Experimental studies concerning the unfolded protein response in glioma pathogenesis

Inaugural-Dissertation

zur Erlangung des Doktorgrades
der Mathematisch-Naturwissenschaftlichen Fakultät
der Heinrich-Heine-Universität Düsseldorf

vorgelegt von

Sascha Steltgens
aus Schwelm

Düsseldorf, Januar 2020

aus dem Institut für Neuropathologie
der Heinrich-Heine-Universität Düsseldorf

Gedruckt mit der Genehmigung der
Mathematisch-Naturwissenschaftlichen Fakultät der
Heinrich-Heine-Universität Düsseldorf

Berichterstatter:

1. Prof. Dr. med. Guido Reifenberger

2. Prof. Dr. Hermann Aberle

Tag der mündlichen Prüfung: 13.03.2020

Teile dieser Arbeit wurden pubilziert oder zur Veröffentlichung eingereicht in:

Chi DL Nguyen, Sebastian Malchow, Stefan Reich, Sascha Steltgens, Stefan Loroch, Christin Lorenz, Albert Sickmann, Christiane B. Knobbe-Thomsen, Björn Tews, Jan Medenbach, Robert Ahrends: A sensitive and simple targeted proteomics approach to quantify transcription factor and membrane proteins of the unfolded protein response pathway in glioblastoma cells. Sci Rep. 2019 Jun 20; 9(1):8836.

Stefan Reich, Chi DL Nguyen, Canan Has, Dominik Conrad, Sascha Steltgens, Himanshu Soni, Christiane B Knobbe-Thomsen, Björn Tews, Grischa Toedt, Dr. Robert Ahrends: Anti-folate resistance and metabolic reprogramming induced by the unfolded protein response.

„[…] *Freiheit bedeutet frei sprechen, frei machen, frei bleiben*
Mauern die, die Angst vorm Versagen errichtet einreißen, Mut haben
Freiheit bedeutet auch zu enttäuschen, sich selbst zu erfüllen
anstatt die Erwartungen von anderen Leuten
Freiheit heißt auch Entscheidungen treffen
Freiheit heißt hin und wieder sich die Freiheit zu nehmen die Meinung zu wechseln
Freiheit heißt es macht manchmal auch Sinn,
dass meine Freiheit da enden muss, wo die Freiheit eines Anderen beginnt
Aber Freiheit darf niemals heißen: entsagen von unseren Rechten […]“

- Curse: *Freiheit*, auf *Freiheit*, Sony BMD 2008

Zusammenfassung

Maligne Gliome stellen eine Tumorerkrankung des zentralen Nervensystems mit oftmals verheerenden Konsequenzen für die betroffenen Patienten dar. Kurative Behandlungsoptionen sind limitiert und eine frühzeitige Diagnose ist kaum möglich, was zu großen medizinischen und wissenschaftlichen Herausforderungen führt. Die molekularen Grundlagen der Gliomgenese sind noch nicht vollständig erforscht. Mutationen im *IDH1*-Gen wurden als eine der initialen Veränderungen in diffusen astrozytären Gliomen und oligodendroglialen Gliomen identifiziert zu der im Rahmen der Tumorprogression weitere genetische Veränderungen in anderen Genen, u.a. Mutationen der Gene *TP53* und *ATRX*, oder Mutationen des Gens *CIC* und des *TERT*- Promoters in den oligodendroglialen Tumoren hinzukommen. Das schnelle Wachstum maligner Gliome stimuliert zwar die Angioneogenese, diese ist aber unzureichend, so dass die Tumorzellen in Gliomen mit einer niedrigen Sauerstoffverfügbarkeit und einer niedrigen Glukosekonzentration konfrontiert sind. Diese Umweltbedingungen können zu einer defekten Proteinfaltung und -prozessierung führen, die wiederum eine gestörte Proteostase im endoplasmatischen Retikulum (ER) bewirken. Veränderungen der Proteostase im ER führen zu einer Aktivierung der drei Transmembranrezeptoren IRE1α, PERK und ATF6, die als *unfolded protein response* (UPR)-Rezeptoren fungieren. Nach der Aktivierung von IRE1α kommt es zum veränderten Splicing der RNA des *XBP1* Genes und Translation eines potenten Transkriptionsfaktors, der die Transkription von Genen fördert, welche die Proteostase wiederherstellen. Aktiviertes PERK phosphoryliert EIF2α und reduziert dadurch die CAP-abhängige Translation, während ATF6 in den Golgi-Apparat transloziert und dort zu einem aktiven Transkriptionsfaktor prozessiert wird.

In dieser Arbeit wurden Behandlungskonzentrationen für die beiden ER-Stress-induzierenden Substanzen Tunicamycin und Thapsigargin experimentell definiert, die es ermöglichten, die UPR in murinen NIH/3T3 Fibroblasten und in humanen LN-308 Gliomzellen zu verschiedenen Zeitpunkten nach Behandlung mit Hilfe von Hochdurchsatz-Methoden im Rahmen eines Kooperationsprojektes zu untersuchen und Transkriptom-, Translatom- und Proteomanalysen durchzuführen. Bei der Analyse der verschiedenen Zeitpunkte nach Behandlung der Zellen zeigte sich, dass die UPR in den beiden untersuchten Zelllinien ähnlich ist, aber auch spezifische Unterschiede aufweist, wie zum Beispiel das konstitutive Expressionsniveau des wichtigsten ER-Chaperons BIP und dessen Veränderung nach Aktivierung des UPR-Signalwegs.

Darüber hinaus wurde der Einfluss des Tumorsuppressorproteins p53 auf die UPR untersucht. Hierbei zeigte sich, dass die Aktivität von IRE1α in murinen neuralen Stamm- und Vorläuferzellen mit *Tp53*-Deletion im Vergleich zu entsprechenden *Tp53*-Wildtyp-Zellen höher ist. Diese Veränderung könnte durch eine veränderte Abundanz des Ko-Chaparones DNAJB9 bedingt sein, welches bereits von anderen Arbeitsgruppen für die Aktivitätsregulation von IRE1α verantwortlich gemacht wurde.

In weiteren eigenen Experimenten ergab sich, dass der von mutiertem IDH1 generierte Onkometabolit 2-Hydroxyglutarat zu einer Aktivierung der UPR in neuralen Stamm- und Vorläuferzellen führt, welche diese resistenter gegenüber ER-Stress macht. Dies legt die Hypothese nahe, dass *Idh1*-mutierte, murine neurale Stamm- und Vorläuferzellen besser mit ER-Stress zurechtkommen, was letztendlich bei der Gliomentstehung von Bedeutung sein könnte. Darüber hinaus wurde untersucht wie sechs etablierte Gliomzelllinien auf das ER-stress-induzierende Chemotherapeutikum Bortezomib reagieren. Hierzu wurden in einem Kooperationsprojekt neue proteomische Methoden entwickelt, die zeigten, dass die sechs untersuchten Zelllinien eine differentielle Expression UPR- relevanter Proteine aufweisen.

Insgesamt wurden in dieser Doktorarbeit molekulare und funktionelle Ergebnisse zur Rolle des UPR in NIH/3T3 Fibroblasten und LN-308 Gliomzellen erzielt. Zudem wurden mögliche Einflüsse Gliom- assoziierter Mutationen auf den UPR untersucht. Zusammengenommen sprechen die eigenen Befunde somit für eine pathogenetische Bedeutung des UPR in Gliomen und bilden den Ausgangspunkt für weitere Analysen der zugrundeliegenden molekularen Pathomechanismen.

Summary

Malignant gliomas are primary cancers of the central nervous system with often devastating consequences for the affected patients. Due to limited treatment options and lack of preventive or early diagnostic opportunities, gliomas are medically and scientifically challenging. The molecular processes in gliomagenesis are not yet fully understood. As initial changes mutations of the *IDH1*-gene were identified in diffuse astrocytic and oligodendroglial gliomas, which additionally acquire other mutations during tumorigenesis, in e.g. mutations in the genes *TP53* and *ATRX* in astrocytic tumors, or *CIC* and *TERT* promotor mutations in oligodendroglial tumors. Further tumor growth stimulates angioneogenesis that is usually insufficient, thus resulting in low oxygen and glucose levels in the tumor tissue. These conditions influence protein folding and processing, thereby resulting in impaired proteostasis, e.g. in the endoplasmic reticulum (ER). Protostatic changes in the ER may activate the three membrane spanning receptors IRE1α, PERK, and ATF6 of the unfolded protein response (UPR). Activity of IRE1α results in unconventional splicing of the *XBP1* mRNA and leading to a translation of the potent transcription factor XBP1, which in turn increases expression of proteins that restore proteostasis in the ER. Active PERK phosphorylates EIF2α and thereby reduces CAP-dependent translation, whereas ATF6 translocates to the Golgi membrane where it is cleaved. The cytosolic cleavage product is a potent transcription factor.

In this thesis, concentrations of two ER stress-inducing drugs, namely Tunicamycin and Thapsigargin, were experimentally defined. This allowed for the molecular analysis of the UPR in mouse fibroblasts (NIH/3T3) and in a human glioma cell line (LN-308) at different time points by using high-throughput methods such as transcriptomics, translatomics, and proteomics. These experiments showed a similar UPR in both cell types, however, with distinct differences, e.g. in the consecutive expression of the major ER resident chaperone BIP as well as its quantitative changes upon UPR activity.

In further experiments, the role of the tumorsuppressor protein p53 in the UPR was elucidated. These studies revealed that the activity of IRE1α in mouse neural stem and progenitor cells (NSC/NPCs) with *Tp53* deletion was higher than in *Tp53*-wildtype cells. Changes in the expression level of the co-chaparone DNAJB9 could be identified as a possible link between p53 and IRE1α activity, as reported before by other groups.

Additional own experiments showed that the oncometabolite 2-hydroxyglutarate that is produced by mutant IDH1 can activate the UPR in murine NSC/NPCs. This physiological endogenous proteostasis challenge renders these cells more resistant against external ER stressors. This observation supports the hypothesis that *Idh1*-mutant glioma precursor cells may be more resistant to ER stress induction during gliomagenesis when compared to wildtype NSC/NPCs. Further studies addressed to effects of the chemotherapeutic drug Bortezomib in six established glioblastoma cell lines. For this purpose, novel proteomic methods were developed in a collaborative project that revealed a different expression of UPR-related proteins in these cell lines.

In summary, this thesis revealed novel molecular and functional insights regarding the role of the UPR in NIH/3T3 fibroblasts and in LN-308 glioma cells. In addition, possible links between glioma-associated gene mutations and the UPR were elucidated. Taken together, the own results highlight a pathogenetic relevance of the UPR in gliomas and lay the grounds for further analyses of the underlying pathomechanisms.

TABLE OF CONTENTS

LIST OF ABBREVIATIONS

2-HG	*D*(-)-2-hydoryglutarate
4-OHT	(E/Z)-4-Hydroxytamoxifen
Aa	Amino acids
Amp	Ampicillin
AP	Alkaline phosphatase
AU	Anson unit
bFGF	Basic fibroblast growth factor
Bor	Bortezomib
BrdU	Bromodeoxyuridine
BSA	Bovine serum albumin
bZIP	Basic leucine zipper
CNS	Central nervous system
CTD	C-terminal domain
DBD	DNA binding domain
DMEM	Dulbecco's Modified Eagle Medium
DMSO	Dimethyl sulfoxide
EGF	Epidermal growth factor
ER	Endoplasmic reticulum
ERAD	ER-associated protein degradation
ERSE	ER stress responsive element
EtOH	Ethanol
FC	Fold change
FCS	Fetal calf serum
G-CIMP	Glioma-CpG island hypermethylation phenotype
GLS	Golgi localization signal
HEPES	4-(2-hydroxyethyl)-1-piperazineethanesulfonic acid
IRES	Internal ribosomal entry site
KO	Knock-out
LB	Lysogeny broth
loxP	Locus of X-over P1
MTT	3-(4,5-dimethylthiazol-2-yl)-2,5-diphenyltetrazolium bromide
Mut	Mutant
NSC/NPCs	Neural stem / progenitor cells
NTD	N-terminal domain
OD	Oligomerization domain
ORF	Open reading frame
p. a.	*Pro analysi*
P/S	Penicillin / Streptomycin
PAGE	Polyacrylamide gel electrophoresis
PBS	Phosphate buffered saline
PCR	Polymerase chain reaction
PEI	Polyethyleneimine
PPR	Proline rich region
PVN	Perivascular niche
qRT-PCR	Semi-quantitative reverse transcripted PCR
RIDD	Regulated IRE1-dependent decay of RNAs
RIPA	Radioimmunoprecipitation assay
RQ	Relative quantity
RT	Room temperature
SDS	Sodium dodecyl sulfate
SEM	Standard error of the mean
SR	SRP receptor

SRP	Signal recognition particle
TAD	Transactivation domain
TAE	TRIS acetate EDTA
TBS	TRIS buffered saline
TE	TRIS EDTA
TET	Ten-eleven translocation
Th	Thapsigargin
Tm	Tunicamycin
TMZ	Temozolomide
TRIS	2-Amino-2-(hydroymethyl)-propane-1,3-diol
UPR	Unfolded protein response
WB	Western Blot
WT	Wildtype

1. INTRODUCTION

1.1 BRAIN TUMORS

Malignancies of the central nervous system (CNS) are devastating diseases because the CNS not only controls physiological necessities but also behavior, mood, and socialization. The CNS is fragile and abnormalities like brain tumors are therefore shattering and of high mortality.

The most common malignancies in the brain are metastases from tumors outside of the brain (*2*). Primary tumors of the brain and the meninges include both benign as well as malignant lesions. However, the group of primary brain tumors with the highest incidence (30 %) of all primary brain tumors are gliomas (*3*). This group of cancers includes 80 % of all primary brain malignancies. Their cell of origin is still unknown, but during gliomagenesis the glioma precursor or stem cell may encompass five phases until inevitable immortalization (*4*). This model is built on the fact that brain tumors are a heterogenous mixture of tumor cells at different developmental stages. Studies in mice suggest that the cells of origin of a glioma could be neural stem cells (NSC/NPCs), astrocytes, or oligodendroglial progenitor cells (*5*).

Gliomas are classified using histological and molecular markers according to the 2016 WHO classification of tumors of the CNS (*6*). Most gliomas are diffuse gliomas which are distinguished based on the presence or absence of alterations in the isocitrate dehydrogenase 1 (*IDH1*) and isocitrate dehydrogenase 2 (*IDH2*) genes, which is further described under 1.1.1. Independent of this differentiation of IDH-mutant and IDH-wildtype tumors, diffuse gliomas exhibit many genetic alterations. In brief, mutations are found in the tumor suppressor protein 53 (*TP53*) gene, the transcriptional regulator ATRX (*ATRX*) gene, the promotor region of the telomerase reverse transcriptase (*TERT*) gene, the phosphatidylinositol 3,4,5-trisphosphate 3-phosphatase and dual-specificity protein phosphatase (*PTEN*) gene, the histone H3.3 (*H3F3A*) gene, as well as the serine/threonine-protein kinase B-raf (*BRAF*) gene. Common chromosomal aberrations are trisomy of chromosome 7 or a gain of 7q, loss of heterozygosity of 17p, or 1p and 19q co-deletion. A gain of chromosome 7 results in an increased gene dose of the epidermal growth factor receptor (*EGFR*) gene, a common alteration in high-grade gliomas. Epigenetic changes include the glioma-CpG island hypermethylation phenotype (g-CIMP), and O6-methylguanin DNA-methyltransferase (*MGMT*)-promoter methylation (*7*). Different combinations of such alterations give rise to subclasses of diffuse gliomas such as diffuse astrocytic and oligodendroglial tumors (*7*). According to the WHO classification diffuse gliomas correspond to WHO grade II, III, or IV tumors depending on the degree of histological malignancy and the associated molecular alterations.

Unfortunately, diffuse gliomas until now are essentially uncurable. Treatment standard for a WHO grade IV glioblastoma, IDH-wildtype is surgical resection followed by radiochemotherapy and chemotherapy with temozolomide (TMZ) (*8*). Despite this aggressive therapy protocol, mean survival of patients is short and remains between 14 to 17 months (*9–11*).

Although the understanding of genetic alterations underlying gliomagenesis has significantly improved over the recent years, and the introduction of molecular markers into glioma classification and grading, as well as the introduction of large-scale DNA sequencing techniques have improved tumor diagnosis, the development of novel therapeutic approaches is lacking behind. Until now, the different glioma-relevant DNA alterations were studied separately from each other. The observation that mutations in *IDH1* are not capable of initiating glioma development by themselves (but have a strong contribution; (*4*)), may put emphasis on the importance of other mutations potentially aiding this particular alteration. Hence, it is most likely that a complex an interplay between different genetic alterations and epigenetic changes drives initiation and progression (*7*).

1.1.1 IDH mutations in gliomas and their implications

As mentioned above, alterations in the *IDH1* gene are thought to be tumor-initiating mutations, but appear to be not sufficient for gliomagenesis (*12, 13*). This observation partially was made using a conditional mouse expressing the mutant IDH1 protein in the CNS which did not cause gliomas but resulted in early death of the mice from severe perinatal brain hemorrhage caused by hindered collagen IV maturation in the ER, and thus a weakened basal membrane (*12*).

Biochemically, the IDH1 missense mutations at base 395 are gain of function mutations. The wildtype (wt) enzyme catalyzes the oxidative decarboxylation of isocitrate to α-ketoglutarate, an NADPH generating reaction, whereas the mutant (mut) enzyme reduces α-ketoglutarate to *D*(-)-2-hydroxyglutarate (2-HG) while consuming NADPH (*14*). This reaction is possible because the exchange of arginine at position 132 of the mutant protein changes the binding properties for isocitrate in the oxidative reaction. Hence, the oxidative reaction in the mutant enzyme becomes very slow, whereas the reductive reaction, α-ketoglutarate to 2-HG, is quick. This reaction is unmeasurable for the wt enzyme (*14*).

The IDH1 R132H mutation is the predominant mutation regarding the IDH enzyme family. It was found in 83-91 % of all *IDH1*-mutant gliomas, whereas R132C (3.6-4.6 %), R132G (0.6-3.8 %), R132S (0.8-2.5 %), and R132L (0.5-4.3 %) were less frequent (*13, 15–17*). IDH2, the only human IDH1 homolog to use $NADP^+$ as an electron acceptor, was found to be mutated at residue R172,

the IDH1 R132 analogue, to R172G, or R172M, or R172K (*15*). IDH2, however, is located in the mitochondria and not in the cytosol like IDH1. Interestingly, eukaryotic cells do express an enzyme able to convert 2-HG back to α-ketoglutarate, i.e., so called D-2-hydroxyglutarate dehydrogenase (D2HGDH), which localizes to the mitochondria. Expression of this enzyme is not deregulated in IDH-mutant gliomas (*18*).

IDH-mutant gliomas are heterozygous for the IDH mutation (*IDH1* or *IDH2*), which means there is no net NADPH yield for the tumor cell with the consequence of possible oxidative stress (*16, 19*). That is why the heterodimer between a mutant and wildtype IDH enzyme is described as catalytically inactive and therefore dominant negative. 2-HG was reported to competitively inhibit α-ketoglutarate-dependent dioxygenases and 5-methylcytosine hydroxylases of the ten-eleven translocation (TET) family (*20*). The former enzyme family includes histone demethylases such as lysine-specific demethylase 7a (KDM7A), thus leading to increases in histone methylation in $IDH1^{R132H}$-expressing cells. Inhibition of the latter enzyme family results in hypermethylation of CpG islands in the DNA of the mutant cell. In gliomas, this DNA-hypermethylation phenotype discriminates IDH-mutant tumors from IDH-wildtype ones and was termed g-CIMP (as mentioned under 1.1) (*21, 22*). However, there are more dioxygenase family members such as the prolyl- and lysyl-hydroxylases that were found to be inhibited by 2-HG. These enzymes physiologically use α-ketoglutarate, molecular oxygen, and Fe^{2+} as cofactor to hydroxylate prolyl and lysyl residues in proteins (*23*). Hydroxyprolyl-residues and hydroxylysyl-residues are important for proper formation of helical structures in collagen proteins which are modified in the endoplasmic reticulum (ER) (*23, 24*). Improperly folded proteins accumulate in the ER and induce a proteostasis pathway known as the unfolded protein response (UPR) (see chapter 1.2) (*25*). 2-HG produced by mutant IDH proteins thus induces the UPR (*12*). Incompletely folded collagen proteins are not secreted and the basal membranes within the vicinity IDH-mutant cells are hence weakened. Another protein with hydroxylated prolyl and lysyl residues is hypoxia-inducible factor 1-α (HIF1α). It was found to be stabilized in mutant IDH expressing mouse brains and that led to an increase in vascular endothelial growth factor (VEGF) and hence growth of aberrant blood vessels (*12*).

Interestingly, patients with IDH-mutant glioblastoma have a better prognosis than IDH-wildtype glioblastoma patients (*26*). This leads to the assumption that mutant IDH proteins are cell biology-wise unfavorable. Since such mutations are also not sufficient to cause glioma development, *IDH* mutations may be the reason why glioma precursor cells accumulate other driver mutations. For example, IDH-mutant tumors carry genomic mutations or alterations in *TP53* and *ATRX* in the case of astrocytic tumors or co-deletions of chromosomal arms 1p and 19q as well as *TERT* promotor

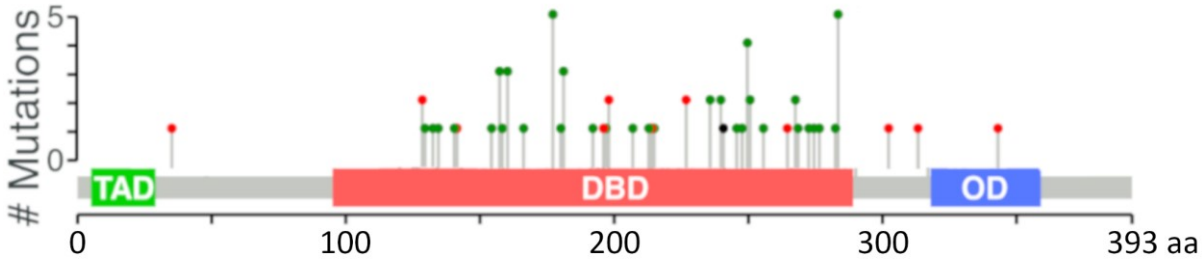

Figure 1- Distribution of mutations in the human *TP53* gene Distributions of mutations in the *TP53* gene over the protein domains of P53 (modified from (*1*)).

mutations in the case of oligodendroglial tumors. Thus, mutant IDH may lay the grounds for the acquisition of additional mutations.

1.1.2 Alterations of p53 function in gliomas

In gliomas the role of mutant p53, a transcription factor mutated in approximately 50 % of all tumors, remains to be elucidated in its comprehensiveness. However, one possibility of interplay with mutant IDH may be related to p53's role in the regulation of DNA methylation through its tight regulation of DNA-methyltransferases (DMNT) and TET protein family enzymes (*27*). Intriguingly, Li-Fraumeni patients, who carry germline *TP53* mutations, secondarily acquire the $IDH1^{R132C}$ mutation in diffuse gliomas, which is the second most common but still rare IDH1 mutation (*3, 17*). The notion that p53 can sense and respond to epigenetic perturbations is supported by the observation that inactivation of p53 rescues embryonic stem cells from apoptosis caused by DMNT1 deficiency (*28*). Chromatin modifications as observed in IDH-mutant cells may result in genes being less or more accessible for p53 transactivation (*29*).

p53 consists of seven domains: a transactivation domain (TAD), a proline rich region (PRR), DNA binding domain (DBD), nuclear localization signal, oligomerization domain (OD), and C-terminal domain (CTD: (*30*)). 95 % of all tumor relevant mutations in the *TP53* gene are observed in the DBD, 28 % of these are hotspot mutations at codons 175, 245, 248, 249, 273, and 283, 75 % of which are missense mutations (*31–33*) (Figure 1). In gliomas, 50 % of the observed mutations in *TP53* are located in the DBD (*34*). Mutations at these positions either alter the DNA-protein interface or destabilize the structure of the DBD (*35, 36*), hence limiting or abolishing the DNA binding capability of p53. Interestingly, also mutant p53 can influence expression of *MYC*, *EGFR*, and multidrug resistance protein 1 (*MDR1*) (*37–39*). The OD is necessary for homo-tetramer assembly and transcriptional activity, whereas the TAD domain is bound by murine double

minute 2 (MDM2), an E3 ubiquitin ligase negatively regulating p53 and thus maintaining low levels of p53 (*40*). MDM2 is within a feedback loop that is transcriptionally increased by p53 f

However, p53 is also activated upon a variety of stress stimuli and governs complex anti-proliferative transcriptional programs tangled into multiple biological responses (*1*). By altering important p53-pathway genes, an inactivating p53 mutation could be mimicked. For example, 53 % of malignant gliomas show tumor suppressor ARF (*$p14^{ARF}$/CDKN2A*) deletions, and 11 % of glioblastoma carry a *MDM2* amplification (*41*). Importantly, p53 is referred to as "guardian of the genome" because it is necessary for a reversible DNA damage-induced G1 phase checkpoint arrest in the cell cycle (*42*). This best understood function of p53 is mediated by transcriptional activation of cyclin-dependent kinase inhibitor 1 (*p21/CDKN1A*) (*43, 44*) and necessary for DNA damage repair prior to cell division. Here, DNA damage activates serine-protein kinase ATM and serine/threonine-protein kinase ATR which phosphorylate and thus activate serine/threonine-protein kinase CHK1 and CHK2, respectively (*32*). The latter phosphorylates p53 and thereby blocks its interaction with MDM2, p53 is therefore stabilized and activates its diverse transcriptional network. However, p53 is additionally able to induce apoptosis by transcriptionally increasing pro-apoptotic regulator BCL-2 (BCL-2) family members (*45–47*), thereby elevating caspase activation and cell death (*48*).

p53 may also play a role in tumor origin. Current theories about the origin of glioma include the glioma stem-like cell as precursor cell (reviewed in (*49*)). There is increasing evidence that p53 has additional functions in non-pathological tissue homeostasis. It may restrict cellular self-renewal in some stem and progenitor cells subjected to oncogenic stress (*50–53*). Consistent with this observation, p53 knock-out mice have elevated numbers of tissue-specific stem cells (*54, 55*).

In contrast to many roles of p53 in cell biology, mutation of this gene has no obvious prognostic implications in gliomas (*26*).

1.1.3 The glioma microenvironment

Several cell types are present within and around gliomas and hence build the cellular environment of the tumor. Generally, the tumor exploits the surrounding environment through recruitment of non-malignant cells providing physiological resources and important factors to facilitate tumor progression (reviewed in (*56*)). Interestingly, a substantial number of subventricular zone neural precursor cells (NPC) migrate towards experimental brain tumors (*57–61*), and were shown to surround the glioma in multiple layers (*61*). Other cell types in the micro-environment communicate with the cancer cells. For example, microglia cells secrete inactive 72 kDa type IV

collagenase (MMP2) which is activated by soluble factors secreted by glioblastomas allowing infiltration of the surrounding tissue (*62*).

The glioma microenvironment also includes endothelial cells, pericytes, and astrocytes forming a neurovascular unit that accompanies tumor progression. Increasing evidence suggests that such structures, namely the perivascular niche (PVN), build a niche for stem cells in physiological and pathological tissue (*56*). Cells of the PVN contribute to stemness of glioma stem cells via endothelial niche derived factors (*63*). These glioma stem cells directly correlate with vasculature of gliomas and therefore, with malignancy. Interestingly, it was shown that glioma stem cells align to vascular structures in co-cultures.

However, before angiogenesis is initiated and due to imperfect neovascularization, the tumor microenvironment is a hostile tissue. Hypoxic conditions arise from fast growing and heavily metabolizing tumor cells which leads to an oxygen pressure of 5-10 mmHg (blood: 40 mmHg) (*64, 65*). This environment results in the upregulation of HIF1α which in turn increases angiogenesis and recruits perivascular progenitor cells to the PVN. The lack of oxygen leads to aerobic glycolysis and thus, lactate production, thereby acidifying the tumor environment. An additional effect of poor oxygen supply is the inability of a cell to properly mature proteins which are then not correctly folded and start to accumulate. This accumulation of misfolded proteins in the cytosol triggers the so-called heat shock response (reviewed in (*66*)), while in the ER they lead to ER stress, the so called unfolded protein response (UPR), which will be introduced in the following chapter.

1.2 THE UNFOLDED PROTEIN RESPONSE AS THE GUARDIAN OF ER PROTEOSTASIS

The equilibrium or homeostasis between folded and misfolded proteins, as well as the ability of a cell to fold all synthesized proteins at a given time point, is called proteostasis. In gliomas it is perturbed by multiple factors, such as mutant IDH proteins, unfavorable microenvironment, and simply the nature of a fast-growing cell's demand for high protein production. All cell surface proteins, transmembrane proteins, and proteins of the extracellular matrix are synthesized in the ER (*67*). These make up approximately 1/3 of a cells protein synthesis load (*68*). Properly folded and glycosylated proteins are transported to the Golgi network via COPII-coated vesicles for further modification, transport to the cell membrane, and secretion. If the biochemical properties of the ER change because of hypoxia, change in calcium homeostasis, low cellular ATP level or a high protein folding demand, proteins will be misfolded. These challenges to the equilibrium between protein synthesis, folding, modification, secretion, and degradation (proteostasis), leads

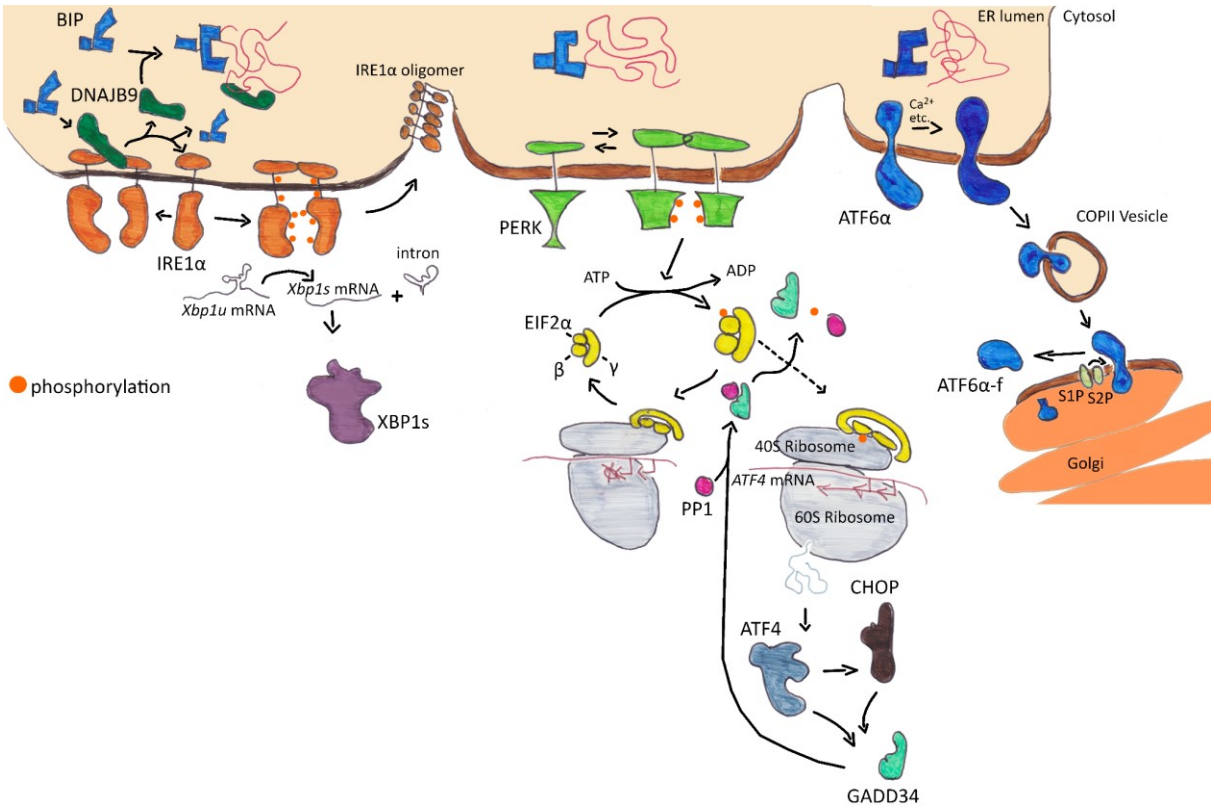

Figure 2- The essential unfolded protein response signaling. The IRE1α pathway is shown on the left, the PERK pathway in the middle, and the ATF6 pathway on the right.

to accumulation of unfolded or misfolded proteins in the ER (*69*). These activate the UPR, which is a signaling and quality control pathway to regain proteostasis or engage cellular apoptosis (*25*). The UPR is built around three signal transducing pathways starting off at three receptors which are ER membrane spanning proteins, two of which in turn are serine/threonine kinases. Inositol-requiring enzyme 1α (IRE1α) and eukaryotic translation initiation factor 2α kinase 3 (PERK) form homodimers upon activation and phosphorylate themselves. Their activity has very different consequences (as descripted under 1.2.1, 1.2.2), however, via synthesis of specific transcription factors they shape the transcriptional landscape of the cell and inevitably the proteome. The cyclic AMP-dependent transcription factor ATF-6α (ATF6) pathway, a third UPR receptor, directly acts as a transcription factor and does not need translation of additional factors and therefore engages transcription of protective targets earlier than the IRE1α and PERK pathway. In general, the UPR increases synthesis of proteins in protective systems like ER-associated protein degradation (ERAD), enzymes in protein modification, and chaperones as well as co-chaperones to reestablish proteostasis in the ER.

1.2.1 IRE1α

IRE1α is a type-I ER membrane protein that is encoded by the *ERN1* gene. Its N-terminal domain (NTD; amino acid (aa) 19-443) serves as an activation domain in the ER lumen. Aa 444-464 build the transmembrane domain. The cytoplasmic part (aa 465-977) consists of two catalytic domains, a kinase and an RNAse domain. IRE1α is active as a homodimer. Upon formation of a homodimer, a trans-autophosphorylation of the two serine/threonine kinase domains occurs on S724 and S726 leading to the activation of the RNAse domain (*70*). Phosphorylations of IRE1α are reverted by the two phosphatases PP2A and PPM1 (*71–73*).

The receptor is activated by accumulation of unfolded proteins in the ER lumen. There are two hypotheses for IRE1α (and PERK) activation. First, active dimers form by direct binding of unfolded proteins to the MHC-like motif of the luminal domain, providing a scaffold for dimerization. Second, a cytosolic heat shock response-like mechanism was proposed where IRE1α is bound by the endoplasmic reticulum chaperone BIP (BIP; gene: *GRP78*/*HSPA5*), the ER resident chaperone, which releases the receptor upon accumulation of unfolded proteins (*74, 75*). Observations made during crystallization of the luminal IRE1α domain, however, shed a different light on the nature of IRE1α. It was shown that the luminal IRE1α domain forms dimers in pure solution (*76, 77*) and when exposed to peptide ligands, the yeast Ire1p formed high-order oligomers form dimers (*78*). Recent work from David Ron's group showed that the luminal domain of human IRE1α forms dimers *in vivo*, which are bound by the DnaJ homolog subfamily B member 9 (DNAJB9) recruiting BIP and inducing ATP hydrolysis in the chaperone leading to disruption of the IRE1α dimer (*79*). BIP-bound IRE1α molecules are then released from the chaperone via nucleotide exchange catalyzed by hypoxia up-regulated protein 1 (HYOU1) and can dimerize again. DNAJB9 and BIP are titrated away from IRE1α upon accumulation of unfolded proteins due to higher affinity to them, leaving the active receptor dimer unaltered, which in turn activates the RNAse domain (*80*).

Upon activation, the RNAse domain of IRE1α splices a 26 bp intron out of the X-box-binding protein 1 (*XBP1*) mRNA. The unspliced mRNA (*XBP1u*) builds a characteristic secondary structure that is recognized and spliced by IRE1α, and is later ligated by the RTCB tRNA ligase complex (*81*). Splicing results in an open reading frame shift, leading upon mRNA translation to a 40 kDa large, very potent, transcription factor able to bind the ER stress responsive element in promoter regions of proteostasis important genes (*82*). However, XBP1s transcriptional activity differs between tissues since it forms heterodimers with other transcription factors (*83*). In general, XBP1s elevates transcription of genes which modulate protein folding, secretion, ERAD, protein translocation into the ER, and lipid synthesis (*84, 85*).

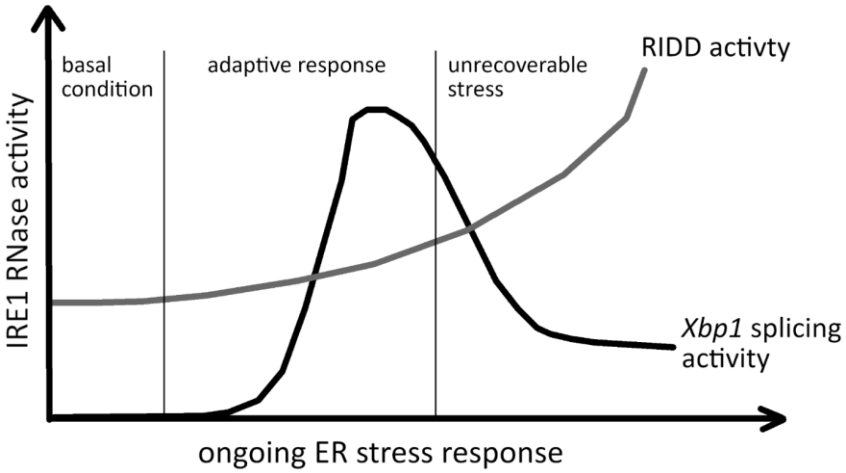

Figure 3- IRE1α RNase domain activity graph. The graph shows the RNase activity of IRE1α under basal, during an adaptive response, and under unrecoverable stress. The activity against the *XBP1u* mRNA increases substantially in an adaptive response but decreases rapidly as soon as the RNase activity against RNAs with a RIDD motive. RIDD cleavage of RNA increases after the adaptive response if the stress from unfolded proteins is unrecoverable. Adapted from (91).

Upon prolonged ER stress, the IRE1α receptor, howsoever, forms higher oligomers resulting in regulated IRE1-dependent decay of mRNAs (RIDD), first described in *Drosophila melanogaster* (*86*) and shown to be conserved in mammals (*87, 88*). Here, IRE1α cleaves an RNA motif similar to the one in *XBP1u* leaving free 5' and 3' ends, which are degraded by exoribonucleases (*89*). RIDD activity under basal conditions, proximal to *XBP1* splicing, is necessary for maintenance of ER homeostasis (*90, 91*), whereas prolonged RIDD activity, under irreversible ER stress, leads to apoptosis (*92*). Cleavage of *XBP1u* and RIDD are in an equilibrium, first there is basal RIDD, then the *XPB1* splicing increases to a maximum and declines from thereon, followed by strong pro-apoptotic RIDD (Figure 3).

IRE1α was shown to additionally interact with TNF receptor associated factor 2 (TRAF2), promoting nuclear factor NF-κB p100 or p105 subunit (NF-κB) activation (*93*). NF-κB is adapted by cytoplasmic protein NCK1 (NCK1) (*94*) and the phosphorylation of mitogen-activated protein kinase 8 (JNK1) to IRE1 (*95*). TRAF2 binding is regulated by the ubiquitination of IRE1α on K545 and K828 by E3 ligase CHIP (*96*). These interactions are thought to couple ER stress with an inflammatory response.

1.2.1.1 *Xbp1* splicing

Splicing of *XBP1u* is tightly regulated. First, the *XBP1* mRNA contains two open reading frames (ORF) that are translated to XBP1u and if spliced by IRE1α to XBP1s. The *XBP1* mRNA is predominantly localized to the ER membrane, despite the XBP1u and XBP1s proteins being soluble in the cytosol (*97*). In addition to the two ORFs, the *XBP1* mRNA contains a translational

(or ribosomal) pausing sequence in the *XBP1u*-ORF, as well as two hydrophobic regions in the resulting polypeptide (*25, 98*). Yanagitani and co-workers reported, that the second hydrophobic region of the XBP1u-ORF polypeptide is necessary for the ER membrane localization of the *XBP1*-mRNA-ribosome-polypeptide intermediate complex. In a follow up study, however, the same group observed that exposure of the second hydrophobic region enables the signal recognition particle (SRP) to bind the polypeptide, bringing the aforementioned complex to the SRP receptor (SR) on the ER membrane (*99*). Here, the complex binds the SEC61 translocon complex but the XBP1u protein is not co-translationally transported into the ER lumen as usual. The authors hypothesize that the XPB1u protein potentially associates with the translocon complex, however, others reported that XBP1u is incorporated in the ER membrane as type-II membrane protein and is subsequently degraded by ERAD (*100*).

Regardless of the nature of the XBP1u protein, the *XBP1* mRNA is localized to the translocon complex mediated by the encoded and translated polypeptide. This mechanism is one piece of the puzzle how a low copy number enzyme like IRE1α, expressed at approximately 416 molecules in HeLa cells (*101*), finds its substrate. The other piece was identified recently by Plumb and co-workers. The authors identified IRE1α to be associated with the SEC61 translocon, bringing it close to the translating ribosome bound complex (*102*). Thereby, the RNAse domain of IRE1α is in close proximity to the mRNA bound to the ribosome and, if active, able to cleave it.

Taken together, the IRE1α arm of the UPR regulates protein influx into the ER predominately at the mRNA level, but additionally increases expression of genes able to reestablish proteostasis.

1.2.2 PERK

PERK is one out of four kinases able to phosphorylate eukaryotic translation initiation factor 2α (EIF2α) (*103*). Like IRE1α, PERK is a type-I transmembrane protein with the sensory part in the ER lumen (aa 30-514), the transmembrane domain (aa 515-535), and the cytoplasmic domain (aa 536-1116) containing the serine/threonine kinase domain. Its activation mechanism remains poorly understood. It is discussed whether PERK is bound by BIP directly or if there is a similar mechanism as for IRE1α activation. Notably, the work of Amin-Wetzel from David Ron's group describes a strong activation of both receptors by deletion of translocon protein SEC63 homolog (DNAJC23/SEC63), possibly a result of its role in protein folding or in repression of IRE1α and PERK signaling (*79*). However, upon activation the receptor dimerizes and undergoes trans-autophosphorylation on T980, stabilizing the activation loop, enhancing EIF2α phosphorylation

(*104, 105*). Additional PERK substrates are NRF2 and forkhead box protein O1 (FOXO1), placing the receptor in proximity to metabolic regulation and redox homeostasis (*106, 107*).

Active PERK phosphorylates EIF2α on S51, inhibiting the nucleotide exchange from GDP to GTP in EIF2-GDP-tRNAiMet tertiary complex between the EIF2 subunits α, β, γ (*108*). This complex is supposed to deliver the starting aa to the ribosome in a GTP dependent manner, its inability to do so shuts down translation globally (*105, 109*). Exceptions to this attenuation are cyclic AMP-dependent transcription factor ATF-4 (ATF4), ATF5, DNA damage-inducible transcript 3 protein (CHOP), and protein phosphatase 1 regulatory subunit 15A (GADD34). Their 5' open reading frames in the 5' untranslated region have been described to be elevated under UPR signaling (*110, 111*). CHOP is the main apoptotic inducer of the UPR. It inhibits transcription of the anti-apoptotic apoptosis regulator BCL-2 (*BCL-2*) and additionally elevates the expression of the pro-apoptotic gene BCL-2-like protein 11 (*BIM*) (*112*). Central to the response of PERK to a disturbed proteostasis is ATF4. This transcription factor increases target genes like *CHOP*, asparagine synthetase (*ASNS*), and insulin-like growth factor-binding protein 1 (*IGFBP-1*) (*113–115*). In a heterodimer with CHOP, the expression of GADD34 is drastically elevated. GADD34 directs protein phosphatase 1 (PP1) in tandem with protein phosphatase 1 regulatory subunit 15B (CReP/PPP1R15B), which both are constitutively expressed, to dephosphorylate p-EIF2α (*116*). The PERK- pathway thereby regulates its own response to accumulating misfolded proteins.

Taken together, the second UPR arm, the PERK pathway, mainly regulates protein influx through regulation of translation directly at the ribosome.

1.2.3 ATF6

ATF6α/β are UPR receptors (encoded by *ATF6α* and *ATF6β*) whose response, in contrast to IRE1α and PERK, does not require protein translation to generate UPR responsive mRNAs. These type-II transmembrane proteins (for ATF6α: cytoplasmic domain: 1-377 aa; transmembrane domain: 378-398 aa; ER luminal domain 399-670 aa) present a Golgi translocation signal (GLS) towards the ER lumen. In the case of ATF6α, the C-terminus contains two GLS signals, whereas ATF6β contains only one (*117*). The two ATF6 proteins have contrasting functions, ATF6α works as a transcriptional activator, whereas ATF6β works as a repressor (*118*). Their response intensity depends on the amount of the β isoform (*118*). Under physiological conditions, both isoforms can form mono-, di-, and, oligomers of homo- or heteromeric nature forming disulfide bridges with their CTD (*119*). The cytosolic N-terminus builds the UPR relevant basic leucine zipper transcription factor (bZIP) (*120*). These molecules serve as sensory modules detecting the redox

state of the ER lumen. Upon accumulation of unfolded proteins BIP unmasks the GLS signal of ATF6α/β, enabling its translocation to the Golgi network. Higa and co-workers reported in 2014, that ATF6α translocation and transcriptional activity is partially regulated by protein disulfide-isomerase A5 (PDIA5) (*121*). The authors also claimed, it may contribute to chemotherapy resistance to Imatinib in patient-derived leukemia cells. The GLS sequences are additionally covered by calreticulin (CALR), introducing another sensory property of the UPR receptor (*122*). In addition, thrombospondin-4 (THBS4) was reported to enhance ATF6α protective function by binding to the ER luminal domain (*123*). The dual specificity mitogen-activated protein kinase kinase 6 (MAPKK6)- mitogen-activated protein kinase P38 α/β (P38α/β/MAPK14)- pathway in dormant human squamous carcinoma cells also partially influences ATF6α activity (*124*). Maiuolo and co-workers published in 2011, that ATF6α is able to, in an unconventional manner, increase expression of genes involved in lipid synthesis upon overload of the ER membrane with membrane proteins (*125*). The activation mechanism, however, remains unknown.

Upon exposure of the GLS, ATF6α/β are packed into COPII vesicles (*126*). Right before the translocation process is initiated, Wolframin (WFS1), an IRE1α branch responsive gene, can retain ATF6α/β at the ER (*127*). The Golgi membrane harbors two serine proteases: membrane-bound transcription factor site-1 protease (S1P/MBTPS1) and S2P (MBTPS2). These proteases cleave ATF6α/β intramembranously, thereby releasing a 50 kDa fragment (ATF6α/β-f), containing the bZIP motive (*128*). ATF6α/β belong to a small family of membrane spanning bZIP transcription factors all cleaved by S1P and S2P (*129*). In the case of ATF6β glycosylation is necessary for its processing in the Golgi (*130*). After cleavage, ATF6α/β-f translocate into the nucleus, where they bind to the ER stress responsive element in tandem with nuclear transcription factor Y (NF-Y) (*131–133*). The ATF6α sequence includes a trans-activation domain overlapping with the degron motif. Ubiquitination and subsequent proteasomal degradation may serve as additional modulators of the response (*134*).

ATF6α-f induces a variety of UPR target genes, for example *XBP1* (*135*), *NF-y* (*136, 137*), interleukin-10 (*IL-10*) (*138, 139*), as well as itself (*ATF6α* (*118, 131*) and *ATF6β* (*118, 140*)). The induction of these target genes is of vital importance for the maintenance of the ATF6 signaling cascade and additionally shapes the UPR. To regain protein processing capacity, ATF6 elevates expression of disulfide bridge building enzymes protein disulfide- isomerase A4 (*PDIA4*) (*141, 142*) and ERO1-like protein α (*ERO1L*) (*141*). This may represent a feedback loop to deactivate the ATF6 branch. Additionally, the chaperones BIP (*85, 141*), endoplasmin (GRP94) (*141, 142*), homocysteine-responsive endoplasmic reticulum-resident ubiquitin-like domain member 1 protein (HERPUD1), calreticulin 2 (CRT2), and HYOU1 were reported to be increased in a ATF6 dependent manner (*135, 141*). ATF6 elevates the level of protein OS-9 (OS9), and protein sel-1

homolog 1 (SEL1L) which are ERAD components (*141*). Interestingly, responders of the ATF6 pathway include pro-apoptotic proteins CHOP (*136, 143*) and BCL-2 (*143*), as well as the sarcoplasmic/endoplasmic reticulum calcium ATPase2 (SERCA2) (*144*) and GTP-binding protein Rheb/Ras homolog enriched in brain (RHEB) (*124*). All these proteins are upregulated with the goal to regain ER proteostasis or engage an apoptotic signaling.

1.2.4 Interplay between the UPR branches

As described above, the UPR signaling appears linear and the branches are separate from each other. However, that does not explain how different inputs lead to distinct but specific UPR outputs. Additionally, the UPR output is cell type-specific, e.g. a cell primed for secretion (e.g. pancreatic islet cells) must have a more robust ER protein folding machinery as compared to e.g. a fibroblast. In part, this specificity is achieved at the transcription factor level but also by the protein tyrosine phosphatase non-receptor type 2 (PTPN2) (*145*).

XBP1s and ATF6α-f both have distinct target genes by themselves but can also dimerize. As heterodimer, they preferentially target genes whose products are involved in protein folding and quality control in comparison to homodimers of either XBP1s or ATF6α-f (*141*). The ATF6α-f/XBP1s heterodimer induces growth arrest and DNA damage inducible 45a (GADD45a), which stimulates DNA excision repair *in vitro* and inhibits the S-phase transition of the cell cycle (*85*). Additional crosstalk between the UPR branches is realized by the ATF6α-f dependent upregulation of DNAJ homolog subfamily C member 3 (DNAJC3/P58IPK) (*146*). It regulates PERK by binding to the kinase domain and inhibiting the autophosphorylation of PERK (*147*). However, physical interactions at the transcription factor level may involve different proteins including ATF6α-f and NF-Y (as described under 1.2.3) as well as XBP1s (*85, 148*), YY1 (*149*), and TATA-binding protein (TBP) (*150*). As described, ATF4 builds heterodimers with CHOP. It was recently shown that this heterodimer may not bind to promoters of apoptosis-promoting genes at all, but rather may induce expression of genes involved in autophagy and translation (*151*). Interestingly, each different interaction partner of ATF4 changes the DNA binding site which than differs from the homodimer (*152–154*). Overall, ATF4 has 18 known interaction partners that all shape its role in cellular processes, such as ER stress, amino acid metabolism, redox detoxification, transcription, mitochondrial function, and microenvironmental shape by increased transcription of type I collagen (*155*).

While interactions between the UPR transcription factors influence the signaling output, the proteins are also fine-tuned by posttranslational modifications. Whereas ATF6α-f is regulated by

phosphorylations (*156*), XBP1s is additionally regulated by phosphorylations, sumoylation, and acetylation (*157–159*). The ATF4 signaling is not only controlled by phosphorylation, but also via its protein stability mediated by selective ubiquitination (*155*).

All these mechanisms further regulate and influence the signaling. Hence, it is very diverse and not as linear as it may seem at first glance. It is under intense research and of increasing interest to elucidate whether tumors or other pathologies can adapt the adaptive UPR response to their benefit.

1.2.5 The UPR in glioma pathology and in therapy

The UPR in glioma is not extensively studied. Nevertheless, several conditions and mutations can trigger the UPR (1.1.1, 1.1.3), which was initially thought to be an adaptive response of the tumor cells to potentially evade threatening conditions. The UPR, however, emerged as a pathway that reprograms the transcriptional landscape of the progressing tumor (*160*). Herein, the UPR participates in determining a range of tumorigenic hallmarks such as cellular transformation, metastatic potential, genomic stability, angiogenesis, immunogenic tolerance, and metabolic status (*161, 162*). It is hence a noteworthy observation that in nervous system tumors in comparison to other cancers, the three UPR receptors show lower mutational rates (*162*).

Lu and co-workers showed that the expression of the transport protein Sec61 subunit gamma (*SEC61γ*) is increased in 77 % of glioblastoma samples investigated (*163*). Interestingly, the *SEC61γ* gene is frequently coamplified with the *EGFR* gene in human glioblastomas (*163*). SEC61γ is responsible for translocation of proteins into the ER membrane and therefore also responsible for EGFR maturation. Chemically induced ER stress leads to increased amounts of SEC61γ and its knock-out has an inhibitory effect on EGFR-dependent Akt survival pathway stimulation (*163*).

The UPR contributes to angiogenesis via induction of vascular endothelial growth factor A (VEGFA) expression under hypoxia or glucose deprivation (*164*). Hypoxia activates the UPR and HIF1α, which leads to ATF4/XBP1s and XBP1s/HIF1α heterodimers, both contributing to transcriptional activation of pro-angiogenic genes such as *VEGF* (*165, 166*). It was also shown by other groups that IRE1α is a key regulator of angiogenesis as observed in IRE1α double negative U-87 MG cells (*167*). Furthermore, by glucose flux analysis, ER stress was shown to increase glucose uptake and thereby glycolysis, amino acid synthesis, as well as the metabolites glutathione and acetate. These changes potentially result in elevated protein synthesis, anti-oxidant defense, and lipid synthesis (*168*). Additionally, under low-glucose conditions the PERK branch was reported to be important for cell survival and hence glioma progression (*169*).

Since treatment options for gliomas are limited, targeting the UPR arose as an interesting pathway for cancer therapy. One possibility is to aggravate the UPR signaling to induce apoptosis by e.g. Bortezomib (Bor), which inhibits the proteasome and thereby leads to an accumulation of unfolded proteins in the cytosol and ER. Bortezomib was approved for treatment of patients with multiple myeloma (*170*). Interestingly, multiply myeloma patients who did not respond to bortezomib treatment showed elevated levels of XBP1 and ATF4 (*171*). Hence, the UPR seems to be involved in mediating resistance to this chemotherapy (*172*) as well as in its mechanism of action (*173*). Initial studies to examine the efficacy of bortezomib in glioblastoma patients were conducted. Bortezomib was shown to be tumor penetrating (*174*). The study, however, did not show a significantly improved survival of patients treated with bortezomib and was done on a small patient cohort. A combination treatment with bortezomib and TMZ resulted in prolonged patient survival (*175*). If combined with e.g. celecoxib or 2,5-dimethyl-celecoxib, both causing leakage of calcium from the ER into the cytosol, bortezomib was shown to be more efficient in killing glioma cells (*176*). However, this treatment option is not well explored in the clinic setting. It remains to be determined if bortezomib will be beneficial for glioma patients.

Surprisingly, the chemotherapeutic agent TMZ itself elevates BIP and CHOP levels upon treatment, and a knock-out of BIP sensitized glioma xenografts to TMZ via increased CHOP levels (*177*). The BIP inhibitor epigallocatechin 3-gallate, a chemical found in green tea, had the same effect on TMZ treated glioma cells, even though epigallocatechin 3-gallate by itself did not alter tumor cell growth (*178*). The prolyl 4-hydroxylase beta polypeptide (P4HB) which is an UPR responsive gene with disulfide isomerase activity has been shown to be associated with TMZ resistance and to be overexpressed in recurrent gliomas (*179*). Besides chemotherapy, radiotherapy is often used to treat glioma patients, particular in case of high-grade tumors. Interestingly, apoptosis induced by radiotherapy was dependent on PERK and IRE1α (*180*). Moreover, an active UPR interferes with EGFR signaling, as mentioned before, but also because it abrogates EGFR trafficking to the cell membrane which in turn enhances radiosensitivity (*181*).

The UPR thus is a promising target for glioma treatment, since on the one hand alterations of UPR signaling pathways are involved in gliomagenesis and glioma progression but on the other hand the UPR interferes with sensitivity to chemo- and radiotherapy.

1.2.6 Role of p53 in the UPR

One way of activating p53 is through the activation of ATM and/or ATR upon DNA damage which then in turn results in the phosphorylation and stabilization of the p53 protein. This

phosphorylation blocks the interaction of p53 with its E3 ubiquitin ligase MDM2. As described above, p53 target genes include DNA damage repair genes but also genes inducing a G1-S phase cell cycle arrest, namely p21 (*CDKN1A*). This arrest allows the cell to repair the response-initiating DNA damage. Additionally, p53 can be stabilized and activated by the UPR responsive gene ATF3 (*182–184*). p53 influences a large network of genes, including over 200 genes involved in 15 different cellular pathways (*1*). Recently it was shown that also ER stress signaling is influenced by p53 signaling (*185*).

Mlynarczyk and Fåhraeus reported that the p53 variant p53/47 (or ΔNp53 or Δ40p53) increases during ER stress (*186*). This isoform lacks 40 amino acids at the N-terminus and displays a different activity and stability than full-length p53 (*186–188*). In their study, the authors claim that p53/47 blocks the p53 dependent increase of P21 and induces expression of the 14-3-3δ protein to induce a G2-M phase arrest. During such cell cycle arrest, the cell can repair a damaged ER. The same group published a study claiming, that under ER stress the p53/47 variant is translated with a similar mechanism as ATF4, and is thus PERK/pEIF2α-dependent (*189*). A similar observation was made by Thomas and co-workers, who provided evidence for a G2-M phase arrest under ER stress, which is PERK dependent, but also showed that p53 is also able to induce a G1-M phase arrest under the same conditions (*190*). Additionally, they observed a reduced translational recovery of p53-mutant cells. The dynamics between p53 and MDM2 seem to be involved in ER stress as well. ER stress activates p53 in a PERK dependent manner, because MDM2 is associated with proteins of the large ribosomal subunit during ER stress rather than with p53. This obviously activates p53 and leads to a p21 dependent G1-S phase arrest (*191*). Also, the apoptotic response of the UPR is reported to involve p53. It was shown that p53 upregulated modulator of apoptosis (PUMA) and NOXA are induced by p53 during the UPR signaling (*192*).

Recently, evidence accumulated that put p53 in direct context to UPR signaling. However, the literature is very diverse. Some reports show an increase and hence, a synergistic effect of p53 during ER stress (*191, 192*), whereas others show an antagonistic effect and degradation of p53 (*193–196*). Dioufa and colleagues investigated p53 knock-out mice with chemically induced ER stress by tunicamycin (*197*). These mice were found to be sensitized to ER stress and showed a potentiated UPR. This empirical conjecture was made on the observation that mouse embryonic fibroblasts (MEFs) derived from the knock-out mice had an elevated *Xbp1s* mRNA level upon treatment. Nevertheless, a similar observation was made, where p53 knock-out cells had an increased *XBP1s* mRNA level and overexpression of p53 led to an *XBP1u* mRNA decrease (*198*).

In summary, p53 is not only involved in cell cycle arrest during ER stress but also appears to influence the expression and splicing of *XBP1*. This effect, however, is intriguing to study. p53, as “guardian of the genome”, influences a key event in a proteostasis pathway. Whether or not this

effect relies on p53's activity as transcription factor or as cytosolic protein remains to be determined. Namba and co-workers observed the same effect, higher splicing of the *XBP1* mRNA in p53 knock-out background (*185*). Since the splicing is mediated by IRE1α, they overexpressed p53 in a p53 knock-out background and measured reduced IRE1α protein levels. The *vice versa* experiment, deletion of p53 in p53 wildtype cells, increased IRE1α. Additionally, IRE1α levels were also found to be increased by overexpression of p53 with hotspot mutations (G245S, R248W, R249S, R273H) in the knock-out background. Cycloheximide chase experiments revealed decreased IRE1α and p53 protein levels in p53 wildtype cells, whereas the p53 knock-out cells did not show a severe decrease in IRE1α. The authors concluded that p53 must control protein stability of IRE1α, and thus conducted a co-immunoprecipitation against p53. The pulled down complex consisted of wildtype p53, E3 ubiquitin-protein ligase synoviolin (SYVN1), and IRE1 and was only observed under proteasome inhibition. SYVN1 was made responsible for the decreased IRE1α levels in p53 wildtype cells. Mechanistically, p53 may serve as adaptor between SYVN1 and IRE1α. Hence, when p53 is absent in the cell, IRE1α is stabilized, because SYVN1 is unable to ubiquitinate the receptor and thus, *XBP1* splicing is higher in p53 knock-out cells (*185*).

2. AIMS OF THE DOCTORAL THESIS

As illustrated above, there is relatively good understanding of the UPR at the biochemical level, including its activation and basic signaling pathways. However, the role of the UPR in tumors, in particular gliomas, is still poorly understood and currently under investigation. This stress responsive signaling is very cell type specific and therefore chemical concentrations used to stimulate the response as well as treatment durations with these chemicals need to be carefully titrated.

The first part of the thesis is based on a collaboration in the context of the BMBF-funded SUPR-G project. This collaborative project addressed the systems biology of the unfolded protein response in glioma (SUPR-G) and focused on the analysis of the UPR in glioma cells via transcriptomics, translatomics, and proteomics. Hence, as a first aim, treatment concentrations and durations were to be established to analyze the UPR with the respective high-throughput methods. These costly and laborious analyses would provide a comprehensive overview of the UPR in glial tumor cells. However, as mRNA and protein synthesis follow different timelines, the analyses should not be performed after the same durations of treatment in different cell culture models. As the project was carried out in close collaboration with the other applicants, parts of the herein presented data were gathered in collaboration with other researchers and are indicated as such.

Further, to assess the influence of glioma associated mutations on the UPR, NSC/NPCs with deletions of *Tp53* were used as an additional *in vitro* model system (*12, 199*). The proposed role of p53 in the UPR, especially on the splicing of *Xbp1*, should be reproduced and a possible mechanism of action should be established.

As a third part of this thesis, the influence of 2-HG, the metabolite synthesized by mutant IDH proteins, on the UPR should be studied. In addition, the role of 2-HG in *Tp53* mutant NSC/NPCs should be studied, since co-existing mutations could possibly benefit each other regarding regulation of the UPR.

3. MATERIALS AND METHODS

3.1 CHEMICALS, KITS, ENZYMES, CELL LINES AND CONSUMABLES

3.1.1 Chemicals and enzymes

If not stated otherwise all conventional chemicals used in this study were "*p.a.*", or for biochemistry, or of research grade. Table 1 provides a list of the chemicals and enzymes used in this thesis.

Table 1 List of chemicals and enzymes

Chemical or enzyme	**Order Number**	**Company**
(2R)-Octyl-α-hydroxyglutarate	16366	Cayman Chemical, Ann Arbor, Michigan, USA
bFGF	AF-100-18B	PeproTech Corporation, Rocky Hill, New Jersey, USA
Benzonase	E1014	Sigma-Aldrich Corporation, St. Louis, Missouri, USA
BglII-FD	FD0083	Thermo Fisher Scientific Corporation, Waltham, Massachusetts, USA
Blasticidin S HCl	A1113903	Thermo Fisher Scientific Corporation, Waltham, Massachusetts, US
Bortezomib	sc-217785	Santa Cruz Biotechnology, Inc., Dallas, Texas, USA
DMEM, high glucose	11965-092	Thermo Fisher Scientific Corporation, Waltham, Massachusetts, USA
DMEM/F-12	1320-033	Thermo Fisher Scientific Corporation, Waltham, Massachusetts, USA
EcoRI-FD	FD0274	Thermo Fisher Scientific Corporation, Waltham, Massachusetts, USA
EGF	AF-100-15	PeproTech Corporation, Rocky Hill, New Jersey, USA
FastAP Thermosensitive Alkaline Phosphatase (1 U/µl)	EF0652	Thermo Fisher Scientific Corporation, Waltham, Massachusetts, USA
Glycogen	R0561	Thermo Fisher Scientific Corporation, Waltham, Massachusetts, USA

Chemical or enzyme	Order Number	Company
HindIII-HF	R3104S	New England BioLabs Inc. Ipswich, Massachusetts, USA
Laminin from Engelberth-Swarm murine sarcoma basement membrane	L2020	Sigma-Aldrich Corporation, St. Louis, Missouri, USA
Lipofectamine 2000	11668019	Thermo Fisher Scientific Corporation, Waltham, Massachusetts, USA
Midori Green Advance	617004	Biozym Scientific GmbH, Hessisch Oldendorf, Germany
MluI-FD	FD0564	Thermo Fisher Scientific Corporation, Waltham, Massachusetts, USA
MluI-HF®	R3198S	New England BioLabs Inc. Ipswich, Massachusetts, USA
N-2 Supplement (100x)	17502048	Thermo Fisher Scientific Corporation, Waltham, Massachusetts, USA
OptiMEM I reduced serum medium	31985047	Thermo Fisher Scientific Corporation, Waltham, Massachusetts, USA
PageRuler Prestained Protein Ladder	26616	Thermo Fisher Scientific Corporation, Waltham, Massachusetts, USA
Penicillin-Streptomycin (5000 U/ml)	15070063	Thermo Fisher Scientific Corporation, Waltham, Massachusetts, USA
Polybrene	H9268	Sigma-Aldrich Corporation, St. Louis, Missouri, USA
Poly-D-Lysine hydrobromide	P6407	Sigma-Aldrich Corporation, St. Louis, Missouri, USA
ProteinaseK	70663-5	Merck KGaA, Darmstadt, Germany
Q5 High-Fidelity Polymerase	M0491S	New England BioLabs Inc. Ipswich, Massachusetts, USA
SalI-FD	FD0644	Thermo Fisher Scientific Corporation, Waltham, Massachusetts, USA
STF-083010	SML0409	Sigma-Aldrich Corporation, St. Louis, Missouri, USA
StuI	ER0421	Thermo Fisher Scientific Corporation, Waltham, Massachusetts, USA

Chemical or enzyme	Order Number	Company
T4 DNA Ligase	15224017	Thermo Fisher Scientific Corporation, Waltham, Massachusetts, USA
T4 polynucleotide Kinase	EK0031	Thermo Fisher Scientific Corporation, Waltham, Massachusetts, USA
Thapsigargin	T9033	Sigma-Aldrich Corporation, St. Louis, Missouri, USA
Trypsin-EDTA (0.05 %)	25300062	Thermo Fisher Scientific Corporation, Waltham, Massachusetts, USA
Trypsin Inhibitor from soybean	17075029	Thermo Fisher Scientific Corporation, Waltham, Massachusetts, USA
Tunicamycin from *Streptomyces* sp.	T7765	Sigma-Aldrich Corporation, St. Louis, Missouri, USA
XhoI-FD	FD0694	Thermo Fisher Scientific Corporation, Waltham, Massachusetts, USA

3.1.2 Kits and other consumables

All kits and other consumables used in this thesis are listed in Table 2.

Table 2 List of used kits and other consumables

Kit	Order Number	Company
GeneJET Gel Extraction Kit	K0692	Thermo Fisher Scientific Corporation, Waltham, Massachusetts, USA
GeneJET PCR Purification Kit	K0701	Thermo Fisher Scientific Corporation, Waltham, Massachusetts, USA
HotStarTaq DNA Polymerase	203203	Qiagen GmbH, Hilden, Germany
MicroAmp Fast Optical 96-Well Reaction Plate with Barcode (0.1 ml)	4346906	Thermo Fisher Scientific Corporation, Waltham, Massachusetts, USA
NEBuilder HiFi DNA Assembly Cloning Kit	E5520S	New England BioLabs Inc. Ipswich, Massachusetts, USA
Neural Tissue Dissociation Kit (P)	130-092-628	Miltenyi Biotec GmbH, Bergisch Gladbach, Germany

Kit	Order Number	Company
Amersham Protran 0.2 µm NC	10600006	GE Healthcare, Little Chalfont, United Kingdom
Pierce™ BSA Protein Assay Kit	23225	Thermo Fisher Scientific Corporation, Waltham, Massachusetts, USA
Plasmid Miniprep Kit I	732-2780	VWR International GmbH, Darmstadt, Germany
RevertAid First Strand cDNA Synthesis Kit	K1621	Thermo Fisher Scientific Corporation, Waltham, Massachusetts, USA
Platinum SyBr Green qRT-PCR SuperMix-UDG w/ROX	11744100	Thermo Fisher Scientific Corporation, Waltham, Massachusetts, USA
StarSeal Advanced Polyolefin Film	E2796-9795	STARLAB GmbH, Hamburg, Germany
TRIzol™ Reagent	15596018	Thermo Fisher Scientific Corporation, Waltham, Massachusetts, USA

3.1.3 Cell lines, cell culture media and added supplements, and plastic ware

The cell lines, cell culture media and added supplements as well as the used plastic ware for cell culture are listed in Table 3.

Table 3 Cell lines, order information respective growth media used for *in vitro* cultivation

Cell line	ATCC® Number[1]	Organism of origin	Media
A-172	CRL-1620	*Homo sapiens*	DMEM with 10 % (v/v) FCS & 10 U/ml P/S
LN-18	CRL-2610		
LN-229	CRL-2611		
SNB-19	CRL-2219		
T98-G	CRL-1690		
U-87 MG	HTB-14		
NIH/3T3	CRL-1658	*Mus musculus*	DMEM with 10 % (v/v) FCS & 10 U/ml P/S

[1] The commercially available cell lines were obtained from American Type Culture Collection (ATCC), Manassas, Virginia. Pheonix retroviral producer cells were kindly provided by the laboratory of Professor Garry Nolan, Stanford University, Stanford, CA. Primary murine neural stem and progenitor cells were obtained from neonatal mice as described in 3.10.

Murine neural stem / progenitor cells (NSC/NPCs)	/	*Mus musculus*	DMEM/F12 with 1 % (v/v) N-2, 10 U/ml P/S, 584.45 fmol/ml bFGF, 3.23 pmol/ml EGF
Phoenix cells	gift from Garry Nolan	*Homo sapiens*	DMEM with 10 % (v/v) FCS & 10 U/ml P/S

All plastic ware used for cell culture work, including sterile Petri dishes and cell culture plates were ordered from Thermo Fisher Scientific Corporation (Waltham, Massachusetts, USA) with Nunclon™ Delta surface. Table 4 provides an overview of the used plastic ware.

Table 4 List of cell culture dishes and plates, as well as information on their surface area and coating for NSC/NPCs

Dish	**Surface area (cm^2)**	**Coating for NSC/NPCs Volume of a 1/250 Laminin dilution in PBS**	**Order number**
6 Well	9.6	1 ml (0.41 µg/cm^2)	140675
96 Well	0.32	0.035 ml (4.4 µg/cm^2)	168136
6 cm	21.5	2 ml (0.37 µg/cm^2)	150288
10 cm	56.7	4 ml (0.28 µg/cm^2)	150350
15 cm	145	(not used for NSC/NPCs)	168381

3.1.3.1 Preparation of basic fibroblast growth factor (bFGF) stock solution

Human recombinant bFGF (Table 1) was solubilized in PBS (-/-) with 0.1 % BSA to 10 µg/ml (584.45 pmol/ml) and stored as aliquots at -20 °C.

3.1.3.2 Preparation of epidermal growth factor (EGF) stock solution

Human EGF (Table 1) was activated by reconstituting lyophilized EGF in 10 mM acetic acid with 0.1 % BSA at a concentration of 2 µg/µl EGF followed by dilution to 10 µg/ml (3.23 nmol/ml) in DMEM/F-12 media. The stock solution was then aliquoted and stored at -80 °C.

3.2 INSTRUMENTS AND SOFTWARE

All laboratory instruments (Table 5), other equipment (Table 6), and software (Table 7) used in this thesis were available at the Institute of Neuropathology or in collaborating laboratories.

Table 5 List of used instruments

Instruments	**Company**
BD FACSCanto	BD Biosciences, San Jose, California, USA
Cell culture incubator: CB160	Binder GmbH, Tuttlingen, Germany
Cell counter: Vi-Cell XR Cell Viability Analyzer	Beckman Coulter GmbH, Krefeld, Germany
NanoDrop ND2000	peQLab Biotechnologie GmbH, Erlangen, Germany
Odyssey CLx	LiCOR, Inc., Lincoln, Nebraska, USA
PCR cycler: Biometra TRIO	Analytik Jena AG, Jena, Germany
Sonicator: Misonix S-4000 with water bath	Thermo Fisher Scientific Corporation, Waltham, Massachusetts, USA
Spectrophotometer: DU 640	Beckman Coulter GmbH, Krefeld, Germany
StepOnePlus Real-Time PCR System	Thermo Fisher Scientific Corporation, Waltham, Massachusetts, USA
Water treatment unit: MilliQ Integral 5	Merck KGaA, Darmstadt, Germany

Table 6 List of used centrifuges and rotors

Centrifuge with rotor	**Company**
Centrifuge 5424	Eppendorf AG, Hamburg, Germany
PerfectSpin 24R	Peqlab Biotechnologie GmbH, Erlangen, Germany
Rotofix 32 with Swing out rotor #1619	Hettich GmbH & Co KG, Tuttlingen, Germany

Table 7 List of software used for data analysis

Software	**Company/Source**
FinchTV v1.4.0	Geospiza Inc., Seattle, Washington, USA
FlowJo v10.0.7r2	FLOWJO, LLC, Ashland, Oregon, USA

Software	Company/Source
GraphPad Prism v5.04	GraphPad Software, Inc., La Jolla, California, USA
Image Studio v2.1.10	LiCOR, Inc., Lincoln, Nebraska, USA
SerialCloner v2.6.1	www.serialbasics.free.fr/Serial_cloner.html
StepOne Software v2.3	Thermo Fisher Scientific Corporation, Waltham, Massachusetts, USA

3.3 ANTIBODIES

The antibodies used in this thesis were ordered from Abcam (Abcam, Cambridge, UK), CST (Cell Signaling Technology, Danvers, Massachusetts, USA), Sigma (Sigma-Aldrich Corporation, St. Louis, Missouri, USA), or LiCOR (LiCOR, Inc., Lincoln, Nebraska, USA). Table 8 summarizes the individual primary antibodies and Table 9 shows the secondary antibodies used for detection of the primary antibody bound to its antigen.

Table 8 List of primary Antibodies

Antibody	Source	Dilution
α1-ACTIN	Sigma #A2066	1/1000 in 5 % BSA/TBS-T
ATF4	CST #11815	1/1000 in 5 % BSA/TBS-T
BIP	CST #3177	1/1000 in 5 % BSA/TBS-T
DNAJB9	Abcam #ab118282	1/166 in 5 % BSA/TBS-T
EIF2α	CST #5324	1/1000 in 5 % BSA/TBS-T
pS51 EIF2α (human cell lysates)	Abcam #ab32157	1/1000 in 5 % BSA/TBS-T
pS51 EIF2α (mouse cell lysates)	CST #3398	1/1000 in 5 % BSA/TBS-T
IRE1	CST #3294	1/1000 in 5 % BSA/TBS-T
p53	CST #2524	1/1000 in 5 % non-fat dry milk in TBS-T
PERK	CST #3192	1/1000 in 5 % BSA/TBS-T
XBP1	Biolegend #619501	1/500 in 5 % BSA/TBS-T

Table 9 List of secondary antibodies

Antibody	Source	Dilution
IRDye 680LT Goat anti-Rabbit IgG	LiCOR #925-68021	1/10000 in 5 % non-fat dry milk in TBS-T
IRDye 800CW Donkey anti-Rabbit IgG	LiCOR #925-32213	1/10000 in 5 % non-fat dry milk in TBS-T
IRDye 680LT Goat anti-Mouse IgG	LiCOR #925-68020	1/5000 in 5 % non-fat dry milk in TBS-T
IRDye® 680LT Donkey anti-Goat IgG	LiCOR #925-68024	1/5000 in 5 % non-fat dry milk in TBS-T

3.4 OLIGONUCLEOTIDE PRIMERS

All oligonucleotides used as primers for polymerase chain reaction (PCR) experiments or cloning purposes were ordered from Sigma-Aldrich Corporation (St. Louis, Missouri, USA) as dried whole synthesis yield and reconstituted in dH_2O to 100 µM. Resulting primer stocks were stored at -20°C and diluted to 10 µM in dH_2O for further use. Table 10 provides a list of primers used for murine genes, whereas Table 11 gives an overview of primers used to amplify human genes, and Table 12 shows oligonucleotides for cloning purposes.

Table 10 List of primer pairs to amplify murine genes

Target gene	Primer name	Sequence (5'-3')	Amplicon length [bp]
Arf1	Mm*Arf1*-F1	GCAGGGAAGACAACAATTCTATACA	108
	Mm*Arf1*-R1	GAAGCTGATATTCTTGTATTCAACAG	
Xbp1s	*Xbp1*-Mm-F1-short	CTGAGTCCGCAGCAGGTGCA	126 (in combination with *Xbp1*-Mm-R1)
Xbp1u	*Xbp1*-Mm-F1-long	CCGCAGCACTCAGACTATGTG	146 (in combination with *Xbp1*-Mm-R1)
Xbp1	*Xbp1*-Mm-R1	GGTCCAACTTGTCCAGAATGC	
Grp78	Hspa5-Mm-F1	GGTGTCCTCTCTGGTGATCAG	125
	Hspa5-Mm-R1	GGTACCACAGTGTTCCTTGGAA	
Ern1	Mm*Ern1*-F2	CCATGCCGAAGTTCAGATGGAA	113

Target gene	Primer name	Sequence (5'-3')	Amplicon length [bp]
	Mm*Ern1*-R2	CCGATGACAAAGTCTGCTGCTT	
Dnajb9	Mm*Dnajb9*-F1	GGCCTTTCACAAATTAGCCATGAAGT	117
	Mm*Dnajb9*-R1	CGACTATTGGCATCCGAGAGTGT	

Table 11 List of primers to amplify human genes

Target gene	Primer name	Sequence (5'-3')	Amplicon length [bp]
XBP1s	*XBP1*-Hs-F1-short	TGAGTCCGCAGCAGGTGCAG	125 (in combination with *Xbp1*-Hs-R1)
XBP1u	*XBP1*-Hs-F1-long	CCGCAGCACTCAGACTACGT	146 (in combination with *Xbp1*-Hs-R1)
XBP1	*XBP1*-Hs-R1	GGTCCAAGTTGTCCAGAATGC	
GRP78	*HSPA5*-Hs-F1	CCTGTCTTCTCAGCATCAAGCAA	128
	HSPA5-Hs-R1	GCTTCATAGTAGACCGGAACAG	
ARF1	*ARF1*-F1	GACCACGATCCTCTACAAGC	111
	ARF1-R1	TCCCACACAGTGAAGCTGATG	

Table 12 List of oligonucleotides used for plasmid cloning or PCR primers to amplify DNA from plasmids

Primer name	Sequence (5'-3')
eGFP-Stop-EcoRI-R1	TAATGAATTCCTACTTGTACAGCTCGTCCATGC
MluI-eGFP-F1	GTAGCACGCGTGTGAGCAAGGGCGAGGAG
pMSCVpuro-Seq-F1	CCTCCTCGTTCGACCCCGCCTCGA
pMSCVpuro-Seq-R1	GCCCAGCGGGGCTGCTAAAGCG
T2A-MluI-R1	TACGTACGCGTAGGGCCAGG
XhoI-SalI-T2A-MluI-EcoRI-F	TCGAGTAGCAGTCGACGGCAGCGGCGAGGGCCGGGGCAGCTTGTTG ACCTGCGGCGACGTAGAGGAGAACCCTGGCCCTACGCGTACGTAG
XhoI-SalI-T2A-MluI-EcoRI-R	AATTCTACGTACGCGTAGGGCCAGGGTTCTCCTCTACGTCGCCGCA GGTCAACAAGCTGCCCCGGCCCTCGCCGCTGCCGTCGACTGCTAC

3.5 CELL CULTURE WORK

Cells were grown on cell culture dishes in an incubator at a constant temperature of 37 °C and in 5 % CO_2 atmosphere. To ensure sufficient humidity, the water compartment was filled with autoclaved dH_2O supplemented with 30 mM copper(II) sulfate.

3.5.1 Thawing and freezing of cells

Cells were stored at -80 °C in heat inactivated fetal calf serum (FCS) supplemented with 10 % dimethyl sulfoxide (DMSO) or in culture medium supplemented with 10 % DMSO for cells growing without FCS. To put cells back into culture the vial was thawed, and the cell suspension was diluted into 5 ml of appropriate cell culture medium. This cell suspension was then centrifuged at 380 *g* for 5 min. After taking off the supernatant the cell pellet was resuspended in the appropriate cell culture medium and plated in a cell culture dish.

3.5.2 Cultivation of cells growing in FCS-containing media

Eukaryotic cells adherently growing in media supplemented with 10 % of heat inactivated (30 min in a water bath at 56 °C) FCS were split as follows: The medium was aspirated, and the cells were rinsed with PBS (-/-). For cell detachment from 10 cm cell culture dishes, 1 ml of 0.05 % Trypsin-EDTA was pipetted onto the cell layer and the cells were incubated for at least 2 min at 37 °C. The enzymatic activity of trypsin was then stopped by diluting the cell suspension with 4 times the volume of FCS-containing cell culture medium. To determine the cell count and cell viability, cells in 500 µl of the cell suspension were counted on the Vi-CELL XR Cell Viability Analyzer™. For experiments, a specific number of viable cells was plated according to the experimental requirements.

3.5.3 Cultivation of cells growing in medium without FCS

Adherently growing cells in medium containing no FCS were split as follows: The medium was aspirated, collected, and the dish was rinsed with 0.05 % Trypsin-EDTA to detach the cells. The trypsinated cell suspension was pooled with the aspirated medium and the cell culture dish was

washed with PBS and trypsin inhibitor solution (25 % of the used volume of trypsin resulting in a 1:1 molar ratio of trypsin to inhibitor), which was also pooled with the cell suspension. Cells were collected by centrifugation at 380 *g* for 5 min and resuspended in fresh medium. Cell number and cell viability were analyzed as described in 3.5.2. The trypsin inhibitor solution constated of 2 g/l Trypsin inhibitor from soybean in PBS (-/-) and was sterile filtrated, aliquoted and stored at -20 °C.

3.5.3.1 Coating of cell culture dishes with laminin for cells growing without FCS

Laminin was diluted to 1 mg/ml in PBS (-/-) before use and stored at 4°C for short-term storage and at -20°C for long-term storage. The cell culture dishes were coated according to Table 4 at 37 °C for at least 15 min and not longer than 4 h.

3.6 Time series experiments with treatment for qRT-PCR and Western Blot analyses

Cells were plated according to Table 13 and incubated overnight or for 48 h in case of murine NSC/NPCs. Medium was aspirated, and the cells were covered with fresh medium according to Table 13 "Volume [ml]". Dependent on the following experiments either 2 µg/ml tunicamycin, 200 nM thapsigargin, or 1 nM bortezomib or the respective solvent controls were administered. Cells were harvested according to 3.7 or 3.8.

Table 13 Experimental conditions for UPR analysis

Cell type	Plate / Dish	Type of analysis	Cell number [#]	Volume [ml]
NSC/NPCs	6 Well (coated)	qRT-PCR	300,000	1.5
	6 cm (coated)	WB	1,000,000	2
NIH/3T3	6 Well	qRT-PCR	500,000	1.5
		WB	500,000	1.5

3.7 PROTEIN ANALYSES BY WESTERN BLOTTING

3.7.1 Cell lysis

Adherently growing cells were rinsed twice with PBS and covered with an appropriate volume of radioimmunoprecipitation assay (RIPA) buffer. The cells were scraped off the dishes using a rubber policeman and the cell lysate was transferred into a microcentrifuge tube. Cells were sonicated in a water bath for 30 s with an amplitude of 100 % (corresponds to ≈ 400 W). Cell lysates were stored at -20 °C for up to three months and at -80 °C for long-term storage.

RIPA:	50.0 mM	2-Amino-2-(hydroymethyl)propane-1,3-diol (TRIS)
	150.0 mM	NaCl
	1.0 % (v/v)	NP-40 analogue
	0.5 % (v/v)	Sodium deoxycholate
	0.1 % (v/v)	SDS

Before use, 10 ml RIPA buffer were supplemented with 1 tablet each of Roche PhosSTOP and cOmplete™ (Phosphatase and Protease Inhibitor cocktails) as well as with 10 µl of Benzonase (Table 1).

3.7.2 Protein quantification

Protein lysates were quantified with the BCA assay kit (Table 2) according to the supplier's instructions. Each assay included standard protein samples (bovine serum albumin (BSA) dissolved in RIPA at concentrations of 0.25, 0.5, 1, 2, 4, 8, 10 mg/ml). The absorbance of each sample at 562 nm was measured with a spectrophotometer on the same plate. Absorbance of the reference samples was plotted against their concentrations to generate a standard curve that was used to calculate the protein concentrations in the experimental samples.

3.7.3 Sodium dodecyl sulfate polyacrylamide gel electrophoresis (SDS-PAGE)

For SDS-PAGE, protein lysates obtained from (3.7.1) were supplemented with SDS sample buffer, heated to 95 °C for 5 min, and loaded onto precast 4-12 % NuPAGE™ Bis- Tris Protein gels. For protein size estimation the marker PageRuler™ Prestained protein ladder (10-140 kDa) was used on each SDS-PAGE gel. The gels were clamped into SDS-PAGE chambers filled with 2-(N-morpholino)-ethanesulfonic acid (MES) containing running buffer. Electrophoresis was performed with constant voltage of 160 V until the bromophenol blue front reached the bottom

of the gel (approximately 65 min). The composition of the SDS sample buffer and the MES buffer were as follows:

SDS-sample buffer (4x):	100 mM	TRIS
	6 % (w/v)	SDS
	4 % (v/v)	β-Mercaptoethanol
	40 % (v/v)	Glycerol
	1 g/l	Bromphenol blue
MES buffer:	50.0 mM	2-(N-morpholino)-ethanesulfonic acid (MES)
	50.0 mM	TRIS
	3.5 mM	SDS
	1.0 mM	EDTA

3.7.4 Western Blotting

To transfer the separated proteins after SDS-PAGE (3.7.3) from the gel to a nitrocellulose membrane (2 µm pore diameter) the tank blot transfer method was used. The membrane was cut to the size of the gel, layered onto the gel, followed by covering gel and membrane with Whatman™ papers. This sandwich was put into the tank filled with transfer buffer and the transfer was performed at a constant current of 250 mA for 2.5 h.

To control for successful protein transfer, the membrane was briefly stained with PonceauS solution to visualize the protein bands. After rinsing off the staining solution with dH_2O, the membrane was incubated in blocking buffer at room temperature (RT) for 1 h. After blocking the membrane was rinsed with TBS-T buffer three times. The membrane was then incubated with the primary antibody (see 3.3) overnight at 4 °C on a stumble shaker. The membrane was washed twice for 10 min in TBS-T at RT. To detect the primary antibody an appropriate secondary antibody was selected depending on the primary antibody species. The selected secondary antibody was then diluted 1:10,000 in blocking buffer and the membrane was incubated with the antibody for 1 h in the dark at RT. Subsequently, the antibody solution was discarded, and the membrane was washed twice for 5 min. To visualize the staining, the membrane was scanned with the Odyssey LiCOR™ system.

The membranes were dried and stored at RT between Whatman™ papers and reconstituted in blocking solution for re-usage. The compositions of the used buffers were as follows:

Transfer buffer:	25.0 mM	TRIS
	0.2 M	Glycine
	20.0 % (v/v)	Methanol

PonceauS solution:	0.1 % (w/v)	Ponceau S
	5.0 % (v/v)	Acidic acid
Blocking buffer:	5 % (w/v)	non- fat dry milk powder (in TBS-T)
TBS-T:	10 mM	TRIS
	150 mM	NaCl
	0.1 % (v/v)	Tween 20

3.7.5 Quantification of bands in Western Blots

Using the Image Studio software (Table 7), bands were circled, and the "Signal"-value was used for quantification. If not otherwise stated, the values of a target protein were normalized to the values obtained for a housekeeping reference (α1-ACTIN) and afterwards normalized again to the target/ACTIN ratios obtained for control cells. The data were plotted as scatter dot plot with standard error of the mean (SEM).

3.8 NUCLEIC ACID EXTRACTION, PURIFICATION, AND ANALYSES

3.8.1 Extraction and purification of RNA from cultured cells

For RNA purification from adherent cells grown in 6 well cell culture plates, the medium was removed from the wells and cells were covered with 1 ml of TRIzol reagent (Table 2). The lysate was transferred into microcentrifuge tubes and the RNA was then isolated according to the manufacturer's instructions, 15 µl of 20 mg/ml glycogen were added to the TRIzol/cell suspension to enhance RNA precipitation. The RNA pellet was dissolved in deionized water (dH_2O), the RNA concentration was determined spectrometric ally using a NanoDrop spectrometer (Table 5), and RNA quality was controlled by agarose gel electrophoresis (3.8.3). RNA was stored at -80 °C.

3.8.2 Reverse transcription of RNA to cDNA

To reverse transcribe RNA into cDNA the RevertAid First Strand cDNA synthesis kit (Table 2) was used according to the manufacturer's instructions. After transcription the reaction mixture was diluted 1/20 in dH_2O depending on the RNA concentration (e.g. 1 µg RNA in 20µl reaction mixture

was diluted in 380 µl dH_2O). cDNA was stored for short-term periods at 4 °C and for long-term storage at -20 °C.

3.8.3 Gel electrophoresis of nucleic acids

For separation of nucleic acids by fragment size, agarose gel electrophoreses were performed. Gels were made by weighing in agarose at 1 to 2 % (w/v) agarose and the agarose was then dissolved in TAE buffer by boiling. The solution was supplemented with 0,035 % (v/v) Midori green and gels were poured into gel trays with combs for the generation of slots. After agarose gel polymerization, samples were supplemented 1:5 with 5x agarose sample buffer and then loaded into the slots. Depending on the DNA/RNA fragment size of the samples, a 100 bp or 1 kbp DNA marker was loaded into one slot as size reference. Gels were run in 1x TAE buffer at 180 V for 20 min. As the agarose gels had been supplemented with Midori green, nucleic acids were made visible under UV light in a gel documentation system (Table 5) or on a UV table. The following buffers were used:

5x Agarose sample buffer:	30 % (v/v)	Glycerol
	0.01 % (w/v)	Xylene Cyanole FF
	0.01 % (w/v)	Bromophenol blue
TAE buffer:	40 mM	TRIS
	0.001 % (v/v)	Acetic acid
	1 mM	EDTA

3.8.4 Polymerase chain reaction

For end-point polymerase chain reaction (PCR), HotStarTaq polymerase (Table 1) was used according to the manufacturer's instructions. Each reaction contained 1.6125 mM $MgCl_2$, 50 µM dNTPs, and 250 nM of each primer (Table 10 or Table 11). The reaction mixture was completed with 1 µl sample DNA or cDNA in a 200 µl reaction vial and the reaction was carried out using a PCR cycler according to the protocol shown in Table 14. After completion of the PCR, the PCR product was stored at 4 °C until analysis.

Table 14 Standard protocol used for PCR analysis

Step	Temperature [°C]	Length [min:sec]	Cycles
1	95	15:00	

Step	Temperature [°C]	Length [min:sec]	Cycles
2	95	00:20	40
3	56	00:20	
4	72	00:20	
5	72	10:00	
6	8	storage	

3.8.5 Semi-quantitative polymerase chain reaction

For relative quantification of mRNA expression levels, the semi-quantitative reverse transcription PCR (qRT-PCR) was used. Here, the target transcript level in a sample is quantified against a reference transcript level from a house-keeping gene (Mm*Arf1* or Hs*ARF1*).

For qRT-PCR the Platinum SyBr green Master Mix (2x) (Thermo Fisher Scientific) was used according to the manufacturer's instructions including the internal reference dye ROX. All primer pairs (3.4) were used at a 500:500 nM ratio. 17 µl of the master mix were loaded into MicroAmp® Fast Optical 96-Well Reaction Plate with Barcode (0.1 ml) and supplemented with 3 µl of diluted cDNA (3.8.2). Plates were then covered with StarSeal Advanced Polyolefin Film. Prepared plates were stored until the qRT-PCR run at 4 °C for not longer than 4 days. Besides the PCR run protocol, a melting curve was added to exclude wells with incorrect product amplification or contamination (Table 15). The mRNA expression relative to the reference target *Arf1*/*ARF1* was calculated using the $2^{-\Delta\Delta Ct}$-method (*200*). This method gives the normalized target amount relative to a reference target termed as relative quantity (RQ) as $2^{-\Delta\Delta Ct}$, were the C_t is the threshold cycle indicating the cycle number were the target amount reaches a fixed threshold. The RQ values were then either plotted or normalized to the RQ value from corresponding DMSO-treated control cells and presented as scatter dot plot with indicated mean ± SEM.

Table 15 qRT-PCR run conditions

Step	Temperature [°C]	Length [min:sec]	Cycles
1	95	10:00	
2	95	00:15	40
3	60	01:00	
4	95	00:15	
5	60	01:00	+ 0.9 °C/min to 95 °C

3.9 OVEREXPRESSION OF DNAJB9 WITH THE PMSCVPURO VECTOR

To overexpress low levels of Mm*Dnajb9* in combination with the fluorescent protein eGFP in murine NSC/NPCs, the retroviral plasmid pMSCVpuro (Clonetech, CA, USA) was used (*201*). The pMSCVpuro-Mm*Dnajb9*-T2A-eGFP plasmid was constructed in three steps as described under 3.9.1, 3.9.2, and 3.9.3. The insert is visualized in Figure 4.

3.9.1 pMSCVpuro with T2A site

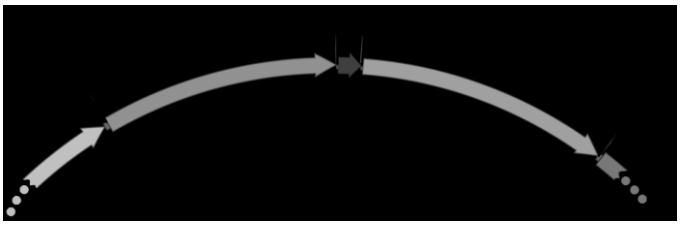

Figure 4- Part of the pMSCVpuro-*Mm*Dnajb9-eGFP plasmid map. The illustration shows the *Mm*Dnajb9-T2A-eGFP insert with indicated restriction sites in the not completely shown pMSCVpuro vector.

The restriction enzymes XhoI-FD and EcoRI-FD were used to open the plasmid while simultaneously dephosphorylating the 5'DNA ends with FastAP (alkaline phosphatase, AP) for 30 min at 37 °C. The insert (T2A site: XhoI-SalI-T2A-MluI-EcoRI-F and XhoI-SalI-T2A-MluI-EcoRI-R) was ordered as an oligonucleotide, phosphorylated with the T4 Polynucleotide Kinase (Table 1) according to the manufacturer's instructions, purified with the PCR purification kit (Table 2) according to the manufacturer's instructions, and annealed in annealing buffer with the program shown in Table 16. Plasmid and insert were separately purified with the PCR purification kit (Table 2) according to the manufacturer's instructions. The products were ligated with T4 DNA ligase (Table 1) as described in Table 17 according to the manufacturer's instructions in at a 1:3 molar ratio (plasmid:insert). 5 µl ligation mixture were transferred into chemo-competent DH5α *Escherichia Coli* bacteria via heat shock (2 min at 42 °C in a water bath) and plated, after at least 30 sec on ice, onto lysogeny broth (LB) agar plates containing 28.61 mM ampicillin (= 100 µg/ml ampicillin; LB-Amp). After overnight incubation at 37 °C, single colonies were picked and transferred into 3 ml LB-Amp medium and grown overnight at 37 °C with shaking. The plasmid was isolated from the bacteria using the MiniPrep Kit (PeqLab) according to the manufacturer's instructions and the cloning process was controlled via PCR (3.8.4) with the primers pMSCV-Seq-F1 and T2A-MluI-R1. Positive clones showed a 166 bp long PCR product, negative ones did not yield a product. Positive clones were sequenced in both directions at StarSEQ GmbH (Mainz, Germany) following amplification with the forward and the reverse primers pMSCVpuro-Seq-F1 or -R1. Sequencing results were analyzed with the FinchTV software (Table 7). Wildtype constructs were named pMSCVpuro-T2A and stored long term at -20 °C.

Table 16 Annealing protocol for XhoI-SalI-T2A-MluI-EcoRI site

Temperature	**Time[min:sec]**
95 °C	5:00
95 °C in -1 °C per minute (→ 86 °C)	9:00
86 °C	30:00
86 °C in -1 °C per minute (→ 8 °C)	78:00
8 °C	storage

Table 17 Ligation protocol

Temperature	**Time[min:sec]**
22 °C	120:00
65 °C	10:00
8 °C	storage

The following buffers and media were prepared and used for the experiments:

Annealing buffer:	10 mM	TRIS
	1 mM	EDTA
	50 mM	NaCl
LB-Amp Agar:	1.00 % (w/v)	Tryptone
	0.50 % (w/v)	Yeast extract
	1.50 % (w/v)	Agar-Agar
	0.17 M	NaCl
	28.61 mM	Ampicillin (= 100 µg/ml)
LB-Amp Media:	1.00 % (w/v)	Tryptone
	0.50 % (w/v)	Yeast extract
	1.50 % (w/v)	Agar-Agar
	28.61 mM	Ampicillin

3.9.2 pMSCVpuro-T2A with eGFP

The green fluorescent protein (GFP) was amplified from pEGFP-C1 (Clonetech, CA, USA) with MluI-eGFP-F1 and eGFP-Stop-EcoRI-R1 using Q5 polymerase (Table 1) according to the manufacturer's instructions with 67 °C for the first and 71 °C for the following annealing steps. The PCR product was analyzed via agarose gel electrophoresis (3.8.3) and the 738 bp product

(MluI-eGFP-Stop-EcoRI) was cut out from the agarose gel and purified using the Gel extraction kit (Table 2) according to the manufacturer's instructions. The pMSCVpuro-T2A vector from 3.9.1 was opened with EcoRI-FD and MluI-FD supplemented with FastAP as described under 3.9.1. This restriction digest product was run on an agarose gel and extracted with the Gel extraction kit according to the manufacturer's instructions. MluI-eGFP-Stop-EcoRI was digested using MluI-FD and EcoRI-FD for 30 min at 37 °C and purified with the PCR purification kit (Table 2). Vector and insert were ligated and amplified as described under 3.9.1. As a control, the plasmids from positive clones were digested with HindIII-HF and MluI-HF at 37 °C for 30 min. Constructs with the correct insert showed bands at 5831 bp and 1244 bp and were sequenced as described under 3.9.1. This protocol resulted in the plasmid pMSCVpuro-T2A-eGFP.

3.9.3 pMSCVpuro-T2A-eGFP with Mm*Dnajb9*

The vector pMSCVpuro-T2A-eGFP from 3.9.2 was digested with BglII-FD and SalI-FD with FastAP for 30 min at 37 °C, followed by gel electrophoresis and extraction of the digested vector from the agarose gel. Mm*Dnajb9* was amplified from murine NSC/NPC cDNA with the Q5 polymerase (Table 1) using the primers DNAJB9-into-2f-F and -R2 at 64 °C as annealing temperature. The PCR product was separated by agarose gel electrophoresis, followed by extraction from the gel. Insert and vector were ligated using the NEBuilder HiFi DNA Assembly Kit according to the manufacturer's instructions and plated on LB-Amp agar plates, which were incubated overnight at 37 °C. Colonies were picked and grown overnight. Plasmids were isolated as described under 3.9.1 and resulting constructs were digested with StuI for 30 min at 37 °C. Positive constructs showed three bands of 5560 bp, 1630 bp, and 557 bp when visualized on an agarose gel. These constructs were sequenced as described under 3.9.1 using the pMSCVpuro-Seq-F1 and T2A-MluI-R1 primers as well as the MluI-eGFP-F1 and pMSCVpuro-Seq-R1 primers. Wildtype constructs were named pMSCVpuro-Mm*Dnajb9*-T2A-eGFP.

3.10 Preparation of murine neural stem and progenitor cells (NSC/NPCs)

To isolate murine neural stem and progenitor cells (NSC/NPCs) newborn mice were decapitated and the scull was opened from the occipital to the frontal pole using sterile surgeon scissors. The scull was bent open, and the brain was removed from the head using curved forceps. Single cell suspensions were prepared using the Neural Tissue Dissociation kit (Table 2) according to the

manufacturer's instructions. In brief, pepsin was utilized to digest the connective tissue of the brain helped by mechanical disruption via pipetting the solution through a 1 ml pipette tip. DNA from disrupted cells was digested by adding 200 µg DNAse for 15 min before centrifugation of the suspension at RT for 5 min at 380 *g*. The pellet was washed twice with PBS (-/-) and once with neural stem cell medium by centrifugation as previously described (3.7.1). The resulting cell suspension was plated onto a laminin-coated 6 cm dish, covered with NSC/NPC medium and incubated at 37 °C and 5 % CO_2 until sub-confluent and then passaged as described above (3.5.3).

3.11 GENERATION OF *TP53* KNOCK-OUT NSC/NPCS

To generate murine *Tp53* knock-out NSC/NPCs cells were isolated from neonatal murine brains of genetically modified mice (*202*). Conditional *Tp53* knock-out NSC/NPCs were then either retrovirally infected with a plasmid carrying the Cre recombinase gene (pMXs-Cre-IRES-Blast, gift from Masato Sasaki, University of Toronto, Canada, model 1) or mice were intercrossed with RosaCreERT1 mice (*203*). The Cre recombinase recognizes the loxP sequence ATAACTTCGTATANNNTANNNTATACGAAGTTAT, cuts and cyclizes the DNA after the first and including the last underlined sequence. In the case of the conditional *Tp53* knock-out mice, the loxP sites are localized between the first and second as well as between the tenth and eleventh exon of the *Tp53* gene (*202*). In the intercrossed mice, cells carry the floxed *Tp53* alleles as well as the (E/Z)-4-hydroxytamoxifen (4-OHT) inducible RosaCreERT1 recombinase (model 2). This modified version of the Cre recombinase is fused to a mutated ligand-binding domain of the estrogen receptor gene. Upon exposure to 4-OHT, the fusion protein translocalizes to the nucleus resulting in the knock-out (KO) genotype $Tp53^{\Delta 2\text{-}10/\Delta 2\text{-}10}$. The cells infected with pMX-Cre (same protocol as in 3.12) were selected by resistance to 1 µg/ml Blasticidin S HCl. With these procedures, two *Tp53* knock-out NSC/NPCs created, one, that upon exposure to 4-OHT loses the *Tp53* gene, and the second one, which loses the *Tp53* gene when retrovirally infected with the pMX-cre plasmid.

For experiments, 300,000 NSC/NPCs were plated onto a 6 cm dish and incubated in the incubator overnight. The medium was exchanged and 3 ml medium containing 500 nM 4-OHT (from a 5 mM stock dissolved in EtOH and stored at -80 °C) were added to the cells for 48 h. Following, the medium was again changed, and the cells were incubated for an additional 72 h and afterwards transferred to 10 cm dishes at sub confluency.

3.12 RETROVIRAL PRODUCTION AND CELL INFECTION

For delivery of pMSCVpuro-Mm*Dnajb9*-T2A-eGFP or pMXs-Cre-IRES-Blast into NSC/NPCs, retroviral gene delivery was used. Retroviral particles were produced in Phoenix cells carrying an ecotropic packaging system (*204*).

Phoenix cells were plated in 6 well plates coated with 1.11 µg/cm^2 poly-D-lysine (see below) at 1,200,000 cells per well. After overnight incubation, 3 µg of pMSCVpuro-Mm*Dnajb9*-T2A-eGFP (3.9.3) were mixed with 1.125 µg pCL-Eco (gift from Inder Verma (Addgene plasmid # 12371) (*205*)) in 200 µl OptiMEM I and vortexed. To the plasmid mixture 9 µl 1 mg/ml Polyethyleneimine (PEI) were added, the solution was vortexed and incubated for 15 min at RT. Cell medium on the cells was exchanged to 2 ml OptiMEM I and the plasmid/PEI mixture was added dropwise to the medium in the 6 well plates. After 4 h of incubation the medium was changed to DMEM containing 10 % FCS and 1 % penicillin/streptomycin (P/S). Cells were washed twice with PBS (-/-) after 24 h incubation and covered with 2 ml of NSC/NPC medium. Virus particle containing medium was harvested 48 h after medium change, filtered through a 0.45 µm filter and stored at -80 °C.

For NSC/NPC infection with retroviral particles, 400,000 cells were seeded on 6 cm dishes. Following overnight incubation, the medium was exchanged to 1 ml retroviral particle containing medium supplemented with 1 ml NSC/NPC medium, 15 µl 1 M 4-(2-hydroxyethyl)-1-piperazineethanesulfonic acid (HEPES), and 8 µg/ml polybrene (Table 1). After 48 h the medium was exchanged, and the cells were incubated for an additional 24 h before selection of infected cells with 1 µM puromycin (pMSCVpuro-Mm*Dnajb9*-T2A-eGFP) or with 1 µg/ml blasticidin S HCl.

Poly-D-Lysine:	0.01 % (w/v)	Poly-D-Lysine hydrobromide
	15 mM	Boric acid

3.13 DOSE-RESPONSE ANALYSES AND READ OUT WITH THE MTT ASSAY

To assess cellular viability, the metabolic activity of cultured treated versus control cells was measured with 3-(4,5-dimethylthiazol-2-yl)-2,5-diphenyltetrazolium bromide (MTT). The chemical is reduced by NAD(P)H- dependent oxidoreductases to insoluble formazan crystals. After solubilization the absorbance of the purple dye was measured, which directly correlates with cell viability. The technique was adapted from (*206*).

In general, the MTT assay was used to prepare dose-response curves of cells treated with various compounds (Table 18) at nine different dilutions and compared to cells treated with a solvent control. Cells were harvested and plated into wells of a 96 well plate as described (3.5) at a maximum of 10,000 cells/well in 50 µl medium (200,000 cells/ml). The outer wells were filled with PBS to account for higher evaporation in these wells and the first column was filled with culture medium as background control for the MTT assay. After incubation with compounds (Table 18) 1.17 mM MTT was added and incubated at 37 °C for 1- 2 h depending on the cell type (NSC/NPCs: 2h; all other cell lines: 1h). To solubilize the formazan, MTT solvent solution was added in a 1:1 (v/v) ratio into the wells and incubated at RT in a dark compartment overnight with constant shaking. Absorbance (A) was measured at 570 nm and 650 nm with a spectrophotometer. The latter value was subtracted from the 570 nm value ($A(ref) = A(570\ nm) - A(650\ nm)$) as this served as reference A(ref) value. To eliminate the background (bkg) absorbance, the absorbance of the wells containing only culture medium was subtracted ($A(cor) = A(ref) - A(bkg)$). The corrected A(cor) values were calculated for each well and a mean was calculated over three technical replicates *per* experiment. These means were normalized to the absorbance means of the solvent control and plotted against the chemical's concentration. In case of dose- response analyses, the obtained normalized absorption was $\log_{10}$ transformed and a "log(inhibitor) vs. normalized response" with variable slope was calculated with the GraphPad PRISM software (Table 7). The following solutions were used:

MTT solution:	11.7 mM	MTT in PBS (-/-) (≈ 10 mg/ml)
MTT solvent:	40 % (v/v) 16 % (w/v) 2 % (v/v) in dH_2O at pH = 4.7	Dimethylformamide SDS Acetic acid

Table 18 Concentrations of compounds used in dose- response analysis

Compound	**Applied concentration**
Bortezomib	0.313, 0.625, 1.25, 2.5, 5, 10, 20, 40, 80 nM
Tunicamycin	0.02, 0.039, 0.078, 0.156, 0.313, 0.625, 1.25, 2.5, 5 µg/ml
Thapsigargin	0.004, 0.008, 0.016, 0.032, 0.064, 0.128, 0.25, 0.5 1 µM

3.14 Inhibition of the IRE1α ribonuclease domain

To inhibit the ribonuclease domain of IRE1α in cultured cells, the small molecule STF-83010 (Table 1) was used (*207*). The compound is cell-permeable and inhibits the splicing of *Xbp1* mRNA as well as the RIDD activity of the receptor. 500,000 cells per well were seeded into a 6 well plate, covered with medium, and incubated overnight. The medium in each well was exchanged to 1.5 ml medium and 20 µM STF-83010 in DMSO. After incubation for 1 h, 2 µg/ml tunicamycin were added for another 6 h. Cells were harvested in TRIzol and RNA was isolated as described under 3.8.1.

3.15 Cell cycle analyses with BrdU and 7-AAD co-staining

Proliferative activity from treated versus control cells was analyzed using bromodeoxyuridine (BrdU) incorporation to label newly synthesized DNA and 7-aminoactinomycin (7-AAD) to stain the total DNA content of a cell using the BrdU Flow Kit (Table 2). In brief, 240,000 cells were plated in a 6 well cell culture plate and incubated overnight. The medium was changed, and cells were incubated in fresh medium containing 2 µg/ml of tunicamycin, or 200 nM of thapsigargin, or 0.03 % (v/v) DMSO. 4 h before the cells were harvested, 15,7 µM of BrdU (= 4.69 µg/ml) were spiked in and the cells were incubated until harvest. The supernatant was collected, and the cells were detached with trypsin and pooled to the supernatant. Afterwards the cells were fixed and stained according to the manufacturer's instructions. Flow cytometry measurements were performed using the FACSCanto (Table 5) at the Department of Transplantation Diagnostics and Cell Therapeutics (ITZ). Compensation controls were included in each experiment. 10,000 events were collected. For data analysis, the FlowJo software (Table 7) was used. Gates were set for 1 N (= G0-G1 cells), 2 N (= G2-M cells), and events with BrdU signal (S-phase). Obtained cellular distributions in percent were normalized to the sum of all gated events and presented as means ± SEM in a staged bar plot.

4. RESULTS

4.1 THE UNFOLDED PROTEIN RESPONSE IS TREATMENT- AND CELL-TYPE SPECIFIC

As described in the introduction, the unfolded protein response (UPR) is highly cell type- and stimulus-specific. This is in a way surprising because the signaling itself is activated by the accumulation of unfolded proteins independent of the cause of the unfolding. Hence, the UPR signaling may incorporate additional regulatory parts and proteins that sense the source of misfolded proteins and fine tune the response to the cellular needs at a given cellular stage. To better understand the phenomenon, which also other groups have addressed before (e.g.: (*84*)), a collaborative multidisciplinary project was established to fully cover the cellular response of a chemically induced unfolded protein response in glioma cells. The consortium was entitled 'System biology of the unfolded protein response' (SUPR-G) and funded for three years by the German Ministry for Education and Research (BMBF). It included research groups which provided expertise in various "omics" methods. Thereby, it was possible to characterize the UPR at the transcriptome level by total RNA sequencing, at the translatom level by sequencing of RNA bound to translating ribosomes, as well as at the proteome level. We also employed targeted proteomics to accurately quantify the major UPR components. However, not every high-throughput approach is feasible at all time points of the signaling. Since the UPR signaling involves different biological level of gene expression regulation, e.g. mRNA, transcription, translational regulation, translation, and post-translational modifications, as well as protein-protein interactions. The own contribution to the consortium was to establish treatment durations and to find concentrations of two known UPR inducers, tunicamycin and thapsigargin, to be used for the different subsequent omics analyses by the consortial partner groups.

4.1.1 The cellular outcome of an activated UPR

To gain insights into the cellular response to unfolded proteins, the global cellular outcome of the signaling was investigated in the mouse fibroblast-derived cell line NIH/3T3. First, nine different concentrations of tunicamycin or thapsigargin ranging from 0.02 – 5 µg/ml or 0.004 – 1 µM, respectively, were applied and the effect on cell viability was measured via the MTT method (3.13). The results shown in Figure 5a display the dose-response curve of NIH/3T3 cells to 0.02 - 5 µg/ml of tunicamycin for 24 h. The cells responded with a nearly linear decrease in absorbance from 0.02 – 0.31 µg/ml of tunicamycin and reached 50 % absorbance with 0.39 µg/ml of tunicamycin treatment. From 0.625 to 5 µg/ml of tunicamycin NIH/3T3 cells showed no

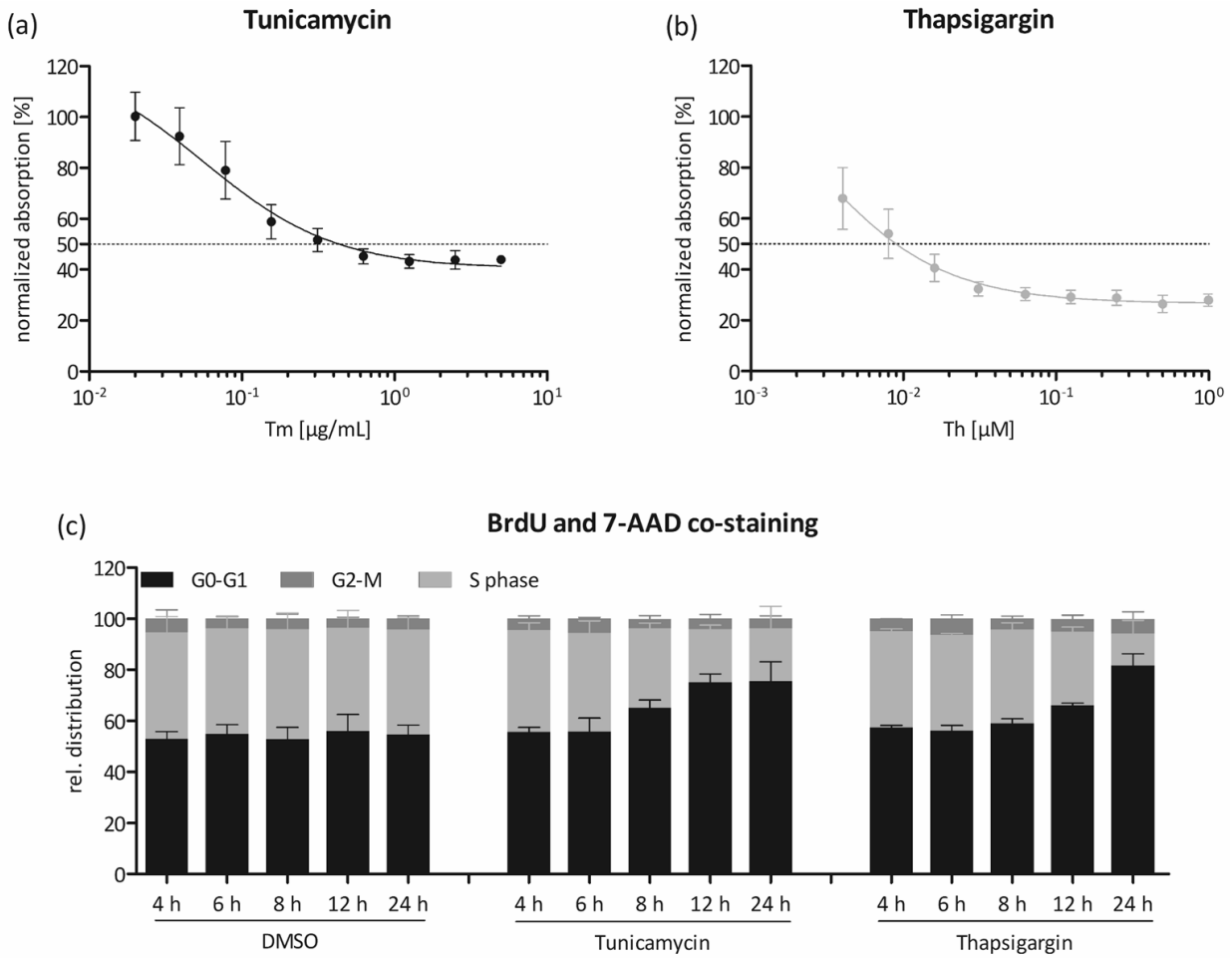

Figure 5- Cellular outcome of the UPR signaling in NIH/3T3 cells. (a) and (b), dose- response curves of tunicamycin (0.02-5 µg/ml) and thapsigargin (0.004-1 µM), respectively. The cellular response was measured with the MTT assay and normalized to DMSO-treated control cells before plotting and curve fitting. The dashed line marks 50 % absorption. (c), BrdU/7AAD co-staining flow cytometry analysis representing the cell cycle distribution of cells under tunicamycin (2 µg/ml) and thapsigargin (200 nM) treatment for the indicated time points. Data is presented as mean ± SEM. Abbreviations: BrdU, bromodeoxyuridine; M, mitosis; S, synthesis; Tm, Tunicamycin; Th, Thapsigargin.

substantial further absorbance decrease. A similar analysis with thapsigargin is shown in Figure 5b. The normalized absorbance of thapsigargin treated cells decreased to 30 % with 63 nM of thapsigargin treatment. Absorbance then maintained a similar level up to 1 µM thapsigargin. NIH/3T3 cells treated with thapsigargin reached 50 % normalized absorption at a concentration of 10 nM thapsigargin.

Cell cycle analysis performed by co-staining of BrdU and 7-AAD in NIH/3T3 cells treated with DMSO (0.12 % (v/v)), tunicamycin (2 µg/ml), or thapsigargin (200 nM) for distinct time points showed a time-dependent accumulation of cells in G0-G1 phase of the cell cycle upon tunicamycin or thapsigargin treatment (Figure 5c). Thapsigargin treatment resulted in a higher fraction of cells in G0-G1 arrest than tunicamycin treatment after 24 h. There was no change in the fraction of G2-M phase cells, and control treatment with DMSO did not interfere with the cell cycle but illustrated that most cells are in G0-G1 phase of the cell cycle. Hence, the cellular outcome of an activated UPR

is a concentration-dependent decrease of cell viability and an accumulation of cells in G1-G0 phase of the cell cycle upon treatment with proteostasis perturbating compounds.

4.1.2 UPR markers in NIH/3T3 cells

For analyses of the UPR and the expression of the markers Xbp1 and pEIF2α as well as the expression of the two UPR receptors IRE1α and PERK, NIH/3T3 cells were treated with tunicamycin or thapsigargin. Analyses of these markers provided more in-depth information about the timing of the UPR signaling. qRT-PCR analysis of RNA extracted from NIH/3T3 cells treated with 2 µg/ml of tunicamycin or 200 nM of thapsigargin for distinct time points (see Figure 6) allowed for a relative quantification of the IRE1α-RNase target mRNA *Xbp1*. Figure 6-a shows the abundance of *Xbp1s* transcripts in tunicamycin-treated cells relative to the expression in

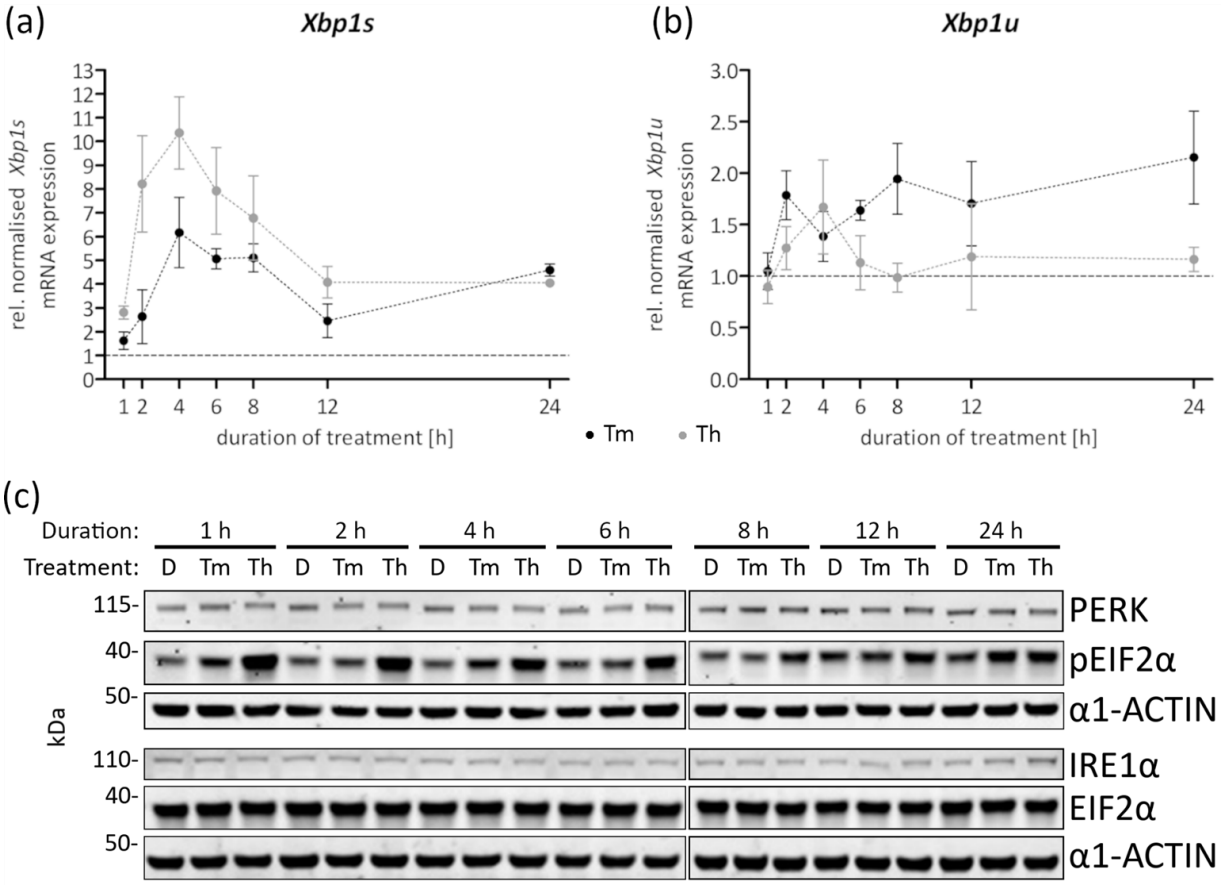

Figure 6- Major UPR marker expression during 24 h of tunicamycin or thapsigargin treatment of NIH/3T3 cells. (a) and (b), qRT-PCR analysis of *Xbp1* spliced and unspliced, respectively, after 2 µg/ml of tunicamycin or 200 nM of thapsigargin treatment. Expression data were normalized to DMSO-treated control cells for the individual treatment durations, the dashed line at y = 1 indicates normalization. The dotted line, connecting the different time points, serves a descriptive purpose only. (c), Western Blot analysis of protein lysates from NIH/3T3 cells treated with DMSO, tunicamycin, or thapsigargin for the indicated duration with antibodies against the stated proteins. α1-ACTIN served as loading control. Data are presented as mean ± SEM. Abbreviations: D, DMSO; rel., relative; s, spliced; Tm, Tunicamycin; Th, Thapsigargin; u, unspliced.

DMSO-treated control cells for the indicated time points. *Xbp1s* expression increased during both treatments with a peak expression of the investigated mRNAs after 4 hours of treatment. Tunicamycin-treated cells showed a 6-fold higher and thapsigargin-treated cells a 10-fold higher *Xbp1s* level than DMSO-treated control cells. Treatment with thapsigargin increased *Xbp1s* to a higher extent than tunicamycin, which, however, maintained a similar *Xbp1s* fold-change after 6 to 8 hours treatment. Thapsigargin exposure led to a plateau phase with no substantial decrease or increase of the *Xbp1s* level between 12 and 24 h. Tunicamycin increased the *Xbp1s* level in the same timespan from 2-fold to 5-fold. At the end of the treatment period (24 h), both drugs increased *Xbp1s* to a comparable level. To gain a complete picture of the IRE1α activity, expression of the unspliced *Xbp1* mRNA *Xbp1u* was measured as well. Figure 6-b shows data as in (a) but with *Xbp1u* as the measured transcript. Tunicamycin-treated cells showed higher *Xbp1u* levels than thapsigargin treated cells. Tunicamycin treatment showed the highest average fold-change after 24 h whereas thapsigargin-treated cells had a peak level after 4 h. Intriguingly, tunicamycin treatment for 4 h showed peak *Xbp1s* level (Figure 6-a), in line with a temporary decrease in *Xbp1u* mRNA abundance (b). After this drop in *Xbp1u*, the fold-change increased to a steady-state level. In thapsigargin treated cells the *Xbp1u* transcription decreased after 4 h to control level and no substantial increase after 24 h was observed.

Western blot analyses of tunicamycin- or thapsigargin-treated NIH/3T3 cells for the same treatment duration as for the qRT-PCR analyses were done for PERK, pEIF2α, EIF2α, and IRE1α (Figure 6-c). Both receptor serine/threonine kinases of the UPR signaling, IRE1α and PERK, did not differ in expression throughout the analyzed time points. A robust read-out for PERK activity is the phosphorylation of EIF2α at S51, which blocks CAP-dependent translation (*208*). After 1 h of thapsigargin treatment the pEIF2α band intensity was noticeably higher than in DMSO-treated control cells and decreased until the 8 h time point. From 8 h – 24 h the band intensity of pEIF2α was not as higher as clearly as compared to DMSO-treated cells before, but it remained stably increased compared to DMSO-treated cells. The pEIF2α band intensity pattern of tunicamycin treated NIH/3T3 cells was different than for thapsigargin treated cells. With tunicamycin treatment, the intensity slowly increased to reach the same intensity as in thapsigargin treated cells after 24 h. During the experiment, there was no visible change in total EIF2α.

Overall, the UPR marker analysis in NIH/3T3 cells revealed a faster and at the beginning more intense response to thapsigargin than to tunicamycin. Tunicamycin treatment, however, had a similar outcome as thapsigargin treatment, but with different kinetics. Interestingly, the treatments differ in the transcription of *Xbp1u* and it only fairly correlates with the abundance of *Xbp1s* (Figure 6-a and -b).

4.1.3 Determination of treatment durations for subsequent high-throughput analyses

With the experiments described above, insights were gained into the UPR and the behavior of cells exposed to tunicamycin and thapsigargin. The following experiments were intended to determine the optimal treatment duration for the different high-throughput analyses planned to be performed after UPR induction. Therefore, qRT-PCR and Western Blot analyses of the ER-resident chaperone BIP (Grp78/GRP78) were carried out in murine NIH/3T3 fibroblasts and LN-308 glioma cells, following tunicamycin and thapsigargin treatment of different time periods. The qRT-PCR and Western Blot analyses of LN-308 were performed in collaboration with Himanshu Soni at the German Cancer Research Center (DKFZ) in Heidelberg.

Figure 7-a shows qRT-PCR results from the same cDNAs analyzed before for *Xbp1s* and *Xbp1u* expression (Figure 6-a, b). Both, tunicamycin and thapsigargin treatment increased the *Grp78* mRNA levels to 25-fold after 6 h or 30-fold after 12 h, respectively. Treatment with tunicamycin resulted in a steady-state mRNA level of the *Grp78* transcript after 6 h treatment between 20 - 25-fold compared to DMSO-treated NIH/3T3 control cells until 24 h. Thapsigargin treatment increased the *Grp78* mRNA level not as substantially as tunicamycin treatment does. There were plateau phases in *Grp78* expression from 2 h – 4 h and 6 h – 8 h treatment that were not observed with tunicamycin treatment.

The analysis of LN-308 cells after treatment with 2.5 µg/ml of tunicamycin or 200 nM of thapsigargin for the distinct time points indicated in Figure 7-b, revealed a similar expression pattern of *GRP78* mRNA under both treatments. The treatments led to a peak fold-change of 15-fold after 12 h. The increase in transcript levels was linear up to 6 h, followed by a plateau phase from 6 h – 8 h under tunicamycin treatment only. *GRP78* mRNA level increased to its peak fold-change and decreased between 12 h – 24 h to 10-fold (thapsigargin) and 5-fold (tunicamycin) compared to DMSO-treated LN-308 control cells.

Western Blot analysis of NIH/3T3 cells using a BIP-specific antibody (Figure 7-c) was performed using the same membranes as in Figure 6-c. This cell line showed no detectable endogenous BIP expression, however, BIP expression increased to a detectable level within 6 h of treatment with tunicamycin or thapsigargin. Both treatments increased the chaperone BIP up to the 24 h time point. LN-308 cells showed, in comparison to NIH/3T3 cells, a high endogenous protein level of BIP. In these cells, the BIP level started to increase after 6 h of treatment as well. Both treatments, as for NIH/3T3 cells, increased BIP protein expression.

Overall, these expression analyses revealed that the mRNA levels of BIP, an important UPR effector gene (*209*), showed the highest fold-change from 2 h to 6 h treatment with the UPR inducers tunicamycin or thapsigargin. The protein levels of BIP, however, started to increase only after 6 h treatment. Based on these results, the following treatment time points were used for the different types of subsequent omics analyses: RNA-based high-throughput approaches (transcriptomics and translatomics): treatment durations of 2 h, 4 h, and 6 h; proteomics-based approaches: treatment durations of 6 h, 16 h, and 24 h.

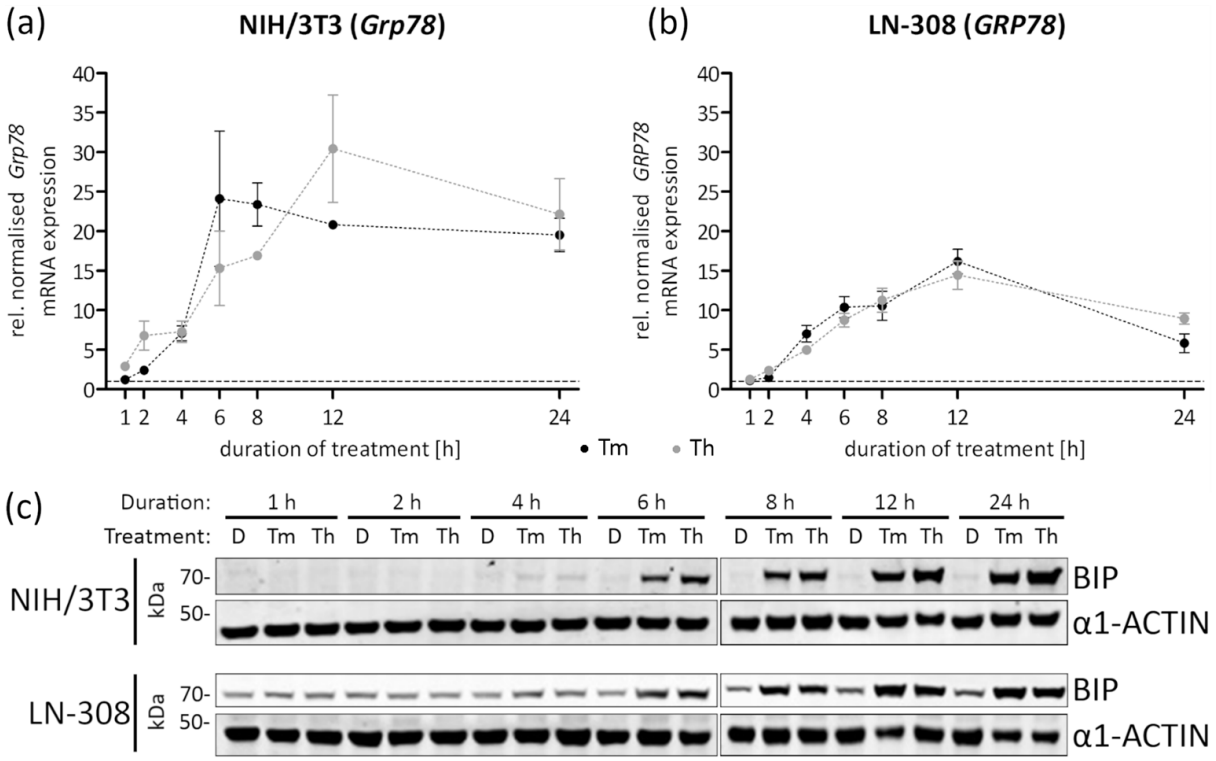

Figure 7- Analyses of *Grp78*/*GRP78* mRNA expression in NIH/3T3 and LN-308 cells following treatment with tunicamycin or thapsigargin for different time periods. (a), qRT-PCR analysis of *Grp78* expression using the same cDNA as in Figure 6. (b), qRT-PCR analysis of *GRP78* expression in LN-308 gliomas cells treated with 2.5 µg/ml of tunicamycin or 200 nM of thapsigargin for the indicated time points. Data were normalized to DMSO-treated control cells for the individual treatment durations, the dashed line at y = 1 indicates normalization. The dotted line, connecting the different time points, serves a descriptive purpose only. (c), Western Blot analysis of the same membrane as in Figure 6 hybridized with a BIP specific antibody in comparison to Western Blots from lysates obtained from LN-308 treated with 2.5 µg/ml of tunicamycin and 200 nM of thapsigargin for the indicated time points. Data are presented as mean ± SEM. Abbreviations: D, DMSO; rel., relative; s, spliced; Tm, Tunicamycin; Th, Thapsigargin; u, unspliced.

4.1.4 UPR marker analyses in LN-308 glioma cells

The glioma cell line LN-308 was used for the high-throughput analyses within the SUPR-G consortium. In parallel to these measurements and to further analyze the applied time points, we analyzed the major UPR markers in LN-308 cells treated with tunicamycin and thapsigargin using Western Blot and qRT-PCR analyses.

Western Blot analysis of lysates from LN-308 cells as shown in Figure 7 were treated with 2.5 µg/ml of tunicamycin and 200 nM of thapsigargin for the durations indicated in Figure 8-a and analyzed for several other UPR markers, including the major UPR receptors IRE1α and PERK, as well as two major transcription factors, XBP1s and ATF4, and the major translational switch pEIF2α. IRE1α protein levels increased starting from 8 h tunicamycin or thapsigargin treatment

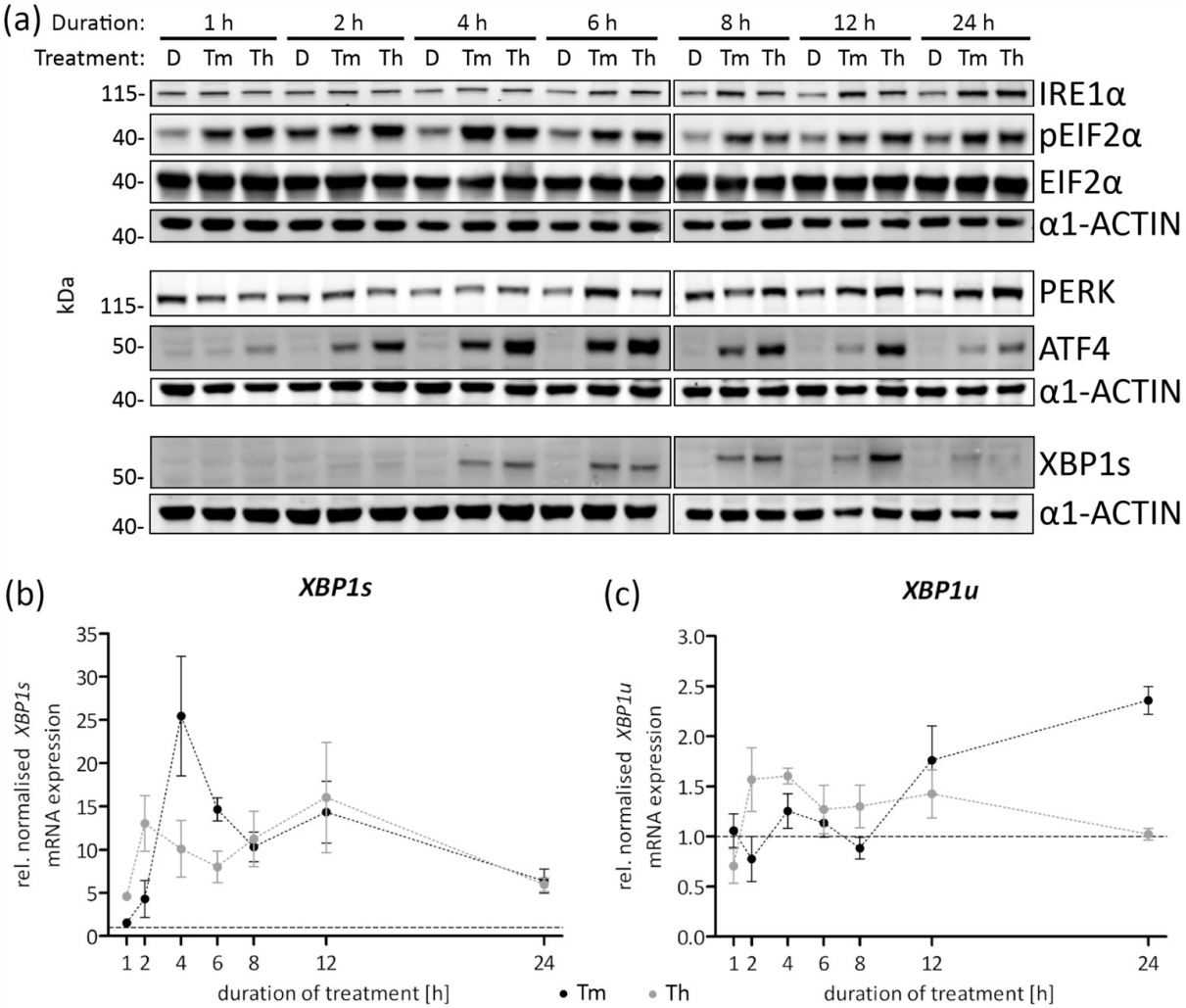

Figure 8- Protein and mRNA expression analyses of important UPR-regulators in LN-308 glioma derived cells. (a) Western Blot analyses of LN-308 cells as in Figure 7 against the indicated proteins. (b) and (c), qRT-PCR analysis of *XBP1s* and *XBP1u* expression in LN-308 cells treated with 2.5 µg/ml of tunicamycin or 200 nM of thapsigargin for the indicated time points. Data were normalized to DMSO-treated control cells for the individual treatment durations as indicated by the dashed line at y = 1. The dotted line, connecting the different time points, serves a descriptive purpose. Data is presented as mean ± SEM. Abbreviations: D, DMSO; rel., relative; s, spliced; Tm, Tunicamycin; Th, Thapsigargin; u, unspliced.

to 24 h treatment. Both treatments resulted in a similar IRE1α band intensity at the end of the investigated time period (Figure 8-a). Thapsigargin or tunicamycin treatment of LN-308 cells increased the PERK protein level after 12 h and 24 h (Figure 8-a). The major kinase substrate upon activation of PERK is EIF2α. The pEIF2α band intensity increased after 1 h treatment with thapsigargin while tunicamycin treatment of LN-308 cells increased pEIF2α expression after 4 h of treatment (Figure 8-a). Treatment with either compound showed the highest induction of pEIF2α after 4 h of exposure. The pEIF2α expression decreased from 4 h to 6 h treatment similarly between the two compounds but stayed higher than the endogenous or background phosphorylation level in DMSO-treated LN-308 control cells for the complete time period analyzed. Total EIF2α protein levels were not influenced by treatment duration nor applied compound (Figure 8-a).

As shown in Figure 8-a, expression of ATF4, a downstream transcription factor of the PERK branch, was increased in tunicamycin-treated LN-308 cells after 2 h of treatment. The ATF4 levels upon treatment with both drugs increased in intensity and reached a peak expression level at 6 h treatment (Figure 8-a), 2 h after CAP-dependent translation was most strongly blocked (phosphorylation of EIF2α is the main switch for CAP-dependent and -independent translation).

The single transcription factor of the IRE1α branch, XBP1, is translated from the spliced *XBP1* mRNA starting after 4 h of tunicamycin or thapsigargin treatment. XBP1s band intensity was steadily higher than in DMSO-treated control cells until the 12 h time point in and fainted after 24 h treatment with either tunicamycin or thapsigargin (Figure 8-a).

Analysis of the *XBP1s* transcript levels in the same cDNA samples as used in Figure 7 showed a marked increase of the transcript in LN-308 cells starting after 2 h of tunicamycin treatment and remaining at an elevated level after 24 h of tunicamycin treatment (Figure 8-b). Similarly, thapsigargin treatment increased the *XBP1s* transcript after 2 h to 13-fold followed by an approximately 8-fold increase over the course of 2 h to 6 h of treatment. Expression of the *XBP1u* transcript in tunicamycin-treated cells fluctuated from 1 h to 8 h of treatment and increased afterwards (Figure 8-c). In comparison, thapsigargin treatment increased *XBP1u* transcription to 1.5-fold after 2 h and 4 h, from where the *XBP1u* transcription level decreased to the transcript levels detected in DMSO-treated control cells after 24 h.

In summary, tunicamycin and thapsigargin treatment increase expression of all major UPR markers investigated in LN-308 cells and additionally resulted in higher expression levels of the two analyzed UPR receptors. These data thus provide a comprehensive analysis of the UPR response in NIH/3T3 and LN-308 following UPR-inducing pharmacological treatments. Certain differences in the response of the two cell lines, NIH/3T3 and LN-308, to tunicamycin and

thapsigargin became evident, including differences in BIP (*Grp78*/*GRP78*) transcription and translation profiles, as well as the mRNA abundance increase of *Xbp1s*/*XBP1s* or *Xbp1u*/*XBP1u* upon treatment with tunicamycin or thapsigargin. Surprisingly, the *Xbp1u* transcripts of both cell lines and treatments displayed a very similar expression pattern.

4.1.5 Timepoints for high throughput experiments

Based on the data reported above, it was concluded that the cells used for RNAseq and ribosomal foot printing have to be treated for 2, 4, and 6 hours with either tunicamycin or thapsigargin. Cells treated under these conditions were subjected to next generation sequencing at the Core Facility of the European Molecular Biology Laboratory, Heidelberg, and data were analyzed there by the bioinformatician Dr. Grischa Tödt. A shotgun proteomic approach was performed with cells treated for 6, 16, and 24 hours with tunicamycin or thapsigargin. Treated and control cells were analyzed by the mass spectrometry in the laboratory of Dr. Robert Ahrends at the *Leibniz-Institut für Analytische Wissenschaften*, Dortmund. RNA and proteome data were bioinformatically integrated by the cooperation partners in Heidelberg and Dortmund. A recent joint publication (*210*) reported on the results obtained by using a novel targeted proteomic approach to quantify expression of proteins linked to the UPR in LN-308 glioma cells. Specifically, the paper demonstrated for the first time that the novel proteomic approach was able to detect and quantify all major UPR-regulators and showcased this in an experiment using UPR perturbation in LN-308 glioma cells.

4.2 p53 INFLUENCES *XBP1* SPLICING BY DOWNREGULATION OF DNAJB9

The *Xbp1* mRNA is unconventionally spliced by the activated and dimerized UPR receptor IRE1α incorporated in the ER membrane (1.2.1, (*211*)). In p53 knock-out cells, this splicing was reported to be increased (1.2.6, (*185*)). Gliomas frequently carry mutations in *TP53* and these tumors are facing ER stress induced by their environment as well as by endogenous sources (1.1.1, 1.1.3 and citations therein). Therefore, it was interesting to evaluate the role of p53 in the IRE1α branch of the UPR.

To do so, NSC/NPCs were prepared from *Tp53*$^{wt/wt}$ and *Tp53*$^{\Delta 2\text{-}10/\Delta 2\text{-}10}$ mice upon exposure to the Cre recombinase as described above (3.11). In addition, NSC/NPCs derived from four different conditional knock-out mice were exposed to 4OHT to then have the original four murine

NSC/NPCs that are still *Tp53*$^{wt/wt}$ and four murine NSC/NPCs from the same animals with *Tp53*$^{\Delta 2\text{-}10/\Delta 2\text{-}10}$ genotype after exposure to 4OHT.

4.2.1 Viability under ER stress is independent of p53

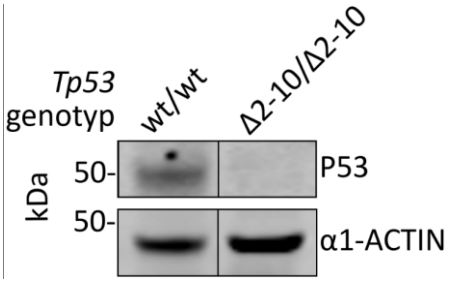

Figure 9- Validation of p53 knock-out NSC/NPCs. Western Blot analyses of whole cell lysates of NCS/NPCs with *Tp53*$^{wt/wt}$ or *Tp53*$^{\Delta 2\text{-}10/\Delta 2\text{-}10}$ using antibodies against p53, and α1-ACTIN as housekeeping control.

To obtain p53 knock-out NSC/NPCs, mouse neural stem and progenitor cells from one wildtype and one p53 loxP neonatal mouse brain. By infecting the isolated NSC/NPCs with pMX-Cre retroviral plasmids, the resulting genotype regarding p53 in control NSC/NPCs was *Tp53*$^{wt/wt}$ while a *Tp53*$^{\Delta 2\text{-}10/\Delta 2\text{-}10}$ was induced in the p53 loxP NSC/NPCs. As shown by Western blot (Figure 9), there was no detectable expression of p53 in the *Tp53*$^{\Delta 2\text{-}10/\Delta 2\text{-}10}$ NSC/NPCs, whereas the wildtype showed p53 expression, indicating that p53 knock-out NSC/NPCs were generated. These cells are referred to as "model 1".

Since p53 is a potent apoptosis-inducer upon DNA damage, dose-response curves with tunicamycin or thapsigargin were performed to investigate an involvement of p53 in ER stress-induced apoptosis. *Tp53*$^{\Delta 2\text{-}10/\Delta 2\text{-}10}$ NSC/NPCs did not display altered reactions in dose-response curves during proteostasis perturbation when compared to *Tp53*$^{wt/wt}$ NSC/NPCs (Figure 10). IC50 values of 0.06 µg/ml and 0.05 µg/ml tunicamycin for *Tp53*$^{wt/wt}$ or *Tp53*$^{\Delta 2\text{-}10/\Delta 2\text{-}10}$ NSC/NPCs, were

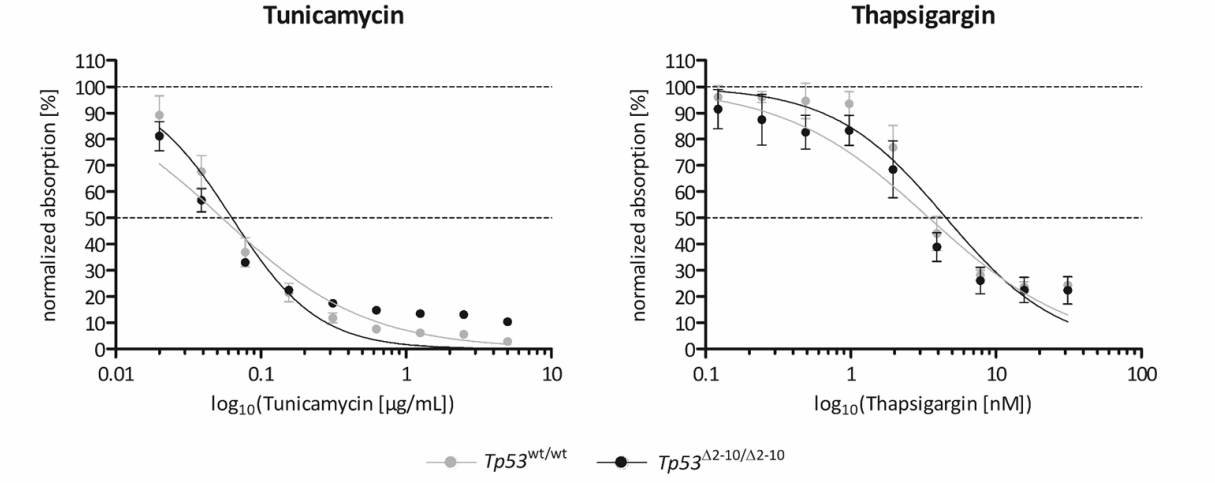

Figure 10- *Tp53*$^{wt/wt}$ and *Tp53*$^{\Delta 2\text{-}10/\Delta 2\text{-}10}$ NCS/NPCs (model 1) show similar viability under tunicamycin or thapsigargin treatment for 24 h. The dose/response curves were obtained with the MTT assay of NSC/NPCs with or without *Tp53* following treatment with tunicamycin (left;(0.02-5 µg/ml) or thapsigargin (right; 0.004-1 µM) for 24 h. Absorbance was normalized to DMSO-treated control cells and a non-linear regression curve was fitted to the data. Data are presented as mean ± SEM.

calculated. For thapsigargin, the IC50 was reached for *Tp53*$^{wt/wt}$ at 0.12 nM and for *Tp53*$^{\Delta 2\text{-}10/\Delta 2\text{-}10}$ at 0.11 nM.

For further experiments, tunicamycin was used to induce the UPR because it inhibits glycosylating enzymes such as GlcNAc phosphotransferase (GPT) and thereby resembles the *in vivo* tumor situation of low glucose availability. It is, hence, more specific towards protein-folding stress than thapsigargin, which blocks the Ca^{2+} sarco/endoplasmic reticulum Ca^{2+} ATPase (SERCA).

4.2.2 Splicing of *Xbp1* is increased in *Tp53*$^{\Delta 2\text{-}10/\Delta 2\text{-}10}$ NSC/NPCs

To validate the reported influence of p53 on *Xbp1* splicing (*185*), a time series from 1 h to 8 h was performed with *Tp53*$^{wt/wt}$ or *Tp53*$^{\Delta 2\text{-}10/\Delta 2\text{-}10}$ NSC/NPCs (model 1) treated with 2 µg/ml of tunicamycin or with DMSO as a control. To compare not only passage replicates of the same cells, as for model 1 cells, but also biological replicates, meaning, cells with *Tp53*$^{wt/wt}$ or *Tp53*$^{\Delta 2\text{-}10/\Delta 2\text{-}10}$ genotype from different mice, termed "model 2". These biological replicates (model 2) were generated by exposure of the NSC/NPCs from floxed *Tp53*$^{wt/wt}$ expressing Cre^{ERT} to 4-OHT as described (3.11). This allowed for the comparison of NSC/NPCs that differed only in their *Tp53* status and their exposure to 4-OHT[2]. By qRT-PCR specific for *Xbp1s* cDNA (Table 10) a mean 10.2-fold and 17.0-fold induction of *Xbp1s* by tunicamycin was measured in model 1 *Tp53*$^{wt/wt}$ and *Tp53*$^{\Delta 2\text{-}10/\Delta 2\text{-}10}$ NSC/NPCs, respectively (Figure 11-a). The difference between the two genotypes was statistically significant in a two-way ANOVA ($p<0.0001$) with Bonferroni correction and was maintained after 8 h (FC(WT) = 8.4; FC(KO) = 16.3) of tunicamycin treatment. After 2 h (FC(WT) = 1.5; FC(KO) = 2.9) and 4 h (FC(WT) = 5.7; FC(KO) = 9.1) of treatment, the fold-change difference between the two genotypes was not statistically significant. However, both NSC/NPC groups showed an increased expression of *Xbp1s* transcripts. In addition to *Xbp1s*, the expression of its precursor *Xbp1u* was significantly different after 8 h of tunicamycin treatment in model 2 (Figure 11-c). In both p53-genotypes, the *Xbp1u* level after 1 h of tunicamycin was lower than in DMSO-treated control cells (FC(WT) = 0.8; FC(KO) = 0.8). The *Tp53*$^{wt/wt}$ NSC/NPCs of model 1 increased *Xbp1u* transcripts over DMSO level after 4 h and 6 h of treatment but did not do so after 8 h of treatment. In contrast, in tunicamycin treated *Tp53*$^{\Delta 2\text{-}10/\Delta 2\text{-}10}$ cells *Xbp1u* increased up to 2.5-fold relative to DMSO-treated control cells over the course of the treatment.

NCS/NPCs of model 2 (biological replicates; Figure 11-b) also increased *Xbp1s* transcripts, but did not show an as striking difference between the p53-genotypes as model 1. Model 2 only showed

[2] The *Tp53*$^{wt/wt}$ NSC/NPC from model 2 were not treated with 4OHT since they then would have become knockouts.

a statistically significant difference in *Xbp1s* transcript levels after 6 h of tunicamycin treatment (FC(WT) = 7.4; FC(KO) = 9.6). Induction of the UPR in model 2, did not result in a different *Xbp1u* level between the p53-genotypes (Figure 11-d). model 2 cells showed a lower *Xbp1u* level after 1 h of tunicamycin treatment than DMSO-treated cells but both p53-genotypes increased the transcript to 2.1-fold (*Tp53*$^{wt/wt}$) or 2.5-fold (*Tp53*$^{\Delta 2\text{-}10/\Delta 2\text{-}10}$). Hence, the results from model 1 were not detected in model 2 of floxed *Tp53*$^{wt/wt}$ expressing Cre^{ERT} NSC/NPCs independently treated with 4-OHT.

To gain a more comprehensive picture of the data observed in the different models, the RQ values (explained in chapter 3.8.5) for *Xbp1s* and *Xbp1u* from DMSO-and tunicamycin-treated cells after 8 h treatment were plotted. RQ values of *Xbp1s* in model 1 *Tp53*$^{\Delta 2\text{-}10/\Delta 2\text{-}10}$ NSC/NPCs was lower in DMSO-treated control model 1 cells than in *Tp53*$^{wt/wt}$ NSC/NPCs (Figure 11-e). Therefore, the observed increase in *Xbp1s* of model 1 cells with *Tp53*$^{\Delta 2\text{-}10/\Delta 2\text{-}10}$ (Figure 11-a) was based on a RQ lower than the RQ in *Tp53*$^{wt/wt}$ cells with DMSO treatment. After 8 h, both p53-genotypes showed a similar RQ for *Xbp1s*, hence the fold change in the *Tp53*$^{\Delta 2\text{-}10/\Delta 2\text{-}10}$ cells of model 1 were higher than in the controls, because the knock-out cells had a lower endogenous level of *Xbp1s*. Similarly, the RQ of *Xbp1u* was also lower in DMSO-treated model 1 cells without p53 than in model 1 cells with p53. The *Tp53*$^{wt/wt}$ cells of model 1 did not increase the transcript after 8 h of tunicamycin treatment. *Xbp1u* increased in the *Tp53*$^{\Delta 2\text{-}10/\Delta 2\text{-}10}$ of model 1 to a higher RQ than in the DMSO-treated cells. The expression levels of the two analyzed transcripts (*Xbp1s* and *Xbp1u*) did not differ between wildtype and knock-out p53 NSC/NPCs in model 2 neither with nor without tunicamycin treatment. Hence, *Xbp1s* transcription level differences in model 1 of p53 knock-out NSC/NPCs were not observed in model 2.

The single observation of a higher fold-change of *Xbp1s* in p53 knock-out model 1 NSC/NPCs was further investigated. Nevertheless, it is intriguing that cells with a lower endogenous *Xbp1s* level were able to reach the same transcript amounts after 8 h of treatment. Namba and co-workers (*185*) postulated that the IRE1α receptor is less stable in p53-deficient cells, which in turn would be responsible for the observed phenotype. Hence, my own investigations were continued by examining the receptor in cells of model 1, since the p53 knock-out NSC/NPCs reached a similar *Xbp1s* level as p53 wildtype NSC/NPCs despite having a lower *Xbp1u* abundance to begin with.

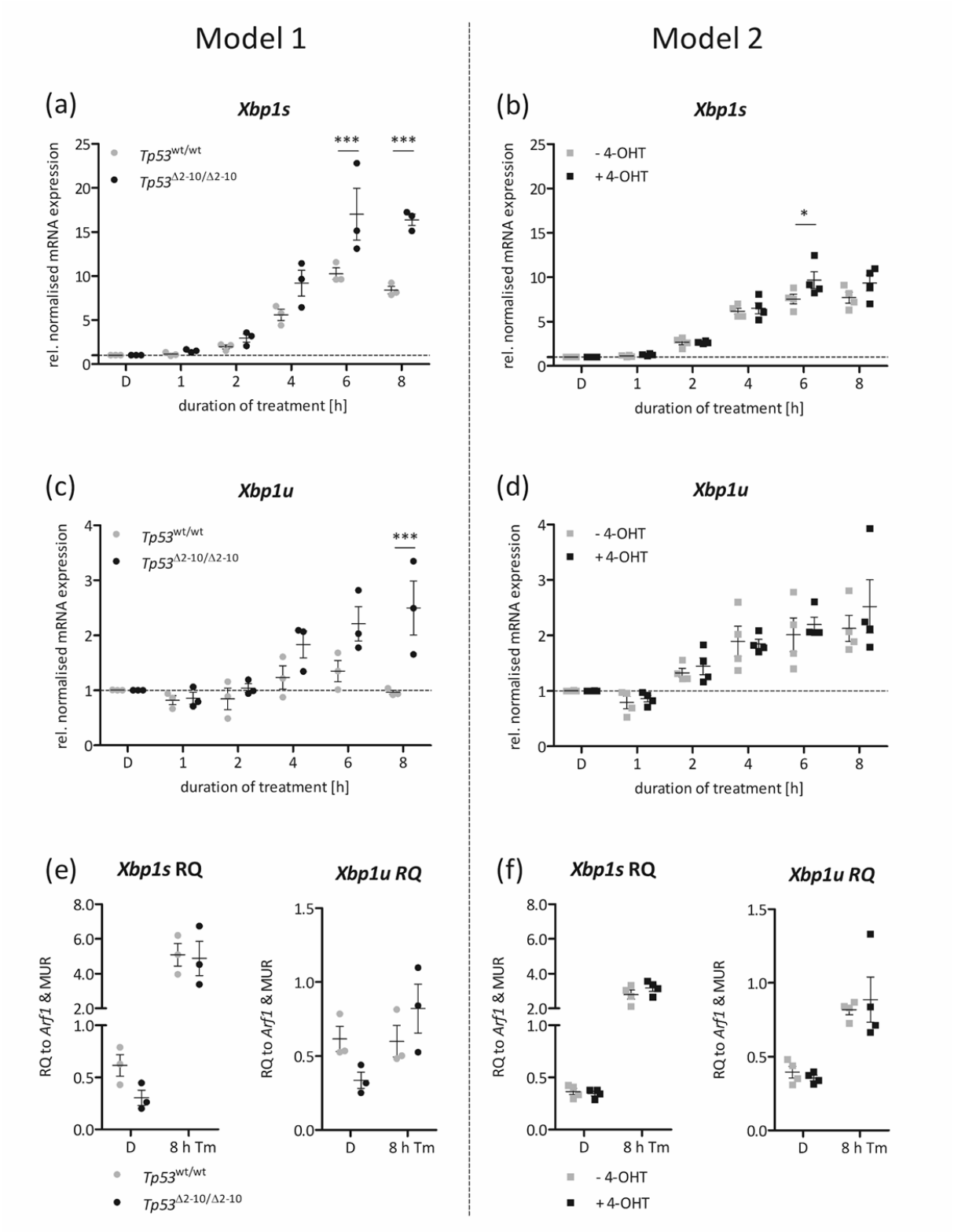

Figure 11- *Xbp1s* and *Xbp1u* mRNA levels differed between *Tp53*$^{wt/wt}$ and *Tp53*$^{\Delta 2\text{-}10/\Delta 2\text{-}10}$ NSC/NPCs. qRT-PCR of NSC/NPCs with the respective genotypes in passage (a, c, and e; model 1) and biological replicates (b, d, and f; model 2), treated for the indicated time points with 2 µg/mL of tunicamycin. Model 1 refers to NSC/NPCs transfected with pMX-cre originating from one mouse (3.11) while model 2 refers to conditional knock-out NSC/NPCs treated with 4OHT. Data are presented as fold change to DMSO-treated control NSC/NPCs, as highlighted by the dashed line at y = 1 in (a)-(d). For both targets the relative quantity (RQ; relative to *Arf1* and mouse universal reverence RNA (MUR)) in DMSO-treated cells versus cell treated for 8 h with tunicamycin in model 1 (e) and model 2 (f) are shown. Statistical significance was determined by two-way ANOVA ($p<0.0001$) with Bonferroni correction. Data are presented as scatter dot plots with indicated mean ± SEM. Abbreviations: MUR, mouse universal reference RNA; rel., relative; RQ, relative quantity; *s*, spliced; tunicamycin, tunicamycin; u, unspliced.

4.2.3 IRE1α abundance is influenced by the p53-genotype in murine NSC/NPCs

To elucidate whether the expression level of IRE1α is responsible for the increased fold change observed for *Xbp1s* expression in *Tp53*$^{\Delta 2\text{-}10/\Delta 2\text{-}10}$ relative to p53-wildtype NSC/NPCs of model 1 (4.2.2) the transcriptional level of the *Ern1* gene encoding IRE1α was determined by qRT-PCR following treatment with tunicamycin. The *Ern1* mRNA expression increased up to a 3-fold induction in *Tp53*$^{wt/wt}$ NCS/NPCs of model 1 during the treatment duration relative to control cells (Figure 12-a). In contrast, increased expression of *Ern1* transcripts was less pronounced in *Tp53*$^{\Delta 2\text{-}10/\Delta 2\text{-}10}$ NSC/NPCs of model 1 following tunicamycin treatment. The difference between the p53-genotypes was significant in a two-way ANOVA ($p<0.0001$) with Bonferroni correction after 2 h, 4 h and 8 h of tunicamycin treatment. The plotted unnormalized RQ in Figure 12-b allows the same observation.

Since only the translated *Ern1* gene product IRE1α can influence *Xbp1* mRNA splicing, IRE1α protein levels were determined in tunicamycin-treated versus control-treated p53-wildtype and p53-deficient NSC/NPCs of model 1. In control treated NSC/NPCs, no difference between the two genotypes could be determined by Western blots hybridized with antibodies specific for IRE1α, with α1-ACTIN serving as the loading control (Figure 12-c). IRE1α band intensities were normalized to the corresponding α1-ACTIN band intensities for all three passage replicates from the corresponding p53-genotypes (model 1) and plotted in Figure 12-d. There was no visible trend observable and an unpaired t-test resulted in an insignificant p-value ($p = 0.81$). During treatment with tunicamycin for up to 6 h, the IRE1α protein levels showed no obvious difference in Western blot analyses (Figure 12-e). Densitometric quantification of the band intensities from three passage replicates (Figure 12-f) only showed a slight but consistent increase of IRE1α in *Tp53*$^{\Delta 2\text{-}10/\Delta 2\text{-}10}$ NSC/NPCs while *Tp53*$^{wt/wt}$ NSC/NPCs demonstrated slight but consistent decrease of IRE1α protein expression (FC to DMSO = 0.75). This difference (FC = 1.4) was significant after 6 h of tunicamycin treatment.

In summary, despite strikingly lower mRNA levels of *Ern1* during tunicamycin treatment in p53 knock-out NSC/NPCs of model 1 the IRE1α protein levels showed a *vice versa* effect.

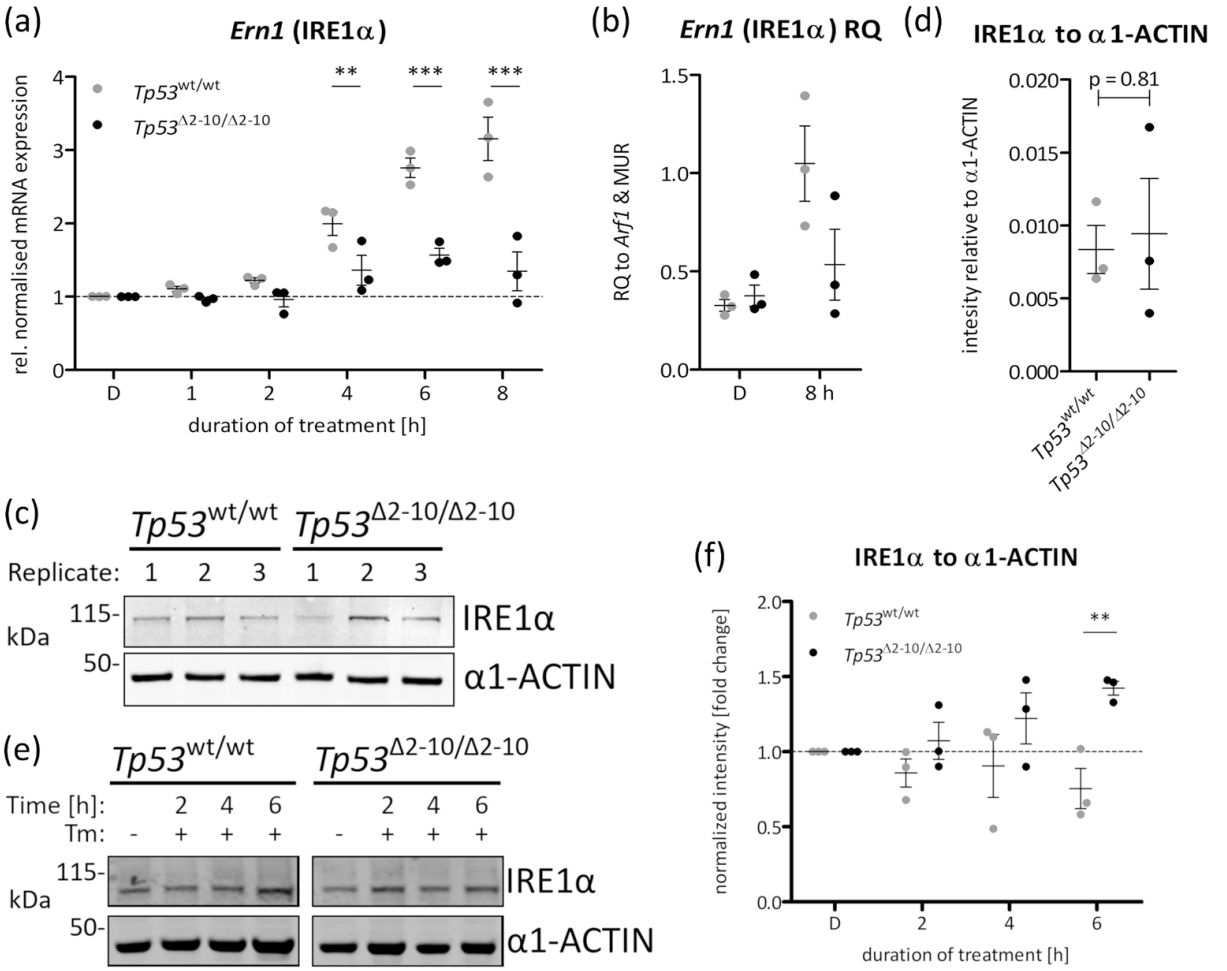

Figure 12- *Ern1* mRNA and IRE1α protein expression changes in p53-wildtype and p53-deficient murine NSC/NPCs of model 1 after tunicamycin treatment. qRT-PCR analyses for *Ern1* expression were performed with cDNA derived from *Tp53*$^{wt/wt}$ and *Tp53*$^{\Delta2\text{-}10/\Delta2\text{-}10}$ NSC/NPCs treated with 2µg/ml of tunicamycin (see also 4.2.2). Data are presented as normalized expression levels relative to DMSO-treated control cells (a) and RQ (b). (c) Western blot analysis for IRE1α in three passage replicates of NSC/NPCs of the indicated genotypes; α1-ACTIN served as loading control. (d) Band intensity measurement and normalization of IRE1α band intensity against α1-ACTIN band intensity plotted against the *Tp53* genotype. (e) Western blots as in (c) but after tunicamycin treatment for the indicated time points. (f) Band intensity quantification as in (d). Lines without tick marks at each end indicate a two-way ANOVA test ((a) $p<0.0001$; (f) $p = 0.0029$) with Bonferroni correction, lines with tick marks at each end indicate an unpaired t-test. The asterisks refer to *, $p < 0.05$; **, $p < 0.01$; ***, $p < 0.001$. Data are presented as scatter dot plots with indicated mean ± SEM. Abbreviations: MUR, mouse universal reference RNA; rel., relative; RQ, relative quantity; *s*, spliced; tunicamycin, tunicamycin; u, unspliced.

4.2.4 Inhibition of IRE1 eliminates the observed *Xbp1s* difference

To further investigate why the *Tp53*$^{\Delta2\text{-}10/\Delta2\text{-}10}$ NSC/NPCs of model 1 showed a higher *Xbp1s* fold change upon tunicamycin treatment when compared to p53-wildtype NSC/NPCs, the activity of the RNase domain of IRE1α was investigated. For this purpose, STF-08310 (STF), a selective inhibitor of the RNase but not the kinase domain of IRE1α (*207*) was used, either alone or in a combined treatment with tunicamycin, followed by qRT-PCR analysis of the *Xbp1s* mRNA levels

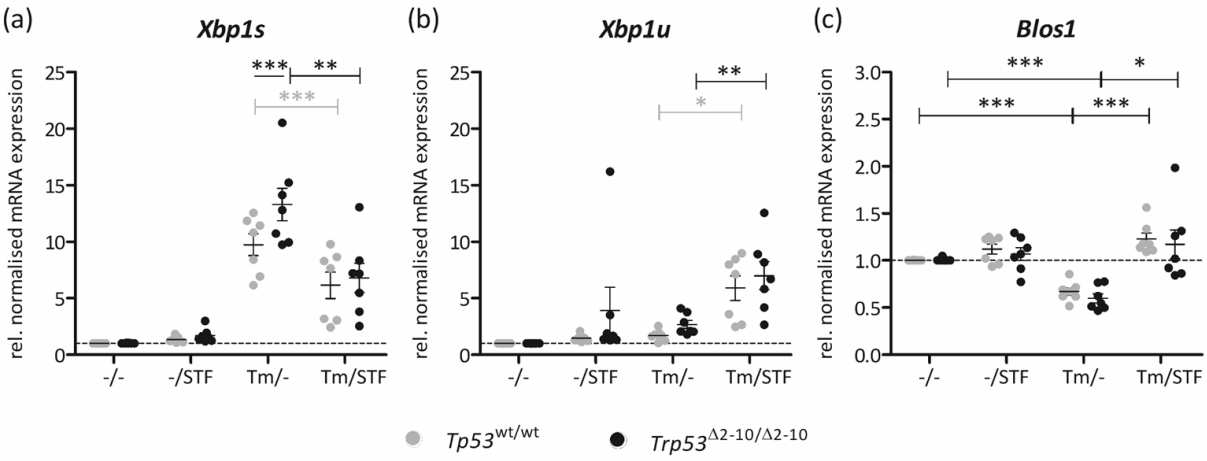

Figure 13- Inhibition of IRE1α activity leads to similar *Xbp1s* expression levels in *Tp53*$^{wt/wt}$ and *Tp53*$^{\Delta 2\text{-}10/\Delta 2\text{-}10}$ NSC/NPCs of model 1 after tunicamycin treatment. qRT-PCR analysis of (a) *Xbp1s*, (b) *Xbp1u*, and (c) *Blos1*, a RIDD-positive control in p53-wildtpye and p53-deficient NSC/NPCs treated with the IRE1α RNase inhibitor STF-08310, tunicamycin, or both. Lines without tick marks at each end indicate a two-way ANOVA ((a) p<0.0001) with Bonferroni correction, lines with tick marks at each end indicate a paired t-test. The asterisks refer to *, p < 0.05; **, p < 0.01; ***, p < 0.001. Data are presented as scatter dot plots with indicated mean ± SEM. Abbreviations: MUR, mouse universal reference RNA; rel., relative; STF, STF-08310; *Xbp1s*, spliced *Xbp1* mRNA; u, unspliced.

in treated versus control cells. STF-08310 treatment alone did not alter the *Xbp1s* mRNA abundance in model 1 NSC/NPCs, while tunicamycin increased the *Xbp1s* level 9.7-fold in *Tp53*$^{wt/wt}$ and 13.3-fold in *Tp53*$^{\Delta 2\text{-}10/\Delta 2\text{-}10}$ NSC/NPCs (Figure 13-a). This difference was significant (two-way ANOVA with Bonferroni correction (p<0.0001)), as it was in the time course experiments in Figure 11 after 6 h. Combined treatment (with tunicamycin and STF-08310) showed a significantly lower *Xbp1s* induction (paired t-test; p(WT) = 0.0004; p(KO) = 0.0015) compared to tunicamycin treated cells. In addition, there was no difference in the mean *Xbp1s* levels according to p53-genotype.

To control the *Xbp1* splicing behavior of IRE1α, expression of *Xbp1u* was also studied in model 1 NSC/NPCs subjected to the different treatments (Figure 13-b). STF-08310 treatment alone did not increase the expression of *Xbp1u* while tunicamycin treatment caused a slight, but insignificant increase of *Xbp1u* transcript levels in *Tp53*$^{\Delta 2\text{-}10/\Delta 2\text{-}10}$ NSC/NPCs (2.8-fold compared to DMSO-treated controls; Figure 13-b). In both p53-genotypes *Xbp1u* increased under combined tunicamycin and STF-08310 treatment to 5.8-fold in p53-wildtype and 6.9-fold in p53-deficient NSC/NPCs relative to control-treated cells. This increase was significant in a paired t-test (p(WT) = 0.01; p(KO) = 0.006) compared to tunicamycin treatment alone.

To assess also for the second splicing activity of IRE1α, termed RIDD (1.2.1), expression of *Blos1* mRNA was determined as a marker commonly used as indicator of RIDD activity (*86*). The *Blos1* gene encodes a protein which is a part of a complex regulating normal lysosome-related organelle biogenesis (*212*). *Blos1* mRNA is degraded by RIDD under high levels of ER stress to decrease its translation serving protective purposes (*213*). RIDD activity of IRE1α decreases its target mRNAs by about 50 % (*86*). The own experiments showed that *Blos1* mRNA expression decreases after

tunicamycin treatment of murine NSC/NPCs of model 1 to a level (0.6-fold in both genotypes) comparable to published data (Figure 13-c) (*86*). Following combination treatment with tunicamycin and STF-08310 *Blos1* transcript levels were elevated relative to control cells, comparable to the expression levels in NSC/NPCs treated with STF-08310 alone. The decrease in *Blos1* expression after tunicamycin treatment relative to control cells was significant for both genotypes (p(WT) = 0.0002; p(KO) = 0.0002). Similarly, expression deficiency between tunicamycin-treated and tunicamycin plus STF-08310-treated cells were significant (p(WT) = 0.0005; p(KO) = 0.01) in paired t-tests.

Based on these experiments, it might be hypothesized that murine *Tp53*$^{\Delta 2\text{-}10/\Delta 2\text{-}10}$ NSC/NPCs may show minor changes in IRE1α protein expression as well as altered *Xbp1* splicing activity from the IRE1α dimer.

4.2.5 DNAJB9 expression is deregulated in *Tp53*$^{\Delta 2\text{-}10/\Delta 2\text{-}10}$ NSC/NPCs

As described before (1.2.1), the BIP co-chaperone ERDJ4/DNAJB9 (*Dnajb9*) regulates IRE1α physiologically occurring dimerization and thus enzymatic activity (*79*). Own qRT-PCR analyses of tunicamycin-treated murine NSC/NPCs of p53-wildtype or knock-out genotypes revealed that *Dnajb9* mRNA is induced by tunicamycin at significantly lower levels in *Tp53*$^{\Delta 2\text{-}10/\Delta 2\text{-}10}$ NSC/NPCs compared to p53-wildtype NSC/NPCs in model 1 (Figure 14-a). This difference was significant in a two-way ANOVA ($p<0.0001$) with Bonferroni correction after 6 h and 8 h of tunicamycin treatment. After 8 hours of tunicamycin treatment the *Dnajb9* mRNA expression level in the *Tp53*$^{wt/wt}$ NSC/NPCs was elevated 10.7-fold relative to DMSO-treated controls but only 3.4-fold in the *Tp53*$^{\Delta 2\text{-}10/\Delta 2\text{-}10}$ NSC/NPCs 3.4-fold. RQ values of DMSO-treated model 1 cells showed no difference between the p53-genotypes, however, after 8 h of exposure to tunicamycin, the *Dnajb9* transcript levels increased to a lesser extend in the *Tp53*$^{\Delta 2\text{-}10/\Delta 2\text{-}10}$ than in the *Tp53*$^{wt/wt}$ NSC/NPCs (Figure 14-b). Western Blots analyses were conducted from untreated lysates of *Tp53*$^{\Delta 2\text{-}10/\Delta 2\text{-}10}$ and *Tp53*$^{wt/wt}$ NSC/NPCs of model 1 (Figure 14-c) and quantified (Figure 14-d). These analyses showed lower DNAJB9 protein expression in p53-deficent NSC/NPCs than in their p53-wildtype counterparts, however, this difference was not significant due to a high variance between the individual replicates. The expression difference became more obvious upon treatment with tunicamycin for up to 6 h (Figure 14-e). While *Tp53*$^{\Delta 2\text{-}10/\Delta 2\text{-}10}$ NSC/NPCs showed no obvious increase in DNAJB9 expression, *Tp53*$^{wt/wt}$ NSC/NPCs clearly upregulated DNAJB9 expression after tunicamycin treatment. These analyses were quantified and indicated that the mean DNAJB9 protein expression was higher in *Tp53*$^{wt/wt}$ than in *Tp53*$^{\Delta 2\text{-}10/\Delta 2\text{-}10}$ NSC/NPCs of model 1 (Figure 14-

f). Lysates from NSC/NPCs infected with pMSCVpuro-Mm*Dnajb9*-T2A-eGFP (cleaved) construct (3.9) served as positive control.

These results indicate that expression of the IRE1α regulating co-chaperone DNAJB9 is increased under ER stress in murine NSC/NPCs and that this increase may be in part dependent on p53 function.

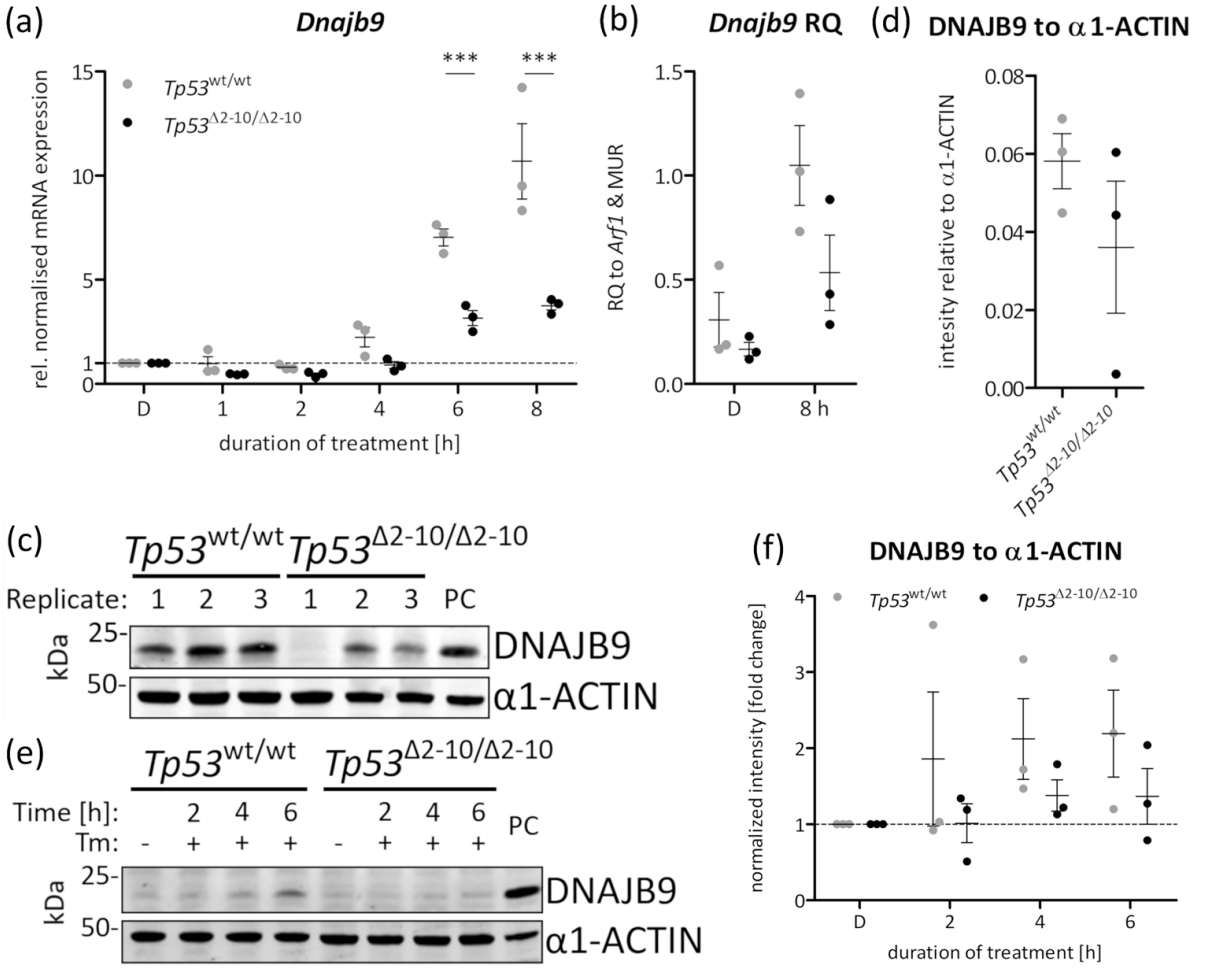

Figure 14- Expression of DNAJB9 under ER stress in P53 KO NSC/NPCs of model 1. (a) qRT-PCR against *Dnajb9* in *Tp53*$^{wt/wt}$ and *Tp53*$^{\Delta2\text{-}10/\Delta2\text{-}10}$ NCSs normalized against DMSO, as indicated by the dashed line at y = 1. (b) RQ data from (a). (c) Western Blot analysis of lysates from NSC/NPCs with the indicated genotypes as passage replicates and their quantification in (d) relative to the corresponding α1-ACTIN signal intensity. (e) representative Western Blot of DNAJB9 in treated NSC/NPCs with tunicamycin for up to 6 h and the fold change relative to α1-ACTIN and DMSO in (f). Data is presented as scatter dot plots with indicated mean ± SEM. Abbreviations: MUR, mouse universal reference RNA; rel., relative; RQ, relative quantity; *s*, spliced; tunicamycin, tunicamycin; u, unspliced.

4.2.6 Heterogeneity of NSC/NPCs in biological replicates

Since the effects observed for *Xbp1s* expression in NSC/NPCs of model 1 of different p53-genotypes were difficult to reproduce in all investigated cultures, additional experiments were performed on conditional p53 knock-out NSC/NPCs after 4-OHT exposure *in vitro* (model 2).

Western blot analysis to evaluate p53 expression before and after 4-OHT exposure of four mouse derived NSC/NPCs ("model 2") with a floxed *Tp53* gene and constitutively expressed Cre recombinase, showed a successful knock down of p53 expression (Figure 15-a). Interestingly, the level of p53 protein expression was variable from cell preparation to cell preparation, i.e. p53 protein levels were higher in Mm1 and Mm2 than in Mm3 and Mm4 cells under steady-state conditions. Analysis of *Ern1* and *Dnajb9* mRNA expression via qRT-PCR showed no differences according to the *Tp53* status of the cells but revealed increased expression levels after prolonged

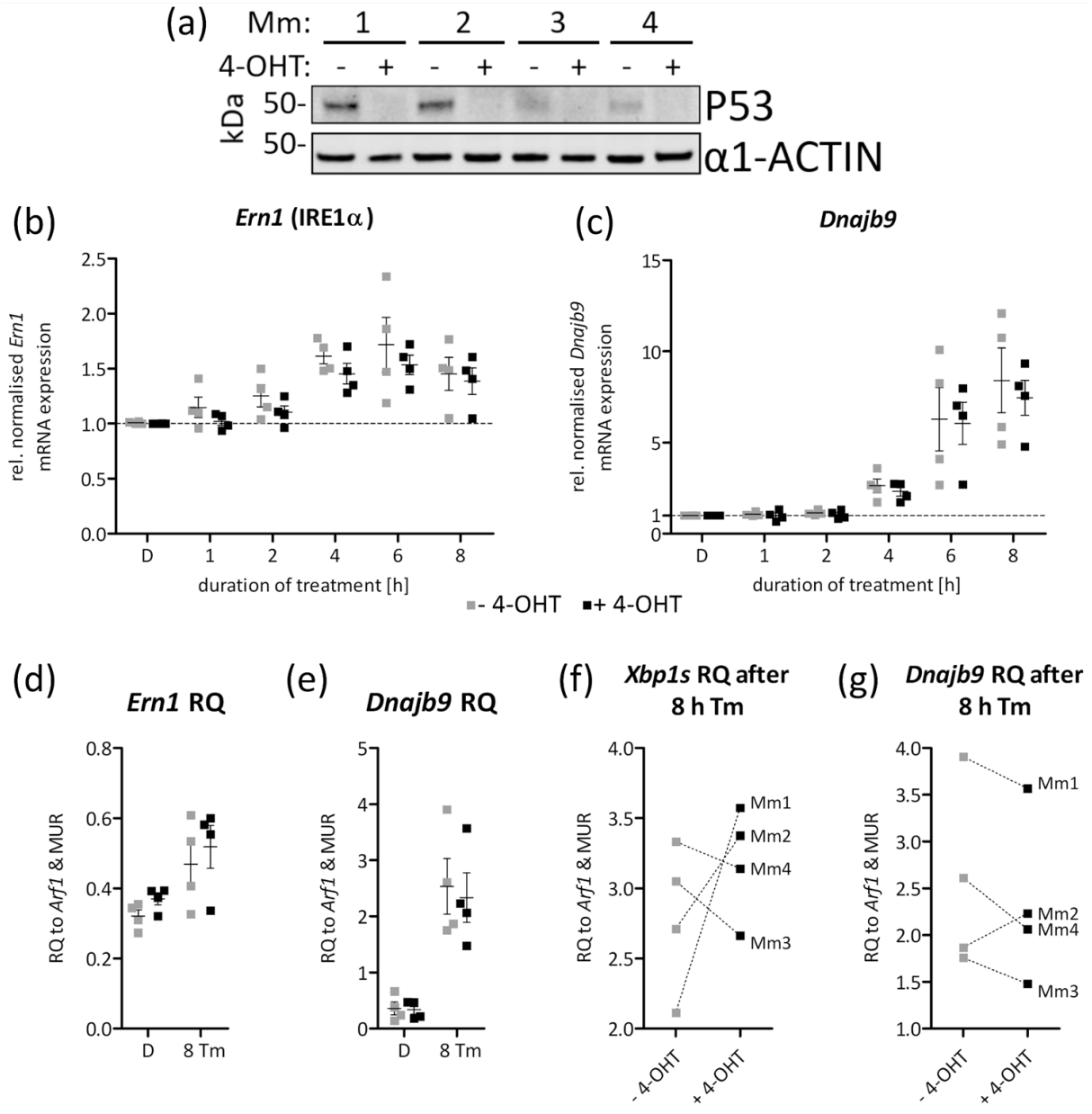

Figure 15- Characterization of NSC/NPCs used as model 2. (a) Western Blot analysis of NSC/NPCs derived from four different mice before and after 4-OHT exposure. (b) Fold change to DMSO of the transcript *Ern1* after treatment with 2 µg/mL tunicamycin for the indicated timepoints and corresponding RQ data (d) analyzed with qRT-PCR. (c) same as (b) but with *Dnajb9* as analyte. (e) same as (d) with *Dnajb9*. (f) *Xbp1s* expression after 8 h 2 µg/mL tunicamycin treatment from Figure 11 (b) with connected mice before and after 4-OHT exposure. (g) same representation as in (f) of data from (c). Data is presented as scatter dot plots with indicated mean ± SEM. Abbreviations: 4-OHT, tamoxifen; Mm: *Mus musculus*; MUR, mouse universal reference RNA; rel., relative; RQ, relative quantity; s, spliced.

tunicamycin treatment in comparison to DMSO-treated cells (Figure 15-b) and c). The RQ data plotted in Figure 15-d of the two transcripts also did not differ between the p53-genotypes. The 8 h timepoint of tunicamycin treatment from Figure 11-b was plotted again in Figure 15-f, and corresponding data points were connected via dotted lines. Hence, it was obvious that NSC/NPCs from two distinct mice (Mm1 and Mm2) increased the *Xbp1s* expression considerably after *Tp53* knock-out whereas NSC/NPC cultures from the two other mice (Mm3 and Mm4) showed slightly decreased *Xbp1s* transcript levels. A similar plot with RQ data for *Dnajb9* (Figure 15-c in g) showed that NSC/NPCs from three mice, decreased the target upon *Tp53* knock-out to some extent while NSC/NPCs from the fourth mouse showed slightly increased expression levels.

Taken together, the own data of model 1 show that p53-deficient NSC/NPCs had a higher *Xbp1s* fold change than comparable p53-wildtpye NSC/NPCs following tunicamycin treatment. This higher fold change may be related to lower expression of DNAJB9 rather than altered IRE1α expression or stability.

4.3 2-HYDROXYGLUTARATE INDUCED UPR IN MURINE NSC/NPCS IS INDEPENDENT OF P53

An intriguing hypothesis is that p53 mutations or functional knock-outs may help a cell to overcome proteostasis perturbations induced by endogenous stressors like mutations in the IDH genes 1 and 2 that result in ER stress induced by the aberrant production of the oncometabolite 2-hydroxyglutarate (2-HG) (*14*). Therefore, *Tp53*-wildtype and knock-out murine NSC/NPCs of model 1 were treated with 0.4 mM octyl-2-HG, a membrane permeable modified version of 2-HG, for 20 h followed by determination of used *Xbp1s* expression as a reporter for ER stress. *Tp53*$^{wt/wt}$ and *Tp53*$^{\Delta 2\text{-}10/\Delta 2\text{-}10}$ NSC/NPCs both significantly (unpaired t-test: p(WT) = 0.0253; p(KO) = 0.0319) increased the splicing of *Xbp1* by IRE1α following octyl-2-HG exposure compared to control cells (0.52 % (v/v) EtOH-treated; FC(WT) = 1.59; FC(KO) = 1.82; Figure 16-a). *Xbp1u* levels were also increased 1.61-fold and 1.65-fold relative to controls (0.52 % (v/v) EtOH treated) but the increase was only significant in *Tp53*$^{wt/wt}$ NSC/NPCs of model 1 (unpaired t-test: p(WT) = 0.0454; Figure 16-b). Surprisingly, 20 h of treatment with 0.4 mM octyl-2-HG did not alter the expression of *Grp78* (Figure 16-c). The expression of the analyzed transcripts did not differ between two distinct p53-genotypes.

The second interesting question concerning a possible role of 2-HG in ER stress was whether exposure to octyl-2-HG preconditions the cells against proteostasis perturbation. To study this hypothesis, p53-wildtype NSC/NPCs derived from four different mice were exposed to 0.4 mM octyl-2-HG for 72 h. Every 24 h half of the medium was replaced with fresh medium including 0.4 mM octyl-2-HG, before adding 2 µg/ml of tunicamycin for 6 h. Alterations in *Xbp1s* expression were then analyzed again by qRT-PCR. Octyl-2-HG exposure for 72 h increased *Xbp1* splicing slightly (FC = 1.57), whereas 6 h treatment with 2 µg/ml tunicamycin increased *Xbp1* splicing substantially (FC = 9.92; Figure 16-d). Double-treated cells increased *Xbp1s* also substantially, but to a lesser degree than cells treated with tunicamycin alone (FC = 6.22). A two-way ANOVA (p = 0.0006) with Bonferroni correction did not show a significant difference between these two treatment groups. However, all treated NSC/NPCs had lower *Xbp1s* levels when pretreated with octyl-2-HG before exposure to tunicamycin (Figure 16-e). As before, octyl-2-HG increased *Xbp1u* as well. Pretreatment with ocytl-2-HG yet did not change its transcription compared to tunicamycin treatment alone (Figure 16-f). *Grp78* expression also was only altered by tunicamycin

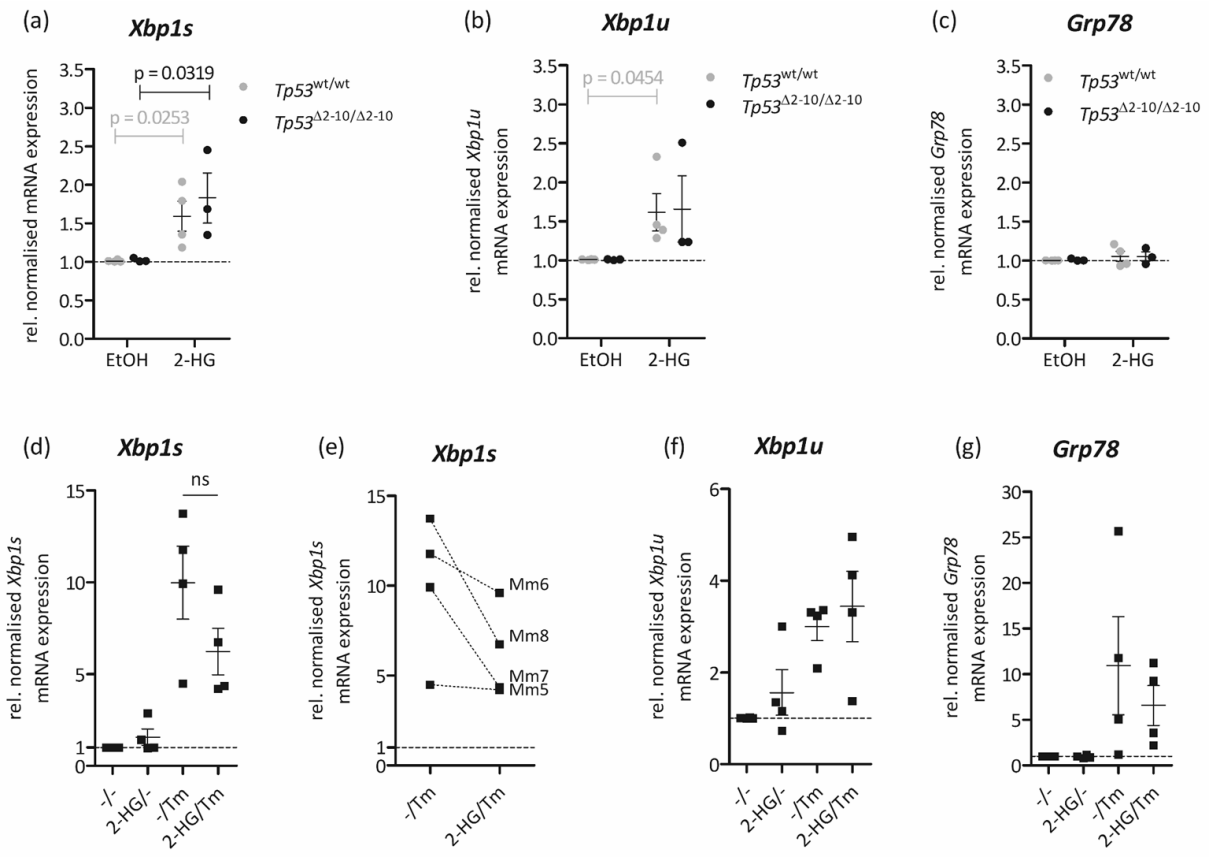

Figure 16- ER stress response upon 2-HG exposure is independent of p53 genotype but preconditions the cell. (a) qRT-PCR against *Xbp1s* in *Tp53*$^{wt/wt}$ and *Tp53*$^{\Delta 2\text{-}10/\Delta 2\text{-}10}$ NSC/NPCs after 20 h exposure to 0.4 mM octyl-2-HG, RQ was normalized against EtOH treated cells, as indicated by the dashed line. (b) and (c) same as in (a) but against *Xbp1u* and *Grp78*, respectively. (d) same as in (a) but after 72 h preconditioning with 0.4 mM octyl-2-HG, half of the medium was exchanged every 24 h including 0.4 mM ocytl-2-HG. Two-way ANOVA (p=0.0006) with Bonferroni correction was not significant. (e) same data as in (a) but with indicated mice individuals. (f) and (g) same as in (a) but against *Xbp1u* and *Grp78*, respectively. Nicked lines indicate an unpaired t-test, lines indicate a two-way ANOVA with Bonferroni correction. Data is presented as scatter dot plots with indicated mean ± SEM. Abbreviations: 2-HG, octyl-2-hydroxyglutarate; -, solvent control; EtOH, ethanol; ns, not significant; rel., relative; s, spliced; tunicamycin, tunicamycin; u, unspliced.

treatment but was lower in the double treatment (Figure 16-g). In both analyses (Figure 16-f and g), however, data showed a high standard error.

Taken together, these results may indicate that continuous exposure of cells to 2-HG, as observed in IDH-mutant gliomas, may precondition the cells towards an ER stress response.

4.4 TREATMENT OF SEVERAL GLIOMA CELL LINES WITH ER STRESS INDUCING CHEMICALS

To investigate the reaction of glioma cells to ER stress inducing agents, tunicamycin and bortezomib, monolayer cultures of six established glioblastoma cell lines (A-172, SNB-19, T98-G, U-87 MG, LN-18, and LN-229) were treated with 0.02 – 5 µg/ml of tunicamycin or 0.313 – 80 nM of bortezomib for 24 h (Figure 17). Treated cells were analyzed with the MTT method and the absorption values were normalized to DMSO-treated controls. In all six cell lines, the mean absorption values for cells treated with tunicamycin did not decrease to values lower than 50 % compared to DMSO-treated control cells. Except for the T98-G cell line, the absorbance of all other cell lines decreased steadily with higher tunicamycin concentrations. In case of the T98-G cell line, the absorbance increased slightly with 0.039 to 0.156 µg/ml of tunicamycin to then slightly decrease under the DMSO absorption level with higher concentrations of tunicamycin. At 5 µg/ml of tunicamycin the cell lines A-172, SNB-19, and T98-G had a normalized absorption level between 70 %- 100 % whereas the remaining cell lines (U-87 MG, LN-18, LN-229) showed a normalized absorption level between 50 % - 70 %. In case of bortezomib treatment, all cell lines showed

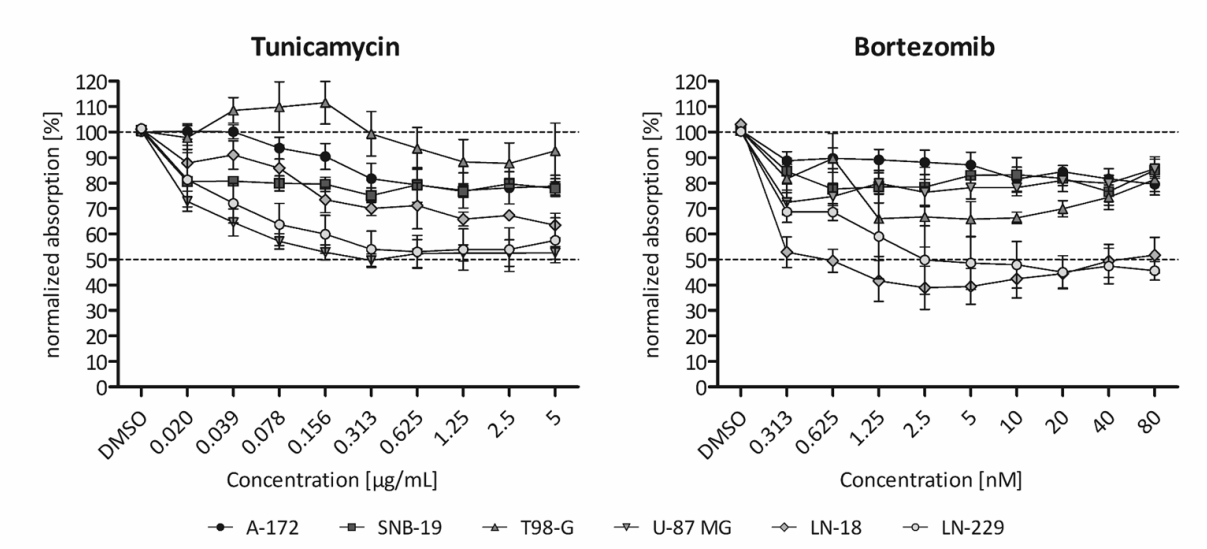

Figure 17- Treatment of six glioma cell lines with different ER stress inducers resulted in reduced cellular viability. MTT analyses of the glioma cell lines A-172, SNB-19, T98-G, U-87 MG, LN-18, and LN-229 treated with either Tunicamycin (0.02- 5 µg/mL) or bortezomib (0.313- 80 nM) for 24 h. Dashed lines indicate 100 % or 50 % absorption. Absorbance was normalized to DMSO-treated control cells. Data are presented as mean ± SEM and connecting lines serve illustrative purposes only.

decreased viability as reflected by lower absorption levels in treated compared to control cells. The cell lines LN-18 and LN-229 showed the highest sensitivity to bortezomib treatment among the six investigated glioma lines.

Taken together, none of the two tested ER stress-inducing drugs were able to decrease the viability of the six investigated glioma cells below 40 % of DMSO-treated control cells. Nevertheless, some cell lines (LN-18 and LN-229) did react more sensitive to either treatment. These experiments set the grounds for more thorough analyses of the UPR in glioma cell lines treated with bortezomib, using high-throughput proteomics-based profiling with a novel quantitative method to comprehensively analyze proteomic changes associated with the UPR in gliomas (*210*).

5. DISCUSSION

In this work, the unfolded protein response (UPR) upon chemical induction of ER stress was investigated in murine fibroblasts as well as neural stem and progenitor cells (NSC/NPCs), and in human glioma cells using different *in vitro* approaches. Parts of the experiments included in this thesis were carried out in the context of a BMBF-funded collaborative research consortium (SUPR-G – The unfolded protein response in glioma) and the first goal of the own work was to establish optimal experimental parameters for high-throughput proteomic and transcriptomic analyzes of the UPR signaling pathway in NIH/3T3 fibroblasts as well as in LN-308 human glioma cells. Independent of these consortium-based investigations, the consequences of two glioma relevant mutations, namely *TP53* mutations and isocitrate dehydrogenase (IDH) mutation, were investigated regarding their possible roles in modulating the UPR pathway in murine NSC/NPCs.

5.1 THE UPR IN GLIOMA CONTEXT – BIP IN THE SPOTLIGHT

Treatment of NIH/3T3 cells with different concentrations of tunicamycin or thapsigargin revealed that thapsigargin is more toxic than tunicamycin at low dosages (Figure 5-a and -b). Both chemicals, however, did not result in 100 % cell death after 24 h of treatment even at the highest concentration used (tunicamycin = 5 µg/ml; thapsigargin = 1 µM). Nevertheless, the own findings do not exclude the possibility that complete cell death may possibly be achieved after treatment with tunicamycin or thapsigargin over longer times of exposure. However, the focus of the own experiments was placed on the characterization of an early response to severe stress. Therefore, 2 µg/ml of tunicamycin and 200 nM of thapsigargin were chosen as the drug concentrations for further analysis, in line with studies from other groups that studied chemical induction of the UPR in cultured cells (*151, 214*).

Following tunicamycin or thapsigargin treatment of NIH/3T3 cells, flow cytometry-based cell cycle analysis using BrdU and 7-AAD revealed a predominant increase in G0-G1 phase cells and an at best transient G2-M arrest after 24 h of treatment (Figure 5-c). A similar observation was made by other authors, who traced the observed effect back to CyclinD1 depletion resulting from translational attenuation via PERK (*215, 216*). As for the complete UPR signaling and its outcomes, other types of cells, such as the human colorectal carcinoma cell line HCT-116, may enter into a G2-M phase arrest (*190*). This decrease in proliferation following tunicamycin or thapsigargin treatment may result in reduced absorption values in an MTT assay. In addition, cell death will

also result in reduced absorption values in an MTT assay. Nevertheless, the cells response observed reproduced the effect seen in other studies. It is also the nature of a chemically perturbed proteostasis that cells inevitably engage an apoptotic response, because they cannot rescue the stress.

Tumor cells in gliomas are, however, not exposed to unsolvable ER stress, they rather experience high protein folding pressure due to high demand of protein secretion whilst facing nutrient and oxygen deprivation (*217*). If such cells slow down their cell cycle progression following UPR signaling (4.1.1), this likely serves the purpose of winning time to reestablish proteostasis and prevent DNA damage and an apoptotic cell death. Thereby, the UPR obliges its cell protective purpose as a shielding mechanism. Analysis of large online data sets revealed that patients suffering from gliomas with active IRE1α demonstrate significantly reduced survival (*41*). This prognostically unfavorable association could also be made for other tumors (*218*) and underlines that an active UPR slowing down the cell cycle may carry an evolutionary advantage for the tumor cell, besides other benefits (as described in 1.2.5). For example, BIP and chaperones in general also seem to play an important role in cancer pathogenesis (*209*).

In the own collaborative experiments, the expression pattern of *Grp78*/*GRP78* mRNA and the resulting protein BIP was studied in mouse NIH/3T3 and LN-308 human glioma cells, respectively. The mRNA expression profile of the chaparone distinguishes NIH/3T3 cells from LN-308 cells in time course and level of induction of baseline expression level of *Grp78*/*GRP78* mRNA, as well as in the endogenous protein expression of BIP (Figure 7-a and -b). Interestingly, the level of induction of the *Grp78* mRNA was almost identical following tunicamycin or thapsigargin treatment. It appeared that LN-308 glioma cells with high endogenous BIP level may not need a marked increase of *GRP78* mRNA to reach a protective BIP level. Protective level meaning that the BIP expression is high enough to bind most of the misfolded proteins and regulate the UPR receptors. In contrast, NIH/3T3 cells showed very low endogenous protein levels of BIP and thus needed a higher increase in mRNA and protein expression to reach a protective BIP abundance. NIH/3T3 cells demonstrated the highest increase in *Grp78* mRNA levels after 6 h of drug treatment. At the same time point, the protein expression level of BIP started to increase, too. The different endogenous protein levels of BIP might be due to the diverse cellular origin differentiation, and immortal versus neoplastic state of NIH/3T3 versus LN-308 cells. It is intriguing to think about possible benefits that glioma cells may gain from a high level of BIP. First of all, glioma patient samples and xenografts of glioma in rat brains showed high protein levels of BIP, ER resident chaparone GRP94 also known as endoplasmin, and HSP90, the major cytosolic chaparone (*168, 219*). The expression level of the two ER chaperones correlates with worse prognosis in glioma patients (*168*). Most surprisingly, BIP and other chaperones (HSP70 and its

co-chaperone HSPBP1) were found on the cell surface of glioma cells and other types of tumor cells (*220–222*). It was be shown that BIP associates with a variety of cell surface proteins like ion channels and major histocompatibility complex class I (MHC-I) receptors as well as DnaJ-like protein MTJ-1 (*223*). These interactions are, however, not yet functionally understood. That cell surface BIP has implications on survival and growth of glioma xenografts has been shown by treatment with an antibody specific for surface BIP, which indeed slowed tumor growth and increased survival of glioma xenograft-bearing mice (*222*). It is intriguing to speculate that cell surface BIP is involved in migration, immune escape, or epidermal growth factor receptor (EGFR) signaling in glioma. In the latter case, it was shown that BIP forms complexes with EGFR intracellularly (*224*), and one might speculate that such protein-protein interactions might happen on the cell surface, possibly, also with the tumor-specific EGFRvIII variant found in a subset of EGFR-amplified glioblastomas (reviewed in (*225*)). The possible roles of the UPR in resistance to chemotherapeutic treatment of glioma and the specific contribution of BIP in this respect are discussed in chapter 5.6.

In conclusion, the UPR is a vital part of glioma biology. Improved mechanistic understanding of the signaling will foster the still limited knowledge of glioma pathogenesis and thereby might possibly provide novel treatment options for this devastating cancer.

5.2 IRE1A AND PERK IN GLIOMAS

As discussed above, BIP as effector of the UPR may support survival and growth of glioma cells under stress conditions. As protective protein it is needed to reestablish proteostasis but also to regulate the UPR receptors. Activation of one of the responsible pathways, the UPR IRE1-XBP1 axis, which is frequently altered in glioma (*162, 226*), was analyzed by qRT-PCR assessment of the expression levels of the two XBP1 mRNA transcripts *Xbp1s* and *Xbp1u* (and human *XBP1s*/*XBP1u*) in NIH/3T3 (4.1.2) and LN-308 (4.1.4) cells following drug induced UPR. Interestingly, the induction of *Xbp1s* in NIH/3T3 cells was stronger upon tunicamycin treatment compared to thapsigargin treatment. Even though both drugs are inducing the UPR the mechanisms of UPR induction are strikingly different: thapsigargin inhibits the SERCA Ca^{2+} pump in the ER membrane and thereby influences Ca^{2+} homeostasis of the organelle and subsequently of the cytosol. Tunicamycin blocks polypeptide chain N-glycosylation by inhibition of GlcNAc phosphotransferase (GPT). Thus, thapsigargin is not specific for ER stress induction. The higher expression levels of *Xbp1u* in tunicamycin treated NIH/3T3 cells compared to thapsigargin treated NIH/3T3 cells may be due to an accumulation of the unspliced transcript. Such an accumulation

does not happen in cells treated with thapsigargin because they have a higher demand of *Xbp1s* since thapsigargin induces the UPR stronger than tunicamycin. An accumulation of *Xbp1u* in NIH/3T3 cells exposed to tunicamycin but no accumulation in thapsigargin treated NIH/3T3 would suggest that *Xbp1u* mRNA transcription is the same for both treatments.

The LN-308 glioma cell line also increased *XBP1s* more excessively upon treatment with tunicamycin compared to treatment with thapsigargin. The pattern of *Xbp1u*/*XBP1u* abundance was similar between NIH/3T3 and LN-308 cells. This is surprising because of the different origins, differentiation and status of the two cell lines. *Xbp1u*/*XBP1u* transcription is regulated by ATF6 (*82*), CCAAT/enhancer-binding protein beta (C/EBPβ) (*227*), myoblast determination protein 1 (MYOD1) (*228*), and XBP1s itself (*82*). However, there is barely any literature on the mechanism how the four mentioned factors influence *Xbp1u*/*XBP1u* transcription and how the factors are expressed in NIH/3T3 and LN-308 cell lines or glioma tissue the own results showing different abundance patterns of *Xbp1s* and *Xbp1u* in NIH/3T3 cells upon treatment with tunicamycin or thapsigargin are in line with data of DuRose and co-workers (*229*). These researchers also reported on different kinetics of *Xbp1s* abundance changes in NIH/3T3 cells treated with either drug (*229*).

The IRE1α-XBP1 axis is of vital importance for glioma cells as indicated by findings showing that overexpression of unfunctional IRE1α in U87-MG glioma cells suppressed vascular endothelial growth factor (VEGF) expression induced by hypoxia or glucose deprivation (*164*) because ATF4/XBP1 and HIF1/XBP1 heterodimers lead to VEGF expression under such conditions (*165, 166*). Also, the relevance of the IRE1α receptor in glioma was recently underlined by the discovery of subclasses in primary glioma cell lines with concern the activity of IRE1 α (*230*). Lhomond and co-workers separated the tumor cells by enrichment in XBP1s (and its targets) and RIDD cleaved mRNAs, correlating with low RIDD activity, ($XBP1s^{+}/RIDD^{-}$) on the one hand and high RIDD activity but depleted in XBP1s and its targets. ($XBP1s^{-}/RIDD^{+}$). By implanting primary glioma cells of both groups in nude mice brains, the authors observed that the $XBP1s^{+}/RIDD^{-}$ group cells did form tumors, whereas the $XBP1s^{-}/RIDD^{+}$ group cells did not (*230*). The authors underline the importance of the adaptive, angiogenic, and immune-escape capacities of the IRE1α -XBP1 axis which may lead to an precision medicine tool keeping IRE1α in RIDD activity rather than *XBP1u* splicing activity to treat gliomas (*230*). IRE1α was also identified as attractive treatment target in gliomas because of the newly identified angiogenesis-increasing capabilities of the kinase domain independent of the RNase domain (*231*). Jabouille et al, were additionally, to their first observation, able to demonstrate, that selective inhibition of IRE1α RNase domain promoted invasiveness in their U87-MG xenograft glioblastoma model. IRE1α mutations that abolished the RNase ability of the receptor expressed in the glioblastoma model led to the exhibition of

mesenchymal features (e.g.: infiltrative phenotype) of the tumors. Collectively, these findings underline the functional relevance of IRE1α in glioma pathogenesis.

The PERK axis is also of vital importance in the survival and development of glioma and other tumors. Since PERK deficient mouse fibroblasts in xenograft models showed compromised angiogenesis and were therefore smaller, the pathway may be of higher relevance to tumor cells (*232, 233*). Additionally, PERK deficiency decreased progression but not initiation of a tumor (*234*). The UPR receptor was recently shown to have elevated activation in WHO grade III glioma and grade IV glioblastoma tissues (*169*). In addition, PERK knockout U87-MG and U-251 glioma cell lines exhibited decreased tumor formation upon xenografting relative to the respective wildtype glioma cells (*169*). Together, the results shown here and reported in the literature point towards a prominent role of PERK in glioma pathogenesis. In the experiments reported in this thesis, PERK protein abundance was unaltered following tunicamycin or thapsigargin treatment but the activity of the receptor increased as determined by the increase in phosphorylation of its substrate EIF2α (Figure 6-c). The phosphorylation of EIF2α to pEIF2α was markedly increased upon thapsigargin treatment and subsequently resulted in an increase of ATF4 protein level. Additionally, increased levels of pEIF2α might contribute to the G1-G0 cell cycle arrest observed under the experimental conditions used (4.1.1). In case of thapsigargin, the level of pEIF2α decreased after 6 h or 8 h which maybe be an effect of increased BIP and thereby decreased PERK activity. Tunicamycin treatment slowly but steadily increased pEIF2α during the treatment duration up to the level of thapsigargin after 24 h of treatment. Tunicamycin inhibits glycosylation of proteins and thus the cellular response to this drug could be slower compared to thapsigargin as the accumulation of misfolded proteins takes more time than in thapsigargin treated cells. Nevertheless, both chemicals increased *Xbp1s* after 1 h already (4.1.2 and 4.1.4), meaning that also tunicamycin treatment led to an activation of IRE1α as early as thapsigargin. As compensatory mechanism against tunicamycin, the cells could increase glycosylating enzymes which need to be translated. Therefore, GADD34 needs to be increased to restart CAP-dependent translation e.g. of the enzyme glycosylating proteins in the ER (e.g.: GPT). The pEIF2α pathway, however, hinders translation and might not be beneficial in dealing with glycosylation stress. This could be one reason why tunicamycin steadily increased pEIF2α in LN-308 glioma cells.

5.3 ESTABLISHMENT OF TREATMENT DURATIONS FOR OMICS EXPERIMENTS

The issues discussed above concerning the relevance and difference of BIP expression between NIH/3T3 and LN-308 cells triggers questions concerning the molecular basis of cell type

specificity of the UPR. The fact that BIP was increased after 6 h of treatment in both cell types (Figure 7) suggests that the underlying signaling pathway is very similar in these two very different cell lines. It shows that cell type specificity of the UPR is not based on the general pathway but regulates the details of the response to a perturbing stimulus. One of these details could be a higher endogenous level of BIP. One reason for a different outcome of the signaling following UPR induction might be related to the diverse transcription factor network involved in the UPR (reviewed in (*218*)).

To further elucidate the link between the UPR and glioma cell biology the SUPR-G consortium project used three omics approaches (transcriptomics, translatomics, and proteomics). For this purpose, preparatory analyses were needed to identify the best treatment conditions and time points of exposure for each individual omics technique. With the data presented in this thesis we finally decided to measure changes at the mRNA level with treatment durations of 2 h, 4 h, and 6 h whereas methods analyzing protein expression were used after 6 h, 16 h, and 24 h of exposure to either tunicamycin or thapsigargin. The main argument for the selection of these time point was, that translation of important protective proteins like BIP started after 6 h, indicating that respective mRNA changes must happen before that treatment duration, which was approximately 4 h earlier (Figure 7).

Taken together, the data presented on tunicamycin and thapsigargin induced UPR in NIH/3T3 and LN-308 cells underlines the differences of the response based on cell type. The two UPR receptors IRE1α and PERK both play important but not yet comprehensively understood roles in glioma biology. Therefore, further studies are needed to untangle the role of the UPR in malignant cancers like glioma that are frequently resistant to standard therapy types like radio- and alkylating chemotherapy.

5.4 Investigations of p53 and the UPR in murine NSC/NPCs

The data in this part of the thesis were gathered to evaluate the role of p53 in the ER stress signaling response of NSC/NPCs, the most likely cell of origin of gliomas (*5*). Based on the observation of Namba *et al.* (*185*) The aim was to elucidate the influence of p53 especially on splicing of *Xbp1*. The hypothesis was, that deletion of p53 increases the abundance of *Xbp1s* as shown before (*185*) and to shed light on molecular pathomechanisms underlying this phenotype.

The initially used passage replicates (termed “model 1”) of NSC/NPCs from one wildtype and one floxed p53 mouse infected retrovirally with pMX-Cre showed a high fold change of *Xbp1s* mRNA

abundance upon tunicamycin treatment and a significantly higher fold change of *Xbp1s* levels in the *Tp53*$^{\Delta 2\text{-}10/\Delta 2\text{-}10}$ compared to p53-wildtype NSC/NPCs (Figure 11-a). This effect was based on the lower endogenous *Xbp1s* level of the knock-outs compared to the wildtype NSC/NPCs resulting from an endogenously lower *Xbp1u* level in the knock-outs compared to the wildtype NSC/NPCs (Figure 11-e). However, the transcript increased on average to more than double relative to the DMSO control (Figure 11-c and -e). The consequence for *Xbp1s* was a similar RQ in the *Tp53*$^{\Delta 2\text{-}10/\Delta 2\text{-}10}$ NSC/NPCs as in the *Tp53*$^{wt/wt}$ NSC/NPCs, meaning, the important difference between *Tp53*$^{wt/wt}$ and *Tp53*$^{\Delta 2\text{-}10/\Delta 2\text{-}10}$ NSC/NPCs of model 1 is related to different *Xbp1u* abundance. It suggests a simple equilibrium change in precursor mRNA (*Xbp1u*) that results logically in a similarly lower splicing of *Xbp1u* under endogenous conditions. Looking closer on the fold change plots (Figure 11-a and -c), the fold change of *Xbp1u* after 8 h tunicamycin between *Tp53*$^{wt/wt}$ and *Tp53*$^{\Delta 2\text{-}10/\Delta 2\text{-}10}$ NSC/NPCs in model 1 is around FC ≈ 2, the fold change of *Xbp1s* at the same timepoint is also FC ≈ 2. Hence, if the amount of precursor doubles, so does the spliced product. In addition, these differences were not detected in model 2 of four independent NSC/NPC cultures (Figure 11-b, -d, and -f) in which the *Tp53*$^{\Delta 2\text{-}10/\Delta 2\text{-}10}$ genotype was induced by *in vitro* 4-OHT treatment. Neither the *Xbp1s* RQ nor the *Xbp1u* RQ were different between *Tp53*$^{wt/wt}$ and *Tp53*$^{\Delta 2\text{-}10/\Delta 2\text{-}10}$ NSC/NPCs in model 2. Taken together, the own results indicate that p53 may not regulate the level of *Xbp1s* and may have only little influence on the expression of *Xbp1u* in mouse NSC/NPCs.

There are two possible explanations for the high fold change of *Xbp1s* or *Xbp1u* originally observed in the *Tp53*$^{wt/wt}$ versus the *Tp53*$^{\Delta 2\text{-}10/\Delta 2\text{-}10}$ NSC/NPCs in model 1: First, p53 had a repressive influence on *Xbp1u* endogenous expression, or second, the expression level of *Xbp1u* level in the two cell lines was different from each other due to additional reasons. The latter seems more likely, comparing the RQ values of all *Xbp1u* qRT-PCRs revealed that, the *Tp53*$^{wt/wt}$ NSC/NPC line used had an average *Xbp1u* RQ nearly twice as high as all other NSC/NPC cells examined in this thesis (Figure 11-e and -f). Lastly, by comparing individual biological replicates from four independent NSC/NPC cultures of model 2 with or without p53, it is interesting that the mice derived NSC/NPC with originally relatively high p53 protein level (Figure 15-a) substantially increased *Xbp1s* after 8 h treatment with tunicamycin if p53 was knocked-out. The ones with relatively low levels of p53 decreased *Xbp1s* upon p53 deletion (Figure 15 -f). It is thus tempting to hypothesize that in cells with high levels of p53, this major regulator may influence the splicing of *Xbp1u* by increasing the *Xbp1u* mRNA but in cells with low levels of p53 there may be no influence on either *Xbp1* specimen. This hypothesis, however, would require further experimental validation.

Since there was essentially no difference between *Xbp1s* levels comparing the *Tp53*$^{wt/wt}$ NSC/NPCs versus cre-infected *Tp53*$^{\Delta 2\text{-}10/\Delta 2\text{-}10}$ NSC/NPCs (model 1), there also was no difference in viability under tunicamycin or thapsigargin (Figure 10). Hence, p53 may not be involved in the apoptosis initiation under ER stress, and further, it may not be involved in resistance of NSC/NPCs to proteostasis stress. However, this may be cell type specific and it is possible, and has been reported, that p53 is involved in the UPR of other cell types (*192*).

In the study by Namba and co-workers (*185*), the cell lines HCT116 (colorectal carcinoma), mouse embryonic fibroblasts, and U2OS (osteosarcoma cells) without p53 had higher levels of IRE1α than their p53 wildtype controls. The protein level of the receptor was also elevated in 23 other human cancer cell lines with mutations in *TP53*. NSC/NPCs in the experiments described in this thesis, did not show a higher IRE1α level upon p53 knock-out *per se* but during tunicamycin treatment *Tp53*$^{\Delta 2\text{-}10/\Delta 2\text{-}10}$ NSC/NPCs increased the receptor whereas *Tp53*$^{wt/wt}$ NSC/NPCs decreased it. The difference in *Ern1* mRNA between the genotypes (Figure 12-a and -b) was not reproducible (Figure 15-b) and thus was possibly due to other reasons, not further examined nor discussed. If SYNV1 is adapted to IRE1α by p53, as hypothesized by Namba and co-workers (*185*), the protein level of IRE1α should be stable under ER stress in cells with p53 deletion and the IRE1α should not increase as shown in Figure 12 -f. It should additionally be noted, that this E3 ligase (SYNV1) was also shown to ubiquitinate p53 (*235*), a matter not discussed by Namba and colleagues (*185*). However, it cannot be excluded that the pathway behaves different in murine cells compared to human cells. Therefore, the pathway proposed by Namba *et* al. (*185*) may not be true for every cell type or organism.

It is challenging to explain how the *Tp53*$^{\Delta 2\text{-}10/\Delta 2\text{-}10}$ NSC/NPCs with a lower endogenous amount of *Xbp1u* than the *Tp53*$^{wt/wt}$ NSC/NPCs of model 1 (Figure 11-e) reach a similar level of *Xbp1s* upon exposure to tunicamycin for 8 h. The increased amount of IRE1α in Figure 12-f may be the responsible regulation of the *Tp53*$^{\Delta 2\text{-}10/\Delta 2\text{-}10}$ NSC/NPCs to balance an endogenously lower *Xbp1u* level with the purpose of increasing *Xbp1s* to a level necessary for an adequate response to the applied ER stress stimulus. To reach an adequate level of *Xbp1s* the *Tp53*$^{wt/wt}$ NSC/NPCs may have decreased IRE1α by degradation, decreased translation, or decreased activity. However, degrading the receptor is possibly the only option for the *Tp53*$^{wt/wt}$ NSC/NPCs to decrease *Xbp1u* splicing, since most DNAJB9 proteins are possibly bound to misfolded proteins and are not available to regulate the IRE1α dimer. As described, DNAJB9 controls IRE1α's activity by recruiting BIP to the dimerized luminal domain of IRE1α and stimulates ATP hydrolysis in BIP to break the IRE1α dimer apart (1.2.1). The *Dnajb9* mRNA was decreased in *Tp53*$^{\Delta 2\text{-}10/\Delta 2\text{-}10}$ NSC/NPCs compared to *Tp53*$^{wt/wt}$ NSC/NPCs of model 1 but not in model 2 of *in vitro* induced *Tp53* knockouts versus *Tp53* wildtype NSC/NPCs. However, the endogenous protein level of DNAJB9 was very low

in the *Tp53*$^{\Delta 2\text{-}10/\Delta 2\text{-}10}$ NSC/NPCs of model 1. Hence, the activity of IRE1α must have been higher in these cells. An altered activity is the only possible explanation for the similar average fold change of *Xbp1s* after 6 h of tunicamycin treatment with inhibition of the RNase domain using STF-083010 (Figure 13-a). The observation that the cells still show *Xbp1u* splicing despite RNase domain inhibition suggests that the inhibitor did not block all IRE1α molecules. Other reasons might be the stability of STF-083010 or timing reasons. Tunicamycin and STF-083010 are administered at the same time but may have different membrane permeability, hence, *Xbp1u* splicing might still have occurred. The inhibitor however blocked the RIDD activity completely, judged from the *Blos1* mRNA being at DMSO level, whereas in the tunicamycin single treatment it was around FC ≈ 0.5 (Figure 13-c). Such a decrease of RIDD through inhibition by STF-083010 is to be expected in mammalian cells (*86*). The increase in *Xbp1u* mRNA upon tunicamycin and STF-083010 treatment suggests a fast compensation mechanism or may be due to an accumulation of the molecule since it is not spliced anymore (Figure 13-b).

The *Tp53*$^{wt/wt}$ and *Tp53*$^{\Delta 2\text{-}10/\Delta 2\text{-}10}$ NSC/NPCs used for model 1 had a similar IRE1α level, the *Tp53*$^{\Delta 2\text{-}10/\Delta 2\text{-}10}$ NSC/NPCs had an endogenously lower *Xbp1u* and *Xbp1s* RQ but increased *Xbp1s* to the same degree as the *Tp53*$^{wt/wt}$ NSC/NPCs with higher precursor level. After 6 h of tunicamycin treatment the IRE1α level in *Tp53*$^{\Delta 2\text{-}10/\Delta 2\text{-}10}$ NSC/NPCs was higher than in *Tp53*$^{wt/wt}$ NSC/NPCs. If the RNase domain is inhibited and only the receptor level would be different, the *Xbp1s* level under tunicamycin and STF-083010 double treatment should be increased in the cells with higher IRE1α level. Since the amount of the receptor differed but the fold change of *Xbp1s* was similar, an altered protein level cannot be the only explanation. Thus, the receptor must have been more active in the *Tp53*$^{\Delta 2\text{-}10/\Delta 2\text{-}10}$ NSC/NPCs, an effect which may be explained by the lower DNAJB9 expression levels in these cells. However, the heterogeneity of the used NSC/NPCs did not allow to find a connection between p53 and IRE1α. Nevertheless, one may speculate that the connecting piece between IRE1α and p53 must be DNAJB9, since it has been shown that its expression is controlled by p53 and that it directly regulates the activity of IRE1α (*79, 236*).

As already discussed, Namba and co-workers showed in an endpoint PCR with primers flanking the spliced-out intron in the *Xbp1u* mRNA and agarose gel electrophoresis, an earlier splicing of *Xbp1u* in p53 knock-out HCT-116 cells, mouse embryonic fibroblast, and U2OS cells compared to their respective p53 wildtype counterparts (*185*). Dioufa *et* al. used the same approach and also reported that the presence of p53 inhibits *Xbp1u* splicing to some extent (*197*). Duplan *et* al. reported an increase in *Xbp1s* on Western Blot in p19^{ARF1} and p53 co-deleted cells compared to p19^{ARF1} deleted ones (*198*). These authors also measured a higher *Xbp1s* mRNA level in p53$^{-/-}$ mouse brains than in p53^{wt} ones with qRT-PCR. The first two studies used a non- quantitative method to draw a quantitative conclusion. However, the last one showed a *Xbp1s* increase upon

p53 knock-out with a variety of methods in a cell line and multiple primary brain samples. Therefore, the hypothesis that p53 may decreases *Xbp1s* may still be correct.

Most studies regarding the discussed points were done in cell lines derived from human tumors of varying origin. These cells naturally carry a high number of mutations and accumulate additional ones over time in cell culture. Furthermore, these cells often have chromosomal alterations that could interfere with gene dosage. Since p53 is mainly involved in DNA damage signaling pathways, it could have been altered by such endogenous genetic alterations in human tumor model cells. This may additionally be a reason why p53 was either identified as UPR agonistic or antagonistic by various groups (1.2.6). It is also difficult to study changes in a very precise and cell type specific signaling pathway, such as the UPR, in cells that may be preconditioned to variable extents to proteostasis perturbations, like neoplastic cells derived from tumors. Therefore, the use of primary cells like NSC/NPCs may be advantageous. However, these primary cells differ in p53 protein levels, despite being of the same cell type and being harvested from similarly young mice. The fact that the different NSC/NPC cultures still differed in the experiments described in this thesis, illustrates the problem of using primary cell cultures. Possibly, that the individual NSC/NPCs used for the biological replicates in the own experiments adapted differently to cell culture conditions and thus, had different p53 levels with respective consequences concerning UPR regulation.

5.5 Exposure to 2-HG preconditions murine NSC/NPCs to ER stress

Diffuse gliomas often carry mutations in the *IDH1* or *IDH2* genes which lead to the production of 2-hydroxygluterate (2-HG). This metabolite inhibits - among others - enzymes that posttranslationally modify collagen precursor molecules and thereby hinders their maturation. Collagens are extracellular matrix proteins and, hence, translated in the ER where they can induce ER stress when not properly modified (*12*). This ER stress induction shown *in vivo* could be reproduced *in vitro* (Figure 16-a). While the increase in *Xbp1s* and *Xbp1u* was significant, 2-HG exposure did not lead to an accumulation of BIP (Figure 16-c). Despite the statistical significance of the altered expression, the increase in *Xbp1s* was small when compared to tunicamycin treated cells (Figure 11-a). However, collagens are not excessively expressed in NSC/NPCs (*237*). Thus, the source of misfolded proteins is possibly smaller than for tunicamycin, since 2-HG leads to misfolding of only a small set of proteins, whereas tunicamycin leads to misfolding of all posttranslationally glycosylated proteins. After 72 h of exposure to 2-HG the increase in *Xbp1s* is not significant anymore and the cells might already have adapted to the stimulus at this time point

(Figure 16-d). Potential adaptation mechanisms could be an increase of prolyl- and lysyl-hydroxylases or a decrease in collagen synthesis because of an active UPR. When an additional ER stress inducing stimulus such as tunicamycin was added after 72 h of pre-exposure to 2-HG, the level of *Xbp1s* induction was reduced relative to exposure to tunicamycin alone. Therefore, the prolonged exposure to 2-HG may predetermine the cellular reaction to proteostasis perturbation.

This predetermination of 2-HG towards proteostasis perturbation may have four possible mechanisms discussed in the following paragraph: 1. a mild but constant activation of the UPR receptors; 2. perturbation-rescuing proteins (e.g.: chaperones, ERAD components, etc.) are already increased; 3. 2-HGs effect on histone methylations; 4. the effect of phosphorylated eIF2α on cellular protein translation.

First, 2-HG activates the receptors constantly, but not to a high extent, hence there is no apoptotic response to the stress but a constant production of *Xbp1s* mRNA and potentially other UPR transcription factors. Consequently, more intense perturbations later do not increase *Xbp1s* because a portion of the protein is already present. The second reason could be an adaptation mechanism in which proteins needed as defense against misfolded proteins already show increased levels and are active by the time the second stimulus is administered. However, this is not the case for BIP, because 2-HG did not change its expression, but the levels of the chaperone were still decreased in the double treatment (2-HG and Tm; Figure 16-g). As third reason, the observed decrease in *Grp78* mRNA is potentially based on increased methylation of histones caused by 2-HG. This would decrease gene expression and might explain why BIP abundance was lower in tunicamycin/2-HG treated NSC/NPCs. So-called hypermethylation of histones would affect a large variety of genes but *Xbp1u* transcription was unaltered, hence, methylation as reason for decreased BIP expression seems less likely. The fourth and last reason leads to the translational decrease caused by 2-HG. It could have led to a lower protein content of the ER prior to tunicamycin exposure. The drug then would have had a smaller impact since there are less proteins to be glycosylated. Subsequent to translational attenuation under ER stress is the increase in CAP-independent translated genes such as ATF4 and BIP. While *Grp78* mRNA transcription does not change, its translation may have. This would lead to a higher BIP protein abundance, would decrease the need of strong mRNA/protein increase upon stimulus, and would lower the UPR receptor activity.

Hence, preconditioning by 2-HG for the accumulation of misfolded proteins can be one of the above-mentioned reasons or an additive effect of a combination of any of these. Nevertheless, IDH mutant NSC/NPCs could have a survival benefit during tumorigenesis as the cells may be more resistant to unfavorable environmental conditions such as low glucose, low pH, or hypoxia. Similar observations were made in stress experiments applying heat shock. Exposing cells to 1 h of 42 °C

caused a heat shock response that almost abolished the apoptotic effect induced via ER stress by administration of tunicamycin or thapsigargin (*238*). Thus, mutant IDH expressing NSC/NPCs could very well be preconditioned to better withstand against ER stress from any stimulus.

5.6 THE USE OF BORTEZOMIB IN GLIOMA TREATMENT

Most gliomas, in particular glioblastomas, are difficult to treat and unfortunately cannot be cured by available therapeutic options, namely surgery combined with irradiation and temozolomide chemotherapy (1.1). Repurposing of drugs developed for other tumors or diseases for glioma therapy may spare decades of preclinical research. Since bortezomib's mechanism of action as proteasomal inhibitor is not cell type specific, and its approval for treatment of human myeloma is already granted (EMEA/H/C/000539 from the European Medicines Agency), it seemed reasonable to test whether bortezomib shows anti-glioma activity *in vitro*. Data on clinical trials testing this drug in the context of malignant glioma are still in an explorative phase (*174, 175*).

The own experiments tested the reaction of commonly used glioma cell lines to tunicamycin or bortezomib (4.4). It is striking that none of the tested cell lines dropped below 50 % of normalized absorption in the MTT assay following tunicamycin treatment. However, the variable reaction of the glioma cell lines to the ER stress inducing chemical underscores the previously mentioned point that the UPR outcome is very cell type dependent. Nevertheless, during the 24 h treatment period even the high concentrations of tunicamycin did not kill all cells. When compared to the dose-response curves from NIH/3T3 cells or NSC/NPCs (Figure 5-a, Figure 10), the response to tunicamycin was remarkably different in glioma cells, especially in the cell lines T98-G and A-172 whereas the cell lines LN-18 and LN-229 showed a comparable dose-response curve as NIH/3T3 cells. The four investigated glioma cell lines had no IDH mutations, and the A-172 cell line is the only one without any *TP53* alteration (*239*). Despite a similar origin their response to tunicamycin was very different and it is thus not surprising that treatment of the cell lines with bortezomib yielded similarly variable results. None of the cell lines was particularly sensitive to bortezomib after 24 h of treatment but there was a clear difference between LN-18 or LN-229 cells and the other four cell lines in the experiment (Figure 17). Both, LN-18 and LN-229, were found among the more sensitive of all tunicamycin or bortezomib treated glioma cell lines, which in conclusion makes them more suitable to treatment with ER stress inducing chemicals. It seems likely that the mutational pattern of each cell line may influence treatment response. Further studies aiming to identify possible genetic, epigenetic, or proteomic alterations associated with differential response of glioma cell lines to bortezomib and other UPR inducing drugs thus are warranted.

To this end, the impact of bortezomib on the UPR of these commonly used glioma cell lines were assessed by proteomic analyses that were performed in cooperation with the group of Robert Ahrends at the Leibnitz Institute for Analytical Science (ISAS, Dortmund). A major problem for conventional proteomic analysis of the UPR relates to the low abundance of the major UPR factors. The UPR proteins are in-fact not observable in standard proteomic procedure, therefore, Chi Nguyen in the group of Robert Ahrends successfully developed a novel proteomic method to identify most UPR proteins from whole cell lysates. The pure identification of proteins, however, provides limited information and to gain reliable and reproducible quantitative data for the UPR proteins it was necessary to develop a targeted proteomic approach. Herein, peptides from lysate digested with trypsin are identified in a mass spectrometer and their abundance is quantified against spiked-in peptides labeled with heavy amino acids resulting in a light to heavy ratio directly corresponding to the measured abundance of the endogenous peptide. Thereby, our cooperation partners were able to reliably quantify the majority of UPR proteins. Together, we validated the method in the glioma cell lines treated with bortezomib and found a marked induction of CHOP, GADD34, XBP1, ATF3, and ATF4 in comparison to DMSO treated controls (data not shown). In contrast, the quantity of the UPR receptors themselves did not change as much. Intriguingly, all investigated cell lines showed different light to heavy ratios of the quantified proteins, again underling the marked heterogeneity of glioma cell line regarding the UPR pathways. The collaborative manuscript describing the successful development of the novel proteomic method to investigate the UPR and its validation in complex samples published (*240*).

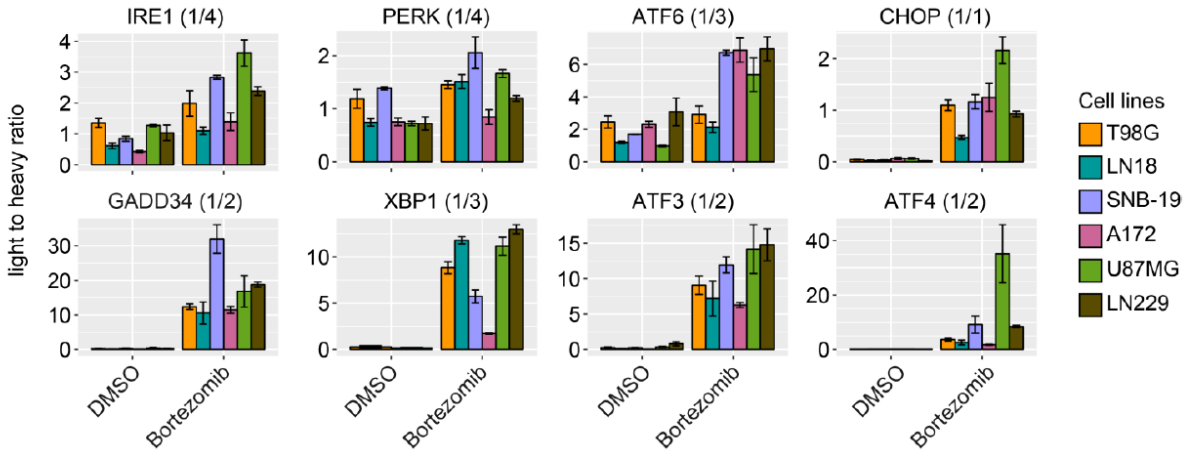

Figure 18- Targeted proteomics approach to quantify the majority of UPR proteins. The cell lines T98-G, LN-18, LN-229, SNB-19, A-172, and U-87 MG were treated with 1 nM of Bor for 24 h and subjected to analysis via targeted proteomics. The number in brackets illustrate that only one of X peptide ratios were plotted. (Figure from: Nguyen *et.* al, 2019 (Reference: *240*))

6. CONCLUSIONS AND OUTLOOK

Taken together, the results summarized in the first part of the thesis formed the basis for an extensive high-throughput molecular profiling study to elucidate the UPR in its comprehensiveness. It was observed, that the UPR responses of two very different cell lines, NIH/3T3 and LN-308, were at first sight comparable but in detail very different. In particular, the different *Xbp1s*/*XBP1s* and *Xbp1u*/*XBP1u* transcriptional profiles showed similarities, whereas the endogenous BIP protein level were different. The high-throughput data will answer questions on how the early UPR is regulated and which mRNAs and proteins are involved in the different stages of the evolving UPR.

In the second part of the thesis, potential mechanisms of how p53 could influence the UPR and the abundance of *Xbp1s* was investigated in *Tp53* knock-out murine NSC/NPC models. However, the hypothesis proposed in previous studies that p53 regulates IRE1α activity by altering the level of the co-chaperone DNAJB9, could not be proven in NSC/NPCs. Rather, this hypothesis had to be abandoned for NSC/NPCs since these cells did not show a reproducible downregulation of DNAJB9 under UPR induction in $Tp53^{\Delta 2\text{-}10/\Delta 2\text{-}10}$ NSC/NPCs. However, the hypothesis that p53 influences *Xbp1s* splicing needs further experimental studies since in NSC/NPCs with high p53 levels, the *Xbp1s* transcript decreased, which was not the case in NSC/NPCs with low p53 levels. *Tp53* and IDH mutations are not the only glioma associated alterations that may modulate the UPR. Another interesting candidate is the epidermal growth factor receptor (EGFR) gene, which is commonly amplified and overexpressed in IDH-wildtype glioblastomas (*225*). EGFR signaling may influence the UPR pathways which in turn could influence EGFR translation and plasma membrane translocation.

Additional experiments performed in this thesis evaluated possible influences of mutant IDH1 derived 2-HG on the UPR in NSC/NPCs. This metabolite induced the UPR pathway and when cells were pre-exposed to 2-HG, they were more resistant to viability decreases when additionally exposed to tunicamycin than without pre-exposition to 2-HG. Further experiments should be conducted to clarify molecular mechanisms underlying this interesting observation that might promote survival of IDH mutant NSC/NPCs and thereby facilitate glioma development.

Finally, treatment of several established human glioma cell lines with bortezomib did not show a striking decrease in viability. However, in cooperation with partners of the SUPR-G consortium, a sensitive and reliable identification and quantification technique for mass spectrometry was developed and validated in bortezomib treated glioma cell lines. Thereby, a marked increase of UPR proteins upon treatment of the cells with bortezomib was demonstrated, enabling further

and more thorough investigations of the involvement of the UPR in bortezomib treated tumor cells.

7. REFERENCES

1. E. R. Kastenhuber, S. W. Lowe, Putting p53 in Context. *Cell*. **170**, 1062–1078 (2017).
2. I. T. Gavrilovic, J. B. Posner, Brain metastases. *Journal of neuro-oncology*. **75**, 5–14 (2005).
3. M. Weller, W. Wick, K. Aldape, M. Brada, M. Berger, S. M. Pfister, R. Nishikawa, M. Rosenthal, P. Y. Wen, R. Stupp, G. Reifenberger, Glioma. *Nature Reviews Disease Primers*, 15017 (2015).
4. F. P. Barthel, P. Wesseling, R. G. W. Verhaak, Reconstructing the molecular life history of gliomas. *Acta neuropathologica*. **135**, 649–670 (2018).
5. H. Zong, L. F. Parada, S. J. Baker, Cell of origin for malignant gliomas and its implication in therapeutic development. *Cold Spring Harbor perspectives in biology*. **7** (2015).
6. D. N. Louis, A. Perry, G. Reifenberger, A. von Deimling, D. Figarella-Branger, W. K. Cavenee, H. Ohgaki, O. D. Wiestler, P. Kleihues, D. W. Ellison, The 2016 World Health Organization Classification of Tumors of the Central Nervous System. *Acta neuropathologica* (2016).
7. G. Reifenberger, H.-G. Wirsching, C. B. Knobbe-Thomsen, M. Weller, Advances in the molecular genetics of gliomas - implications for classification and therapy. *Nature reviews. Clinical oncology* (2016).
8. M. Weller, M. van den Bent, K. Hopkins, J. C. Tonn, R. Stupp, A. Falini, E. Cohen-Jonathan-Moyal, D. Frappaz, R. Henriksson, C. Balana, O. Chinot, Z. Ram, G. Reifenberger, R. Soffietti, W. Wick, EANO guideline for the diagnosis and treatment of anaplastic gliomas and glioblastoma. *The Lancet. Oncology*. **15**, e395-403 (2014).
9. M. R. Gilbert, M. Wang, K. D. Aldape, R. Stupp, M. E. Hegi, K. A. Jaeckle, T. S. Armstrong, J. S. Wefel, M. Won, D. T. Blumenthal, A. Mahajan, C. J. Schultz, S. Erridge, B. Baumert, K. I. Hopkins, T. Tzuk-Shina, P. D. Brown, A. Chakravarti, W. J. Curran, M. P. Mehta, Dose-dense temozolomide for newly diagnosed glioblastoma. *Journal of clinical oncology : official journal of the American Society of Clinical Oncology*. **31**, 4085–4091 (2013).
10. O. L. Chinot, W. Wick, W. Mason, R. Henriksson, F. Saran, R. Nishikawa, A. F. Carpentier, K. Hoang-Xuan, P. Kavan, D. Cernea, A. A. Brandes, M. Hilton, L. Abrey, T. Cloughesy, Bevacizumab plus radiotherapy-temozolomide for newly diagnosed glioblastoma. *N Engl J Med*. **370**, 709–722 (2014).
11. M. R. Gilbert, J. J. Dignam, T. S. Armstrong, J. S. Wefel, D. T. Blumenthal, M. A. Vogelbaum, H. Colman, A. Chakravarti, S. Pugh, M. Won, R. Jeraj, P. D. Brown, K. A. Jaeckle, D. Schiff, V. W. Stieber, D. G. Brachman, M. Werner-Wasik, I. W. Tremont-Lukats, E. P. Sulman, K. D. Aldape, W. J. Curran, M. P. Mehta, A randomized trial of bevacizumab for newly diagnosed glioblastoma. *N Engl J Med*. **370**, 699–708 (2014).
12. M. Sasaki, C. B. Knobbe, M. Itsumi, A. J. Elia, I. S. Harris, I. I. C. Chio, R. A. Cairns, S. McCracken, A. Wakeham, J. Haight, A. Y. Ten, B. Snow, T. Ueda, S. Inoue, K. Yamamoto, M. Ko, A. Rao, K. E.

Yen, S. M. Su, T. W. Mak, D-2-hydroxyglutarate produced by mutant IDH1 perturbs collagen maturation and basement membrane function. *Genes & Development*. **26**, 2038–2049 (2012).

13. T. Watanabe, S. Nobusawa, P. Kleihues, H. Ohgaki, IDH1 mutations are early events in the development of astrocytomas and oligodendrogliomas. *The American journal of pathology*. **174**, 1149–1153 (2009).
14. L. Dang, D. W. White, S. Gross, B. D. Bennett, M. A. Bittinger, E. M. Driggers, V. R. Fantin, H. G. Jang, S. Jin, M. C. Keenan, K. M. Marks, R. M. Prins, P. S. Ward, K. E. Yen, L. M. Liau, J. D. Rabinowitz, L. C. Cantley, C. B. Thompson, M. G. Vander Heiden, S. M. Su, Cancer-associated IDH1 mutations produce 2-hydroxyglutarate. *Nature*. **462**, 739–744 (2009).
15. H. Yan, D. W. Parsons, G. Jin, R. McLendon, B. A. Rasheed, W. Yuan, I. Kos, I. Batinic-Haberle, S. Jones, G. J. Riggins, H. Friedman, A. Friedman, D. Reardon, J. Herndon, K. W. Kinzler, V. E. Velculescu, B. Vogelstein, D. D. Bigner, IDH1 and IDH2 mutations in gliomas. *N Engl J Med*. **360**, 765–773 (2009).
16. J. Balss, J. Meyer, W. Mueller, A. Korshunov, C. Hartmann, A. von Deimling, Analysis of the IDH1 codon 132 mutation in brain tumors. *Acta neuropathologica*. **116**, 597–602 (2008).
17. T. Watanabe, A. Vital, S. Nobusawa, P. Kleihues, H. Ohgaki, Selective acquisition of IDH1 R132C mutations in astrocytomas associated with Li-Fraumeni syndrome. *Acta neuropathologica*. **117**, 653–656 (2009).
18. D. Krell, M. Assoku, M. Galloway, P. Mulholland, I. Tomlinson, C. Bardella, Screen for IDH1, IDH2, IDH3, D2HGDH and L2HGDH mutations in glioblastoma. *PloS one*. **6**, e19868 (2011).
19. Z. J. Reitman, H. Yan, Isocitrate dehydrogenase 1 and 2 mutations in cancer. *Journal of the National Cancer Institute*. **102**, 932–941 (2010).
20. W. Xu, H. Yang, Y. Liu, Y. Yang, P. Wang, S.-H. Kim, S. Ito, C. Yang, P. Wang, M.-T. Xiao, L.-x. Liu, W.-q. Jiang, J. Liu, J.-y. Zhang, B. Wang, S. Frye, Y. Zhang, Y.-h. Xu, Q.-y. Lei, K.-L. Guan, S.-m. Zhao, Y. Xiong, Oncometabolite 2-hydroxyglutarate is a competitive inhibitor of α-ketoglutarate-dependent dioxygenases. *Cancer cell*. **19**, 17–30 (2011).
21. S. Turcan, D. Rohle, A. Goenka, L. A. Walsh, F. Fang, E. Yilmaz, C. Campos, A. W. M. Fabius, C. Lu, P. S. Ward, C. B. Thompson, A. Kaufman, O. Guryanova, R. Levine, A. Heguy, A. Viale, L. G. T. Morris, J. T. Huse, I. K. Mellinghoff, T. A. Chan, IDH1 mutation is sufficient to establish the glioma hypermethylator phenotype. *Nature*. **483**, 479–483 (2012).
22. H. Noushmehr, D. J. Weisenberger, K. Diefes, H. S. Phillips, K. Pujara, B. P. Berman, F. Pan, C. E. Pelloski, E. P. Sulman, K. P. Bhat, R. G. W. Verhaak, K. A. Hoadley, D. N. Hayes, C. M. Perou, H. K. Schmidt, L. Ding, R. K. Wilson, D. van den Berg, H. Shen, H. Bengtsson, P. Neuvial, L. M. Cope, J. Buckley, J. G. Herman, S. B. Baylin, P. W. Laird, K. Aldape, Identification of a CpG island methylator phenotype that defines a distinct subgroup of glioma. *Cancer cell*. **17**, 510–522 (2010).

23. K. I. Kivirikko, R. Myllylä, T. Pihlajaniemi, Protein hydroxylation. *The FASEB Journal*. **3**, 1609–1617 (1989).
24. J. Myllyharju, K. I. Kivirikko, Collagens, modifying enzymes and their mutations in humans, flies and worms. *Trends in genetics : TIG*. **20**, 33–43 (2004).
25. C. Hetz, F. R. Papa, The Unfolded Protein Response and Cell Fate Control. *Molecular cell*. **69**, 169–181 (2018).
26. M. Weller, J. Felsberg, C. Hartmann, H. Berger, J. P. Steinbach, J. Schramm, M. Westphal, G. Schackert, M. Simon, J. C. Tonn, O. Heese, D. Krex, G. Nikkhah, T. Pietsch, O. Wiestler, G. Reifenberger, A. von Deimling, M. Loeffler, Molecular Predictors of Progression-Free and Overall Survival in Patients With Newly Diagnosed Glioblastoma. *Journal of Clinical Oncology*. **27**, 5743–5750 (2009).
27. A. Tovy, A. Spiro, R. McCarthy, Z. Shipony, Y. Aylon, K. Allton, E. Ainbinder, N. Furth, A. Tanay, M. Barton, M. Oren, p53 is essential for DNA methylation homeostasis in naïve embryonic stem cells, and its loss promotes clonal heterogeneity. *Genes Dev*. **31**, 959–972 (2017).
28. L. Jackson-Grusby, C. Beard, R. Possemato, M. Tudor, D. Fambrough, G. Csankovszki, J. Dausman, P. Lee, C. Wilson, E. Lander, R. Jaenisch, Loss of genomic methylation causes p53-dependent apoptosis and epigenetic deregulation. *Nature genetics*. **27**, 31–39 (2001).
29. D. Su, X. Wang, M. R. Campbell, L. Song, A. Safi, G. E. Crawford, D. A. Bell, Interactions of chromatin context, binding site sequence content, and sequence evolution in stress-induced p53 occupancy and transactivation. *PLoS genetics*. **11**, e1004885 (2015).
30. The Universal Protein Resource (UniProt). *Nucleic Acids Res*. **35**, D193-7 (2007).
31. D. P. Guimaraes, P. Hainaut, TP53. *Biochimie*. **84**, 83–93 (2002).
32. K. H. Vousden, C. Prives, Blinded by the Light. *Cell*. **137**, 413–431 (2009).
33. B. England, T. Huang, M. Karsy, Current understanding of the role and targeting of tumor suppressor p53 in glioblastoma multiforme. *Tumour biology : the journal of the International Society for Oncodevelopmental Biology and Medicine*. **34**, 2063–2074 (2013).
34. A. Zacher, K. Kaulich, S. Stepanow, M. Wolter, K. Köhrer, J. Felsberg, B. Malzkorn, G. Reifenberger, Molecular Diagnostics of Gliomas Using Next Generation Sequencing of a Glioma-Tailored Gene Panel. *Brain pathology (Zurich, Switzerland)*. **27**, 146–159 (2017).
35. A. N. Bullock, A. R. Fersht, Rescuing the function of mutant p53. *Nature reviews. Cancer*. **1**, 68–76 (2001).
36. Y. Cho, S. Gorina, P. D. Jeffrey, N. P. Pavletich, Crystal structure of a p53 tumor suppressor-DNA complex. *Science (New York, N.Y.)*. **265**, 346–355 (1994).
37. M. W. Frazier, X. He, J. Wang, Z. Gu, J. L. Cleveland, G. P. Zambetti, Activation of c-myc gene expression by tumor-derived p53 mutants requires a discrete C-terminal domain. *Mol Cell Biol*. **18**, 3735–3743 (1998).

38. S. Strano, S. Dell'Orso, S. Di Agostino, G. Fontemaggi, A. Sacchi, G. Blandino, Mutant p53. *Oncogene*. **26**, 2212–2219 (2007).
39. J. H. Ludes-Meyers, M. A. Subler, C. V. Shivakumar, R. M. Munoz, P. Jiang, J. E. Bigger, D. R. Brown, S. P. Deb, S. Deb, Transcriptional activation of the human epidermal growth factor receptor promoter by human p53. *Mol Cell Biol*. **16**, 6009–6019 (1996).
40. J. D. Oliner, K. W. Kinzler, P. S. Meltzer, D. L. George, B. Vogelstein, Amplification of a gene encoding a p53-associated protein in human sarcomas. *Nature*. **358**, 80–83 (1992).
41. Cancer Genome Atlas Research Network, Comprehensive genomic characterization defines human glioblastoma genes and core pathways. *Nature*. **455**, 1061–1068 (2008).
42. M. B. Kastan, O. Onyekwere, D. Sidransky, B. Vogelstein, R. W. Craig, Participation of p53 protein in the cellular response to DNA damage. *Cancer Res*. **51**, 6304–6311 (1991).
43. W. S. el-Deiry, T. Tokino, V. E. Velculescu, D. B. Levy, R. Parsons, J. M. Trent, D. Lin, W. E. Mercer, K. W. Kinzler, B. Vogelstein, WAF1, a potential mediator of p53 tumor suppression. *Cell*. **75**, 817–825 (1993).
44. J. W. Harper, G. R. Adami, N. Wei, K. Keyomarsi, S. J. Elledge, The p21 Cdk-interacting protein Cip1 is a potent inhibitor of G1 cyclin-dependent kinases. *Cell*. **75**, 805–816 (1993).
45. A. R. Clarke, C. A. Purdie, D. J. Harrison, R. G. Morris, C. C. Bird, M. L. Hooper, A. H. Wyllie, Thymocyte apoptosis induced by p53-dependent and independent pathways. *Nature*. **362**, 849–852 (1993).
46. S. W. Lowe, E. M. Schmitt, S. W. Smith, B. A. Osborne, T. Jacks, p53 is required for radiation-induced apoptosis in mouse thymocytes. *Nature*. **362**, 847–849 (1993).
47. E. Yonish-Rouach, D. Resnitzky, J. Lotem, L. Sachs, A. Kimchi, M. Oren, Wild-type p53 induces apoptosis of myeloid leukaemic cells that is inhibited by interleukin-6. *Nature*. **352**, 345–347 (1991).
48. T. Miyashita, S. Krajewski, M. Krajewska, H. G. Wang, H. K. Lin, D. A. Liebermann, B. Hoffman, J. C. Reed, Tumor suppressor p53 is a regulator of bcl-2 and bax gene expression in vitro and in vivo. *Oncogene*. **9**, 1799–1805 (1994).
49. R. Azzarelli, B. D. Simons, A. Philpott, The developmental origin of brain tumours. *Development (Cambridge, England)*. **145** (2018).
50. D. Friedmann-Morvinski, E. A. Bushong, E. Ke, Y. Soda, T. Marumoto, O. Singer, M. H. Ellisman, I. M. Verma, Dedifferentiation of neurons and astrocytes by oncogenes can induce gliomas in mice. *Science (New York, N.Y.)*. **338**, 1080–1084 (2012).
51. D. Tosoni, S. Zecchini, M. Coazzoli, I. Colaluca, G. Mazzarol, A. Rubio, M. Caccia, E. Villa, O. Zilian, P. P. Di Fiore, S. Pece, The Numb/p53 circuitry couples replicative self-renewal and tumor suppression in mammary epithelial cells. *J Cell Biol*. **211**, 845–862 (2015).
52. D. F. Tschaharganeh, W. Xue, D. F. Calvisi, M. Evert, T. V. Michurina, L. E. Dow, A. Banito, S. F. Katz, E. R. Kastenhuber, S. Weissmueller, C.-H. Huang, A. Lechel, J. B. Andersen, D. Capper, L.

Zender, T. Longerich, G. Enikolopov, S. W. Lowe, p53-dependent Nestin regulation links tumor suppression to cellular plasticity in liver cancer. *Cell*. **158**, 579–592 (2014).

53. Z. Zhao, J. Zuber, E. Diaz-Flores, L. Lintault, S. C. Kogan, K. Shannon, S. W. Lowe, p53 loss promotes acute myeloid leukemia by enabling aberrant self-renewal. *Genes Dev*. **24**, 1389–1402 (2010).
54. T. Bondar, R. Medzhitov, p53-mediated hematopoietic stem and progenitor cell competition. *Cell stem cell*. **6**, 309–322 (2010).
55. Y. Liu, S. E. Elf, Y. Miyata, G. Sashida, Y. Liu, G. Huang, S. Di Giandomenico, J. M. Lee, A. Deblasio, S. Menendez, J. Antipin, B. Reva, A. Koff, S. D. Nimer, p53 regulates hematopoietic stem cell quiescence. *Cell stem cell*. **4**, 37–48 (2009).
56. N. A. Charles, E. C. Holland, R. Gilbertson, R. Glass, H. Kettenmann, The brain tumor microenvironment. *Glia*. **59**, 1169–1180 (2011).
57. M. Assanah, R. Lochhead, A. Ogden, J. Bruce, J. Goldman, P. Canoll, Glial progenitors in adult white matter are driven to form malignant gliomas by platelet-derived growth factor-expressing retroviruses. *The Journal of neuroscience : the official journal of the Society for Neuroscience*. **26**, 6781–6790 (2006).
58. M. C. Assanah, J. N. Bruce, S. O. Suzuki, A. Chen, J. E. Goldman, P. Canoll, PDGF stimulates the massive expansion of glial progenitors in the neonatal forebrain. *Glia*. **57**, 1835–1847 (2009).
59. S. R. Chirasani, A. Sternjak, P. Wend, S. Momma, B. Campos, I. M. Herrmann, D. Graf, T. Mitsiadis, C. Herold-Mende, D. Besser, M. Synowitz, H. Kettenmann, R. Glass, Bone morphogenetic protein-7 release from endogenous neural precursor cells suppresses the tumourigenicity of stem-like glioblastoma cells. *Brain : a journal of neurology*. **133**, 1961–1972 (2010).
60. R. Glass, M. Synowitz, G. Kronenberg, J.-H. Walzlein, D. S. Markovic, L.-P. Wang, D. Gast, J. Kiwit, G. Kempermann, H. Kettenmann, Glioblastoma-induced attraction of endogenous neural precursor cells is associated with improved survival. *The Journal of neuroscience : the official journal of the Society for Neuroscience*. **25**, 2637–2646 (2005).
61. J.-H. Walzlein, M. Synowitz, B. Engels, D. S. Markovic, K. Gabrusiewicz, E. Nikolaev, K. Yoshikawa, B. Kaminska, G. Kempermann, W. Uckert, L. Kaczmarek, H. Kettenmann, R. Glass, The antitumorigenic response of neural precursors depends on subventricular proliferation and age. *Stem cells (Dayton, Ohio)*. **26**, 2945–2954 (2008).
62. D. S. Markovic, R. Glass, M. Synowitz, N. van Rooijen, H. Kettenmann, Microglia stimulate the invasiveness of glioma cells by increasing the activity of metalloprotease-2. *Journal of neuropathology and experimental neurology*. **64**, 754–762 (2005).
63. C. Calabrese, H. Poppleton, M. Kocak, T. L. Hogg, C. Fuller, B. Hamner, E. Y. Oh, M. W. Gaber, D. Finklestein, M. Allen, A. Frank, I. T. Bayazitov, S. S. Zakharenko, A. Gajjar, A. Davidoff, R. J. Gilbertson, A perivascular niche for brain tumor stem cells. *Cancer cell*. **11**, 69–82 (2007).

64. M. Höckel, K. Schlenger, S. Höckel, P. Vaupel, Hypoxic cervical cancers with low apoptotic index are highly aggressive. *Cancer Res*. **59**, 4525–4528 (1999).
65. M. Hockel, P. Vaupel, Tumor Hypoxia. *JNCI Journal of the National Cancer Institute*. **93**, 266–276 (2001).
66. S. Joshi, T. Wang, T. L. S. Araujo, S. Sharma, J. L. Brodsky, G. Chiosis, Adapting to stress - chaperome networks in cancer. *Nature reviews. Cancer* (2018).
67. R. Bravo, V. Parra, D. Gatica, A. E. Rodriguez, N. Torrealba, F. Paredes, Z. V. Wang, A. Zorzano, J. A. Hill, E. Jaimovich, A. F.G. Quest, S. Lavandero, in *International Review of Cell and Molecular Biology*, International Review of Cell and Molecular Biology, K. W. Jeon, ed. (Elsevier Science, Burlington, 2013), pp. 215–290.
68. E. Dufey, H. Urra, C. Hetz, ER proteostasis addiction in cancer biology. *Seminars in cancer biology*. **33**, 40–47 (2015).
69. W. E. Balch, R. I. Morimoto, A. Dillin, J. W. Kelly, Adapting proteostasis for disease intervention. *Science (New York, N.Y.)*. **319**, 916–919 (2008).
70. F. Prischi, P. R. Nowak, M. Carrara, M. M. U. Ali, Phosphoregulation of Ire1 RNase splicing activity. *Nature communications*. **5**, 3554 (2014).
71. G. Lu, A. Ota, S. Ren, S. Franklin, C. D. Rau, P. Ping, T. F. Lane, Z. H. Zhou, K. Reue, A. J. Lusis, T. Vondriska, Y. Wang, PPM1l encodes an inositol requiring-protein 1 (IRE1) specific phosphatase that regulates the functional outcome of the ER stress response. *Molecular metabolism*. **2**, 405–416 (2013).
72. Q. Qiu, Z. Zheng, L. Chang, Y.-S. Zhao, C. Tan, A. Dandekar, Z. Zhang, Z. Lin, M. Gui, X. Li, T. Zhang, Q. Kong, H. Li, S. Chen, A. Chen, R. J. Kaufman, W.-L. Yang, H.-K. Lin, D. Zhang, H. Perlman, E. Thorp, K. Zhang, D. Fang, Toll-like receptor-mediated IRE1α activation as a therapeutic target for inflammatory arthritis. *Embo j*. **32**, 2477–2490 (2013).
73. Y. Qiu, T. Mao, Y. Zhang, M. Shao, J. You, Q. Ding, Y. Chen, D. Wu, D. Xie, X. Lin, X. Gao, R. J. Kaufman, W. Li, Y. Liu, A crucial role for RACK1 in the regulation of glucose-stimulated IRE1alpha activation in pancreatic beta cells. *Science signaling*. **3**, ra7 (2010).
74. T. Tomoyasu, T. Ogura, T. Tatsuta, B. Bukau, Levels of DnaK and DnaJ provide tight control of heat shock gene expression and protein repair in Escherichia coli. *Mol Microbiol*. **30**, 567–581 (1998).
75. K. Abravaya, M. P. Myers, S. P. Murphy, R. I. Morimoto, The human heat shock protein hsp70 interacts with HSF, the transcription factor that regulates heat shock gene expression. *Genes Dev*. **6**, 1153–1164 (1992).
76. C. Y. Liu, M. Schröder, R. J. Kaufman, Ligand-independent dimerization activates the stress response kinases IRE1 and PERK in the lumen of the endoplasmic reticulum. *J Biol Chem*. **275**, 24881–24885 (2000).

77. J. Zhou, C. Y. Liu, S. H. Back, R. L. Clark, D. Peisach, Z. Xu, R. J. Kaufman, The crystal structure of human IRE1 luminal domain reveals a conserved dimerization interface required for activation of the unfolded protein response. *Proc Natl Acad Sci U S A*. **103**, 14343–14348 (2006).
78. B. M. Gardner, P. Walter, Unfolded proteins are Ire1-activating ligands that directly induce the unfolded protein response. *Science (New York, N.Y.)*. **333**, 1891–1894 (2011).
79. N. Amin-Wetzel, R. A. Saunders, M. J. Kamphuis, C. Rato, S. Preissler, H. P. Harding, D. Ron, A J-Protein Co-chaperone Recruits BiP to Monomerize IRE1 and Repress the Unfolded Protein Response. *Cell* (2017).
80. A. V. Korennykh, P. F. Egea, A. A. Korostelev, J. Finer-Moore, C. Zhang, K. M. Shokat, R. M. Stroud, P. Walter, The unfolded protein response signals through high-order assembly of Ire1. *Nature*. **457**, 687–693 (2009).
81. J. Peschek, D. Acosta-Alvear, A. S. Mendez, P. Walter, A conformational RNA zipper promotes intron ejection during non-conventional XBP1 mRNA splicing. *EMBO reports*. **16**, 1688–1698 (2015).
82. H. Yoshida, T. Matsui, A. Yamamoto, T. Okada, K. Mori, XBP1 mRNA Is Induced by ATF6 and Spliced by IRE1 in Response to ER Stress to Produce a Highly Active Transcription Factor. *Cell*. **107**, 881–891 (2001).
83. C. Hetz, The unfolded protein response. *Nature reviews. Molecular cell biology*. **13**, 89–102 (2012).
84. D. Acosta-Alvear, Y. Zhou, A. Blais, M. Tsikitis, N. H. Lents, C. Arias, C. J. Lennon, Y. Kluger, B. D. Dynlacht, XBP1 controls diverse cell type- and condition-specific transcriptional regulatory networks. *Molecular cell*. **27**, 53–66 (2007).
85. A.-H. Lee, N. N. Iwakoshi, L. H. Glimcher, XBP-1 Regulates a Subset of Endoplasmic Reticulum Resident Chaperone Genes in the Unfolded Protein Response. *Mol Cell Biol*. **23**, 7448–7459 (2003).
86. J. Hollien, J. S. Weissman, Decay of endoplasmic reticulum-localized mRNAs during the unfolded protein response. *Science (New York, N.Y.)*. **313**, 104–107 (2006).
87. D. Han, A. G. Lerner, L. Vande Walle, J.-P. Upton, W. Xu, A. Hagen, B. J. Backes, S. A. Oakes, F. R. Papa, IRE1alpha kinase activation modes control alternate endoribonuclease outputs to determine divergent cell fates. *Cell*. **138**, 562–575 (2009).
88. J. Hollien, J. H. Lin, H. Li, N. Stevens, P. Walter, J. S. Weissman, Regulated Ire1-dependent decay of messenger RNAs in mammalian cells. *J Cell Biol*. **186**, 323–331 (2009).
89. J. Iqbal, K. Dai, T. Seimon, R. Jungreis, M. Oyadomari, G. Kuriakose, D. Ron, I. Tabas, M. M. Hussain, IRE1beta inhibits chylomicron production by selectively degrading MTP mRNA. *Cell Metabolism*. **7**, 445–455 (2008).

90. P. Kimmig, M. Diaz, J. Zheng, C. C. Williams, A. Lang, T. Aragón, H. Li, P. Walter, The unfolded protein response in fission yeast modulates stability of select mRNAs to maintain protein homeostasis. *eLife*. **1**, e00048 (2012).
91. M. Safra, S. Ben-Hamo, C. Kenyon, S. Henis-Korenblit, The ire-1 ER stress-response pathway is required for normal secretory-protein metabolism in C. elegans. *J Cell Sci*. **126**, 4136–4146 (2013).
92. M. Maurel, E. Chevet, J. Tavernier, S. Gerlo, Getting RIDD of RNA. *Trends in biochemical sciences*. **39**, 245–254 (2014).
93. P. Hu, Z. Han, A. D. Couvillon, R. J. Kaufman, J. H. Exton, Autocrine tumor necrosis factor alpha links endoplasmic reticulum stress to the membrane death receptor pathway through IRE1alpha-mediated NF-kappaB activation and down-regulation of TRAF2 expression. *Mol Cell Biol*. **26**, 3071–3084 (2006).
94. D. T. Nguyên, S. Kebache, A. Fazel, H. N. Wong, S. Jenna, A. Emadali, E.-H. Lee, J. J. M. Bergeron, R. J. Kaufman, L. Larose, E. Chevet, Nck-dependent activation of extracellular signal-regulated kinase-1 and regulation of cell survival during endoplasmic reticulum stress. *Mol Biol Cell*. **15**, 4248–4260 (2004).
95. F. Urano, X. Wang, A. Bertolotti, Y. Zhang, P. Chung, H. P. Harding, D. Ron, Coupling of stress in the ER to activation of JNK protein kinases by transmembrane protein kinase IRE1. *Science (New York, N.Y.)*. **287**, 664–666 (2000).
96. X. Zhu, J. Zhang, H. Sun, C. Jiang, Y. Dong, Q. Shan, S. Su, Y. Xie, N. Xu, X. Lou, S. Liu, Ubiquitination of inositol-requiring enzyme 1 (IRE1) by the E3 ligase CHIP mediates the IRE1/TRAF2/JNK pathway. *J Biol Chem*. **289**, 30567–30577 (2014).
97. S. B. Stephens, R. D. Dodd, J. W. Brewer, P. J. Lager, J. D. Keene, C. V. Nicchitta, Stable ribosome binding to the endoplasmic reticulum enables compartment-specific regulation of mRNA translation. *Mol Biol Cell*. **16**, 5819–5831 (2005).
98. K. Yanagitani, Y. Imagawa, T. Iwawaki, A. Hosoda, M. Saito, Y. Kimata, K. Kohno, Cotranslational targeting of XBP1 protein to the membrane promotes cytoplasmic splicing of its own mRNA. *Molecular cell*. **34**, 191–200 (2009).
99. S. Kanda, K. Yanagitani, Y. Yokota, Y. Esaki, K. Kohno, Autonomous translational pausing is required for XBP1u mRNA recruitment to the ER via the SRP pathway. *Proc Natl Acad Sci U S A*. **113**, E5886-E5895 (2016).
100. C.-y. Chen, N. S. Malchus, B. Hehn, W. Stelzer, D. Avci, D. Langosch, M. K. Lemberg, Signal peptide peptidase functions in ERAD to cleave the unfolded protein response regulator XBP1u. *Embo j*. **33**, 2492–2506 (2014).
101. N. A. Kulak, G. Pichler, I. Paron, N. Nagaraj, M. Mann, Minimal, encapsulated proteomic-sample processing applied to copy-number estimation in eukaryotic cells. *Nature methods*. **11**, 319–324 (2014).

102. R. Plumb, Z.-R. Zhang, S. Appathurai, M. Mariappan, A functional link between the co-translational protein translocation pathway and the UPR. *eLife*. **4** (2015).

103. N. Donnelly, A. M. Gorman, S. Gupta, A. Samali, The eIF2α kinases. *Cell Mol Life Sci*. **70**, 3493–3511 (2013).

104. K. Ma, K. M. Vattem, R. C. Wek, Dimerization and release of molecular chaperone inhibition facilitate activation of eukaryotic initiation factor-2 kinase in response to endoplasmic reticulum stress. *J Biol Chem*. **277**, 18728–18735 (2002).

105. A. G. Hinnebusch, eIF2alpha kinases provide a new solution to the puzzle of substrate specificity. *Nature structural & molecular biology*. **12**, 835–838 (2005).

106. S. B. Cullinan, D. Zhang, M. Hannink, E. Arvisais, R. J. Kaufman, J. A. Diehl, Nrf2 is a direct PERK substrate and effector of PERK-dependent cell survival. *Mol Cell Biol*. **23**, 7198–7209 (2003).

107. W. Zhang, V. Hietakangas, S. Wee, S. C. Lim, J. Gunaratne, S. M. Cohen, ER stress potentiates insulin resistance through PERK-mediated FOXO phosphorylation. *Genes Dev*. **27**, 441–449 (2013).

108. A. G. Rowlands, K. S. Montine, E. C. Henshaw, R. Panniers, Physiological stresses inhibit guanine-nucleotide-exchange factor in Ehrlich cells. *Eur J Biochem*. **175**, 93–99 (1988).

109. D. Scheuner, B. Song, E. McEwen, C. Liu, R. Laybutt, P. Gillespie, T. Saunders, S. Bonner-Weir, R. J. Kaufman, Translational control is required for the unfolded protein response and in vivo glucose homeostasis. *Molecular cell*. **7**, 1165–1176 (2001).

110. Y. Ma, L. M. Hendershot, Delineation of a negative feedback regulatory loop that controls protein translation during endoplasmic reticulum stress. *J Biol Chem*. **278**, 34864–34873 (2003).

111. P. D. Lu, H. P. Harding, D. Ron, Translation reinitiation at alternative open reading frames regulates gene expression in an integrated stress response. *J Cell Biol*. **167**, 27–33 (2004).

112. H. Urra, E. Dufey, F. Lisbona, D. Rojas-Rivera, C. Hetz, When ER stress reaches a dead end. *Biochimica et biophysica acta*. **1833**, 3507–3517 (2013).

113. L. R. Palam, T. D. Baird, R. C. Wek, Phosphorylation of eIF2 facilitates ribosomal bypass of an inhibitory upstream ORF to enhance CHOP translation. *J Biol Chem*. **286**, 10939–10949 (2011).

114. I. P. Barbosa-Tessmann, C. Chen, C. Zhong, S. M. Schuster, H. S. Nick, M. S. Kilberg, Activation of the unfolded protein response pathway induces human asparagine synthetase gene expression. *J Biol Chem*. **274**, 31139–31144 (1999).

115. A. Marchand, C. Tomkiewicz, L. Magne, R. Barouki, M. Garlatti, Endoplasmic reticulum stress induction of insulin-like growth factor-binding protein-1 involves ATF4. *J Biol Chem*. **281**, 19124–19133 (2006).

116. H. P. Harding, Y. Zhang, D. Scheuner, J.-J. Chen, R. J. Kaufman, D. Ron, Ppp1r15 gene knockout reveals an essential role for translation initiation factor 2 alpha (eIF2alpha) dephosphorylation in mammalian development. *Proc Natl Acad Sci U S A*. **106**, 1832–1837 (2009).

117. J. Shen, X. Chen, L. Hendershot, R. Prywes, ER Stress Regulation of ATF6 Localization by Dissociation of BiP/GRP78 Binding and Unmasking of Golgi Localization Signals. *Developmental Cell*. **3**, 99–111 (2002).

118. D. J. Thuerauf, L. Morrison, C. C. Glembotski, Opposing roles for ATF6alpha and ATF6beta in endoplasmic reticulum stress response gene induction. *The Journal of Biological Chemistry*. **279**, 21078–21084 (2004).

119. S. Nadanaka, T. Okada, H. Yoshida, K. Mori, Role of disulfide bridges formed in the luminal domain of ATF6 in sensing endoplasmic reticulum stress. *Mol Cell Biol*. **27**, 1027–1043 (2007).

120. K. Haze, H. Yoshida, H. Yanagi, T. Yura, K. Mori, Mammalian transcription factor ATF6 is synthesized as a transmembrane protein and activated by proteolysis in response to endoplasmic reticulum stress. *Mol Biol Cell*. **10**, 3787–3799 (1999).

121. A. Higa, S. Taouji, S. Lhomond, D. Jensen, M. E. Fernandez-Zapico, J. C. Simpson, J.-M. Pasquet, R. Schekman, E. Chevet, Endoplasmic reticulum stress-activated transcription factor ATF6alpha requires the disulfide isomerase PDIA5 to modulate chemoresistance. *Mol Cell Biol*. **34**, 1839–1849 (2014).

122. M. Hong, S. Luo, P. Baumeister, J.-M. Huang, R. K. Gogia, M. Li, A. S. Lee, Underglycosylation of ATF6 as a novel sensing mechanism for activation of the unfolded protein response. *The Journal of Biological Chemistry*. **279**, 11354–11363 (2004).

123. J. M. Lynch, M. Maillet, D. Vanhoutte, A. Schloemer, M. A. Sargent, N. S. Blair, K. A. Lynch, T. Okada, B. J. Aronow, H. Osinska, R. Prywes, J. N. Lorenz, K. Mori, J. Lawler, J. Robbins, J. D. Molkentin, A thrombospondin-dependent pathway for a protective ER stress response. *Cell*. **149**, 1257–1268 (2012).

124. D. M. Schewe, J. A. Aguirre-Ghiso, ATF6alpha-Rheb-mTOR signaling promotes survival of dormant tumor cells in vivo. *Proc Natl Acad Sci U S A*. **105**, 10519–10524 (2008).

125. J. Maiuolo, S. Bulotta, C. Verderio, R. Benfante, N. Borgese, Selective activation of the transcription factor ATF6 mediates endoplasmic reticulum proliferation triggered by a membrane protein. *Proceedings of the National Academy of Sciences of the United States of America*. **108**, 7832–7837 (2011).

126. A. J. Schindler, R. Schekman, In vitro reconstitution of ER-stress induced ATF6 transport in COPII vesicles. *Proceedings of the National Academy of Sciences of the United States of America*. **106**, 17775–17780 (2009).

127. S. G. Fonseca, S. Ishigaki, C. M. Oslowski, S. Lu, K. L. Lipson, R. Ghosh, E. Hayashi, H. Ishihara, Y. Oka, M. A. Permutt, F. Urano, Wolfram syndrome 1 gene negatively regulates ER stress signaling in rodent and human cells. *The Journal of clinical investigation*. **120**, 744–755 (2010).

128. J. Ye, R. B. Rawson, R. Komuro, X. Chen, U. P. Davé, R. Prywes, M. S. Brown, J. L. Goldstein, ER Stress Induces Cleavage of Membrane-Bound ATF6 by the Same Proteases that Process SREBPs. *Molecular cell*. **6**, 1355–1364 (2000).

129. M. Llarena, D. Bailey, H. Curtis, P. O.' Hare, Different Mechanisms of Recognition and ER Retention by Transmembrane Transcription Factors CREB-H and ATF6. *Traffic*. **11**, 48–69 (2010).

130. D. Guan, H. Wang, V. E. Li, Y. Xu, M. Yang, Z. Shen, N-glycosylation of ATF6beta is essential for its proteolytic cleavage and transcriptional repressor function to ATF6alpha. *Journal of cellular biochemistry*. **108**, 825–831 (2009).

131. H. Yoshida, K. Haze, H. Yanagi, T. Yura, K. Mori, Identification of the cis-Acting Endoplasmic Reticulum Stress Response Element Responsible for Transcriptional Induction of Mammalian Glucose-regulated Proteins; 1999. *The Journal of Biological Chemistry*. **1998**, 33741–33749 (1998).

132. B. Roy, A. S. Lee, Transduction of calcium stress through interaction of the human transcription factor CBF with the proximal CCAAT regulatory element of the grp78/BiP promoter. *Mol Cell Biol*. **15**, 2263–2274 (1995).

133. B. Roy, W. W. Li, A. S. Lee, Calcium-sensitive transcriptional activation of the proximal CCAAT regulatory element of the grp78/BiP promoter by the human nuclear factor CBF/NF-Y. *The Journal of Biological Chemistry*. **271**, 28995–29002 (1996).

134. D. J. Thuerauf, L. E. Morrison, H. Hoover, C. C. Glembotski, Coordination of ATF6-mediated transcription and ATF6 degradation by a domain that is shared with the viral transcription factor, VP16. *The Journal of Biological Chemistry*. **277**, 20734–20739 (2002).

135. P. J. Belmont, A. Tadimalla, W. J. Chen, J. J. Martindale, D. J. Thuerauf, M. Marcinko, N. Gude, M. A. Sussman, C. C. Glembotski, Coordination of growth and endoplasmic reticulum stress signaling by regulator of calcineurin 1 (RCAN1), a novel ATF6-inducible gene. *J Biol Chem*. **283**, 14012–14021 (2008).

136. H. Yoshida, T. Okada, K. Haze, H. Yanagi, T. Yura, M. Negishi, K. Mori, ATF6 activated by proteolysis binds in the presence of NF-Y (CBF) directly to the cis-acting element responsible for the mammalian unfolded protein response. *Mol Cell Biol*. **20**, 6755–6767 (2000).

137. H. Yoshida, T. Okada, K. Haze, H. Yanagi, T. Yura, M. Negishi, K. Mori, Endoplasmic reticulum stress-induced formation of transcription factor complex ERSF including NF-Y (CBF) and activating transcription factors 6alpha and 6beta that activates the mammalian unfolded protein response. *Mol Cell Biol*. **21**, 1239–1248 (2001).

138. J. Rao, S. Yue, Y. Fu, J. Zhu, X. Wang, R. W. Busuttil, J. W. Kupiec-Weglinski, L. Lu, Y. Zhai, ATF6 mediates a pro-inflammatory synergy between ER stress and TLR activation in the pathogenesis of liver ischemia-reperfusion injury. *American journal of transplantation : official journal of the American Society of Transplantation and the American Society of Transplant Surgeons*. **14**, 1552–1561 (2014).

139. A. Shkoda, P. A. Ruiz, H. Daniel, S. C. Kim, G. Rogler, R. B. Sartor, D. Haller, Interleukin-10 blocked endoplasmic reticulum stress in intestinal epithelial cells. *Gastroenterology*. **132**, 190–207 (2007).

140. T. Odisho, L. Zhang, A. Volchuk, ATF6β regulates the Wfs1 gene and has a cell survival role in the ER stress response in pancreatic β-cells. *Experimental cell research*. **330**, 111–122 (2015).

141. M. D. Shoulders, L. M. Ryno, J. C. Genereux, J. J. Moresco, P. G. Tu, C. Wu, J. R. Yates, A. I. Su, J. W. Kelly, R. L. Wiseman, Stress-independent activation of XBP1s and/or ATF6 reveals three functionally diverse ER proteostasis environments. *Cell reports*. **3**, 1279–1292 (2013).

142. D. L. Howarth, C. Lindtner, A. M. Vacaru, R. Sachidanandam, O. Tsedensodnom, T. Vasilkova, C. Buettner, K. C. Sadler, Activating transcription factor 6 is necessary and sufficient for alcoholic fatty liver disease in zebrafish. *PLoS genetics*. **10**, e1004335 (2014).

143. K. Nakanishi, T. Sudo, N. Morishima, Endoplasmic reticulum stress signaling transmitted by ATF6 mediates apoptosis during muscle development. *J Cell Biol*. **169**, 555–560 (2005).

144. D. J. Thuerauf, H. Hoover, J. Meller, J. Hernandez, L. Su, C. Andrews, W. H. Dillmann, P. M. McDonough, C. C. Glembotski, Sarco/endoplasmic reticulum calcium ATPase-2 expression is regulated by ATF6 during the endoplasmic reticulum stress response. *The Journal of Biological Chemistry*. **276**, 48309–48317 (2001).

145. S. H. Kasper, M. R. Spalinger, T. Raselli, M. Scharl, A cell type-specific role of protein tyrosine phosphatase non-receptor type 2 in regulating ER stress signalling. *Digestion*. **91**, 248–256 (2015).

146. R. van Huizen, J. L. Martindale, M. Gorospe, N. J. Holbrook, P58IPK, a novel endoplasmic reticulum stress-inducible protein and potential negative regulator of eIF2alpha signaling. *The Journal of Biological Chemistry*. **278**, 15558–15564 (2003).

147. D. T. Rutkowski, S.-W. Kang, A. G. Goodman, J. L. Garrison, J. Taunton, M. G. Katze, R. J. Kaufman, R. S. Hegde, The role of p58IPK in protecting the stressed endoplasmic reticulum. *Mol Biol Cell*. **18**, 3681–3691 (2007).

148. K. Yamamoto, T. Sato, T. Matsui, M. Sato, T. Okada, H. Yoshida, A. Harada, K. Mori, Transcriptional induction of mammalian ER quality control proteins is mediated by single or combined action of ATF6alpha and XBP1. *Developmental Cell*. **13**, 365–376 (2007).

149. M. Li, P. Baumeister, B. Roy, T. Phan, D. Foti, S. Luo, A. S. Lee, ATF6 as a transcription activator of the endoplasmic reticulum stress element. *Mol Cell Biol*. **20**, 5096–5106 (2000).

150. R. Luo, J.-F. Lu, Q. Hu, S. N. Maity, CBF/NF-Y controls endoplasmic reticulum stress induced transcription through recruitment of both ATF6(N) and TBP. *Journal of cellular biochemistry*. **104**, 1708–1723 (2008).

151. J. Han, S. H. Back, J. Hur, Y.-H. Lin, R. Gildersleeve, J. Shan, C. L. Yuan, D. Krokowski, S. Wang, M. Hatzoglou, M. S. Kilberg, M. A. Sartor, R. J. Kaufman, ER-stress-induced transcriptional regulation increases protein synthesis leading to cell death. *Nature cell biology*. **15**, 481–490 (2013).

152. T. Hai, T. Curran, Cross-family dimerization of transcription factors Fos/Jun and ATF/CREB alters DNA binding specificity. *Proc Natl Acad Sci U S A*. **88**, 3720–3724 (1991).

153. M. Vallejo, D. Ron, C. P. Miller, J. F. Habener, C/ATF, a member of the activating transcription factor family of DNA-binding proteins, dimerizes with CAAT/enhancer-binding proteins and directs their binding to cAMP response elements. *Proc Natl Acad Sci U S A*. **90**, 4679–4683 (1993).

154. C. R. Vinson, T. Hai, S. M. Boyd, Dimerization specificity of the leucine zipper-containing bZIP motif on DNA binding. *Genes Dev*. **7**, 1047–1058 (1993).

155. K. Ameri, A. L. Harris, Activating transcription factor 4. *The International Journal of Biochemistry & Cell Biology*. **40**, 14–21 (2008).

156. P. Gade, S. B. Manjegowda, S. C. Nallar, U. B. Maachani, A. S. Cross, D. V. Kalvakolanu, Regulation of the death-associated protein kinase 1 expression and autophagy via ATF6 requires apoptosis signal-regulating kinase 1. *Mol Cell Biol*. **34**, 4033–4048 (2014).

157. J. Lee, C. Sun, Y. Zhou, J. Lee, D. Gokalp, H. Herrema, S. W. Park, R. J. Davis, U. Ozcan, p38 MAPK-mediated regulation of Xbp1s is crucial for glucose homeostasis. *Nature medicine*. **17**, 1251–1260 (2011).

158. F.-M. Wang, Y.-J. Chen, H.-J. Ouyang, Regulation of unfolded protein response modulator XBP1s by acetylation and deacetylation. *The Biochemical journal*. **433**, 245–252 (2011).

159. H. Chen, L. Qi, SUMO modification regulates the transcriptional activity of XBP1. *The Biochemical journal*. **429**, 95–102 (2010).

160. N. M. Penaranda Fajardo, C. Meijer, F. A. E. Kruyt, The endoplasmic reticulum stress/unfolded protein response in gliomagenesis, tumor progression and as a therapeutic target in glioblastoma. *Biochemical pharmacology*. **118**, 1–8 (2016).

161. M. Wang, R. J. Kaufman, The impact of the endoplasmic reticulum protein-folding environment on cancer development. *Nature reviews. Cancer*. **14**, 581–597 (2014).

162. E. Chevet, C. Hetz, A. Samali, Endoplasmic reticulum stress-activated cell reprogramming in oncogenesis. *Cancer discovery*. **5**, 586–597 (2015).

163. Z. Lu, L. Zhou, P. Killela, A. B. Rasheed, C. Di, W. E. Poe, R. E. McLendon, D. D. Bigner, C. Nicchitta, H. Yan, Glioblastoma proto-oncogene SEC61gamma is required for tumor cell

survival and response to endoplasmic reticulum stress. *Cancer research*. **69**, 9105–9111 (2009).

164. B. Drogat, P. Auguste, D. T. Nguyen, M. Bouchecareilh, R. Pineau, J. Nalbantoglu, R. J. Kaufman, E. Chevet, A. Bikfalvi, M. Moenner, IRE1 signaling is essential for ischemia-induced vascular endothelial growth factor-A expression and contributes to angiogenesis and tumor growth in vivo. *Cancer Res*. **67**, 6700–6707 (2007).

165. X. Chen, D. Iliopoulos, Q. Zhang, Q. Tang, M. B. Greenblatt, M. Hatziapostolou, E. Lim, W. L. Tam, M. Ni, Y. Chen, J. Mai, H. Shen, D. Z. Hu, S. Adoro, B. Hu, M. Song, C. Tan, M. D. Landis, M. Ferrari, S. J. Shin, M. Brown, J. C. Chang, X. S. Liu, L. H. Glimcher, XBP1 promotes triple-negative breast cancer by controlling the HIF1α pathway. *Nature*. **508**, 103–107 (2014).

166. Y. Wang, G. N. Alam, Y. Ning, F. Visioli, Z. Dong, J. E. Nör, P. J. Polverini, The unfolded protein response induces the angiogenic switch in human tumor cells through the PERK/ATF4 pathway. *Cancer Res*. **72**, 5396–5406 (2012).

167. G. Auf, A. Jabouille, S. Guerit, R. Pineau, M. Delugin, M. Bouchecareilh, N. Magnin, A. Favereaux, M. Maitre, T. Gaiser, A. von Deimling, M. Czabanka, P. Vajkoczy, E. Chevet, A. Bikfalvi, M. Moenner, Inositol-requiring enzyme 1alpha is a key regulator of angiogenesis and invasion in malignant glioma. *Proc Natl Acad Sci U S A*. **107**, 15553–15558 (2010).

168. L. M. Epple, R. D. Dodd, A. L. Merz, A. M. Dechkovskaia, M. Herring, B. A. Winston, A. M. Lencioni, R. L. Russell, H. Madsen, M. Nega, N. L. Dusto, J. White, D. D. Bigner, C. V. Nicchitta, N. J. Serkova, M. W. Graner, Induction of the unfolded protein response drives enhanced metabolism and chemoresistance in glioma cells. *PloS one*. **8**, e73267 (2013).

169. X. Hou, Y. Liu, H. Liu, X. Chen, M. Liu, H. Che, F. Guo, C. Wang, D. Zhang, J. Wu, X. Chen, C. Shen, C. Li, F. Peng, Y. Bi, Z. Yang, G. Yang, J. Ai, X. Gao, S. Zhao, PERK silence inhibits glioma cell growth under low glucose stress by blockage of p-AKT and subsequent HK2's mitochondria translocation. *Scientific reports*. **5**, 9065 (2015).

170. S. Gandolfi, J. P. Laubach, T. Hideshima, D. Chauhan, K. C. Anderson, P. G. Richardson, The proteasome and proteasome inhibitors in multiple myeloma. *Cancer metastasis reviews*. **36**, 561–584 (2017).

171. M. Ri, Endoplasmic-reticulum stress pathway-associated mechanisms of action of proteasome inhibitors in multiple myeloma. *International journal of hematology*. **104**, 273–280 (2016).

172. N. Nikesitch, J. M. Lee, S. Ling, T. L. Roberts, Endoplasmic reticulum stress in the development of multiple myeloma and drug resistance. *Clinical & translational immunology*. **7**, e1007 (2018).

173. T. H. Landowski, C. J. Megli, K. D. Nullmeyer, R. M. Lynch, R. T. Dorr, Mitochondrial-mediated disregulation of Ca2+ is a critical determinant of Velcade (PS-341/bortezomib) cytotoxicity in myeloma cell lines. *Cancer Res*. **65**, 3828–3836 (2005).

174. J. J. Raizer, J. P. Chandler, R. Ferrarese, S. A. Grimm, R. M. Levy, K. Muro, J. Rosenow, I. Helenowski, A. Rademaker, M. Paton, M. Bredel, A phase II trial evaluating the effects and intra-tumoral penetration of bortezomib in patients with recurrent malignant gliomas. *Journal of neuro-oncology*. **129**, 139–146 (2016).

175. D. J. McCracken, E. C. Celano, A. D. Voloschin, W. L. Read, J. J. Olson, Phase I trial of dose-escalating metronomic temozolomide plus bevacizumab and bortezomib for patients with recurrent glioblastoma. *Journal of neuro-oncology*. **130**, 193–201 (2016).

176. A. Kardosh, E. B. Golden, P. Pyrko, J. Uddin, F. M. Hofman, T. C. Chen, S. G. Louie, N. A. Petasis, A. H. Schönthal, Aggravated endoplasmic reticulum stress as a basis for enhanced glioblastoma cell killing by bortezomib in combination with celecoxib or its non-coxib analogue, 2,5-dimethyl-celecoxib. *Cancer Res*. **68**, 843–851 (2008).

177. P. Pyrko, A. H. Schönthal, F. M. Hofman, T. C. Chen, A. S. Lee, The unfolded protein response regulator GRP78/BiP as a novel target for increasing chemosensitivity in malignant gliomas. *Cancer Res*. **67**, 9809–9816 (2007).

178. T. C. Chen, W. Wang, E. B. Golden, S. Thomas, W. Sivakumar, F. M. Hofman, S. G. Louie, A. H. Schönthal, Green tea epigallocatechin gallate enhances therapeutic efficacy of temozolomide in orthotopic mouse glioblastoma models. *Cancer letters*. **302**, 100–108 (2011).

179. S. Sun, D. Lee, A. S. W. Ho, J. K. S. Pu, X. Q. Zhang, N. P. Lee, P. J. R. Day, W. M. Lui, C. F. Fung, G. K. K. Leung, Inhibition of prolyl 4-hydroxylase, beta polypeptide (P4HB) attenuates temozolomide resistance in malignant glioma via the endoplasmic reticulum stress response (ERSR) pathways. *Neuro-Oncology*. **15**, 562–577 (2013).

180. K. Suzuki, A. Gerelchuluun, Z. Hong, L. Sun, J. Zenkoh, T. Moritake, K. Tsuboi, Celecoxib enhances radiosensitivity of hypoxic glioblastoma cells through endoplasmic reticulum stress. *Neuro-Oncology*. **15**, 1186–1199 (2013).

181. J. N. Contessa, M. S. Bhojani, H. H. Freeze, A. Rehemtulla, T. S. Lawrence, Inhibition of N-linked glycosylation disrupts receptor tyrosine kinase signaling in tumor cells. *Cancer Res*. **68**, 3803–3809 (2008).

182. J. N. Hayner, J. Shan, M. S. Kilberg, Regulation of the ATF3 gene by a single promoter in response to amino acid availability and endoplasmic reticulum stress in human primary hepatocytes and hepatoma cells. *Biochimica et biophysica acta*. **1861**, 72–79 (2018).

183. C. Yan, D. D. Boyd, ATF3 regulates the stability of p53. *Cell cycle (Georgetown, Tex.)*. **5**, 926–929 (2006).

184. C. Yan, D. Lu, T. Hai, D. D. Boyd, Activating transcription factor 3, a stress sensor, activates p53 by blocking its ubiquitination. *Embo j*. **24**, 2425–2435 (2005).

185. T. Namba, K. Chu, R. Kodama, S. Byun, K. W. Yoon, M. Hiraki, A. Mandinova, S. W. Lee, Loss of p53 enhances the function of the endoplasmic reticulum through activation of the IRE1α/XBP1 pathway. *Oncotarget*. **6**, 19990–20001 (2015).

186. C. Mlynarczyk, R. Fåhraeus, Endoplasmic reticulum stress sensitizes cells to DNA damage-induced apoptosis through p53-dependent suppression of p21(CDKN1A). *Nature communications*. **5**, 5067 (2014).

187. D. J. Powell, R. Hrstka, M. Candeias, K. Bourougaa, B. Vojtesek, R. Fåhraeus, Stress-dependent changes in the properties of p53 complexes by the alternative translation product p53/47. *Cell cycle (Georgetown, Tex.)*. **7**, 950–959 (2008).

188. Y. Yin, C. W. Stephen, M. G. Luciani, R. Fåhraeus, p53 Stability and activity is regulated by Mdm2-mediated induction of alternative p53 translation products. *Nat Cell Biol*. **4**, 462–467 (2002).

189. K. Bourougaa, N. Naski, C. Boularan, C. Mlynarczyk, M. M. Candeias, S. Marullo, R. Fåhraeus, Endoplasmic reticulum stress induces G2 cell-cycle arrest via mRNA translation of the p53 isoform p53/47. *Molecular cell*. **38**, 78–88 (2010).

190. S. E. Thomas, E. Malzer, A. Ordóñez, L. E. Dalton, E. F. A. van 't Wout, E. Liniker, D. C. Crowther, D. A. Lomas, S. J. Marciniak, p53 and translation attenuation regulate distinct cell cycle checkpoints during endoplasmic reticulum (ER) stress. *The Journal of Biological Chemistry*. **288**, 7606–7617 (2013).

191. F. Zhang, R. B. Hamanaka, E. Bobrovnikova-Marjon, J. D. Gordan, M.-S. Dai, H. Lu, M. C. Simon, J. A. Diehl, Ribosomal stress couples the unfolded protein response to p53-dependent cell cycle arrest. *J Biol Chem*. **281**, 30036–30045 (2006).

192. J. Li, B. Lee, A. S. Lee, Endoplasmic reticulum stress-induced apoptosis. *J Biol Chem*. **281**, 7260–7270 (2006).

193. L. Qu, S. Huang, D. Baltzis, A.-M. Rivas-Estilla, O. Pluquet, M. Hatzoglou, C. Koumenis, Y. Taya, A. Yoshimura, A. E. Koromilas, Endoplasmic reticulum stress induces p53 cytoplasmic localization and prevents p53-dependent apoptosis by a pathway involving glycogen synthase kinase-3beta. *Genes Dev*. **18**, 261–277 (2004).

194. L. Qu, A. E. Koromilas, Control of tumor suppressor p53 function by endoplasmic reticulum stress. *Cell cycle (Georgetown, Tex.)*. **3**, 567–570 (2004).

195. O. Pluquet, L.-K. Qu, D. Baltzis, A. E. Koromilas, Endoplasmic reticulum stress accelerates p53 degradation by the cooperative actions of Hdm2 and glycogen synthase kinase 3beta. *Mol Cell Biol*. **25**, 9392–9405 (2005).

196. D. Baltzis, O. Pluquet, A. I. Papadakis, S. Kazemi, L.-K. Qu, A. E. Koromilas, The eIF2alpha kinases PERK and PKR activate glycogen synthase kinase 3 to promote the proteasomal degradation of p53. *J Biol Chem*. **282**, 31675–31687 (2007).

197. N. Dioufa, I. Chatzistamou, E. Farmaki, A. G. Papavassiliou, H. Kiaris, p53 antagonizes the unfolded protein response and inhibits ground glass hepatocyte development during endoplasmic reticulum stress. *Experimental biology and medicine (Maywood, N.J.)*. **237**, 1173–1180 (2012).

198. E. Duplan, E. Giaime, J. Viotti, J. Sévalle, O. Corti, A. Brice, H. Ariga, L. Qi, F. Checler, C. Alves da Costa, ER-stress-associated functional link between Parkin and DJ-1 via a transcriptional cascade involving the tumor suppressor p53 and the spliced X-box binding protein XBP-1. *J Cell Sci*. **126**, 2124–2133 (2013).

199. M. Cayre, P. Canoll, J. E. Goldman, Cell migration in the normal and pathological postnatal mammalian brain. *Progress in Neurobiology*. **88**, 41–63 (2009).

200. K. J. Livak, T. D. Schmittgen, Analysis of relative gene expression data using real-time quantitative PCR and the 2(-Delta Delta C(T)) Method. *Methods (San Diego, Calif.)*. **25**, 402–408 (2001).

201. E. H. Akama-Garren, N. S. Joshi, T. Tammela, G. P. Chang, B. L. Wagner, D.-Y. Lee, W. M. Rideout, T. Papagiannakopoulos, W. Xue, T. Jacks, A Modular Assembly Platform for Rapid Generation of DNA Constructs. *Scientific reports*. **6**, 16836 (2016).

202. J. Jonkers, R. Meuwissen, H. van der Gulden, H. Peterse, M. van der Valk, A. Berns, Synergistic tumor suppressor activity of BRCA2 and p53 in a conditional mouse model for breast cancer. *Nature genetics*. **29**, 418–425 (2001).

203. B. Sauer, N. Henderson, Site-specific DNA recombination in mammalian cells by the Cre recombinase of bacteriophage P1. *Proc Natl Acad Sci U S A*. **85**, 5166–5170 (1988).

204. S. Swift, J. Lorens, P. Achacoso, G. P. Nolan, Rapid production of retroviruses for efficient gene delivery to mammalian cells using 293T cell-based systems. *Current protocols in immunology*. **Chapter 10**, Unit 10.17C (2001).

205. R. K. Naviaux, E. Costanzi, M. Haas, I. M. Verma, The pCL vector system. *Journal of virology*. **70**, 5701–5705 (1996).

206. T. L. Riss, R. A. Moravec, A. L. Niles, S. Duellman, H. A. Benink, T. J. Worzella, L. Minor, in *Assay Guidance Manual*, G. S. Sittampalam, N. P. Coussens, K. Brimacombe, A. Grossman, M. Arkin, D. Auld, C. Austin, J. Baell, B. Bejcek, T. D.Y. Chung, J. L. Dahlin, V. Devanaryan, T. L. Foley, M. Glicksman, M. D. Hall, J. V. Hass, J. Inglese, P. W. Iversen, S. D. Kahl, S. C. Kales, M. Lal-Nag, Z. Li, J. McGee, O. McManus, T. Riss, O. J. Trask, J. R. Weidner, M. Xia, X. Xu, eds. (Bethesda (MD), 2004).

207. I. Papandreou, N. C. Denko, M. Olson, H. van Melckebeke, S. Lust, A. Tam, D. E. Solow-Cordero, D. M. Bouley, F. Offner, M. Niwa, A. C. Koong, Identification of an Ire1alpha endonuclease specific inhibitor with cytotoxic activity against human multiple myeloma. *Blood*. **117**, 1311–1314 (2011).

208. Y.-Y. Lee, R. C. Cevallos, E. Jan, An upstream open reading frame regulates translation of GADD34 during cellular stresses that induce eIF2alpha phosphorylation. *J Biol Chem*. **284**, 6661–6673 (2009).

209. C. Casas, GRP78 at the Centre of the Stage in Cancer and Neuroprotection. *Frontiers in neuroscience*. **11**, 177 (2017).

210. C. D. L. Nguyen, S. Malchow, S. Reich, S. Steltgens, S. Loroch, C. Lorenz, A. Sickmann, "A sensitive and simple targeted proteomics approach to quantify transcription factor and membrane proteins of the unfolded protein response pathway in glioblastoma cells". -*submitted*-.

211. C. Hetz, F. R. Papa, The Unfolded Protein Response and Cell Fate Control. *Molecular cell* (2017).

212. G. Salazar, B. Craige, M. L. Styers, K. A. Newell-Litwa, M. M. Doucette, B. H. Wainer, J. M. Falcon-Perez, E. C. Dell'Angelica, A. A. Peden, E. Werner, V. Faundez, BLOC-1 complex deficiency alters the targeting of adaptor protein complex-3 cargoes. *Mol Biol Cell*. **17**, 4014–4026 (2006).

213. D. Bae, K. A. Moore, J. M. Mella, S. Y. Hayashi, J. Hollien, Degradation of Blos1 mRNA by IRE1 repositions lysosomes and protects cells from stress. *The Journal of cell biology*. **218**, 1118–1127 (2019).

214. Son1p is a component of the 26S proteasome of the yeast Saccharomyces cerevisiae.

215. J. W. Brewer, L. M. Hendershot, C. J. Sherr, J. A. Diehl, Mammalian unfolded protein response inhibits cyclin D1 translation and cell-cycle progression. *Proc Natl Acad Sci U S A*. **96**, 8505–8510 (1999).

216. J. W. Brewer, J. A. Diehl, PERK mediates cell-cycle exit during the mammalian unfolded protein response. *Proc Natl Acad Sci U S A*. **97**, 12625–12630 (2000).

217. P.-J. Le Reste, T. Avril, V. Quillien, X. Morandi, E. Chevet, Signaling the Unfolded Protein Response in primary brain cancers. *Brain Research*. **1642**, 59–69 (2016).

218. J. Obacz, T. Avril, P.-J. Le Reste, H. Urra, V. Quillien, C. Hetz, E. Chevet, Endoplasmic reticulum proteostasis in glioblastoma-From molecular mechanisms to therapeutic perspectives. *Science signaling*. **10** (2017).

219. M. W. Graner, The unfolded protein response in glioblastomas. *Future science OA*. **1**, FSO45 (2015).

220. M. W. Graner, R. I. Cumming, D. D. Bigner, The heat shock response and chaperones/heat shock proteins in brain tumors. *The Journal of neuroscience : the official journal of the Society for Neuroscience*. **27**, 11214–11227 (2007).

221. M. W. Graner, D. A. Raynes, D. D. Bigner, V. Guerriero, Heat shock protein 70-binding protein 1 is highly expressed in high-grade gliomas, interacts with multiple heat shock

protein 70 family members, and specifically binds brain tumor cell surfaces. *Cancer science*. **100**, 1870–1879 (2009).

222. B. R. Kang, S.-H. Yang, B.-R. Chung, W. Kim, Y. Kim, Cell surface GRP78 as a biomarker and target for suppressing glioma cells. *Scientific reports*. **6**, 34922 (2016).

223. M. Gonzalez-Gronow, M. A. Selim, J. Papalas, S. V. Pizzo, GRP78. *Antioxidants & redox signaling*. **11**, 2299–2306 (2009).

224. G. Liu, Y. Shang, Y. Yu, Induced endoplasmic reticulum (ER) stress and binding of over-expressed ER specific chaperone GRP78/BiP with dimerized epidermal growth factor receptor in mammalian cells exposed to low concentration of N-methyl-N'-nitro-N-nitrosoguanidine. *Mutation research*. **596**, 12–21 (2006).

225. Z. An, O. Aksoy, T. Zheng, Q.-W. Fan, W. A. Weiss, Epidermal growth factor receptor and EGFRvIII in glioblastoma. *Oncogene*. **37**, 1561–1575 (2018).

226. D. W. Parsons, S. Jones, X. Zhang, J. C.-H. Lin, R. J. Leary, P. Angenendt, P. Mankoo, H. Carter, I.-M. Siu, G. L. Gallia, A. Olivi, R. McLendon, B. A. Rasheed, S. Keir, T. Nikolskaya, Y. Nikolsky, D. A. Busam, H. Tekleab, L. A. Diaz, J. Hartigan, D. R. Smith, R. L. Strausberg, S. K. N. Marie, S. M. O. Shinjo, H. Yan, G. J. Riggins, D. D. Bigner, R. Karchin, N. Papadopoulos, G. Parmigiani, B. Vogelstein, V. E. Velculescu, K. W. Kinzler, An integrated genomic analysis of human glioblastoma multiforme. *Science (New York, N.Y.)*. **321**, 1807–1812 (2008).

227. H. Sha, Y. He, H. Chen, C. Wang, A. Zenno, H. Shi, X. Yang, X. Zhang, L. Qi, The IRE1alpha-XBP1 pathway of the unfolded protein response is required for adipogenesis. *Cell Metabolism*. **9**, 556–564 (2009).

228. A. Blais, M. Tsikitis, D. Acosta-Alvear, R. Sharan, Y. Kluger, B. D. Dynlacht, An initial blueprint for myogenic differentiation. *Genes Dev*. **19**, 553–569 (2005).

229. J. B. DuRose, A. B. Tam, M. Niwa, Intrinsic capacities of molecular sensors of the unfolded protein response to sense alternate forms of endoplasmic reticulum stress. *Mol Biol Cell*. **17**, 3095–3107 (2006).

230. S. Lhomond, T. Avril, N. Dejeans, K. Voutetakis, D. Doultsinos, M. McMahon, R. Pineau, J. Obacz, O. Papadodima, F. Jouan, H. Bourien, M. Logotheti, G. Jégou, N. Pallares-Lupon, K. Schmit, P.-J. Le Reste, A. Etcheverry, J. Mosser, K. Barroso, E. Vauléon, M. Maurel, A. Samali, J. B. Patterson, O. Pluquet, C. Hetz, V. Quillien, A. Chatziioannou, E. Chevet, Dual IRE1 RNase functions dictate glioblastoma development. *EMBO molecular medicine*. **10** (2018).

231. A. Jabouille, M. Delugin, R. Pineau, A. Dubrac, F. Soulet, S. Lhomond, N. Pallares-Lupon, H. Prats, A. Bikfalvi, E. Chevet, C. Touriol, M. Moenner, Glioblastoma invasion and cooption depend on IRE1α endoribonuclease activity. *Oncotarget*. **6**, 24922–24934 (2015).

232. J. D. Blais, V. Filipenko, M. Bi, H. P. Harding, D. Ron, C. Koumenis, B. G. Wouters, J. C. Bell, Activating transcription factor 4 is translationally regulated by hypoxic stress. *Mol Cell Biol*. **24**, 7469–7482 (2004).

233. M. Bi, C. Naczki, M. Koritzinsky, D. Fels, J. Blais, N. Hu, H. Harding, I. Novoa, M. Varia, J. Raleigh, D. Scheuner, R. J. Kaufman, J. Bell, D. Ron, B. G. Wouters, C. Koumenis, ER stress-regulated translation increases tolerance to extreme hypoxia and promotes tumor growth. *Embo j*. **24**, 3470–3481 (2005).

234. E. Bobrovnikova-Marjon, C. Grigoriadou, D. Pytel, F. Zhang, J. Ye, C. Koumenis, D. Cavener, J. A. Diehl, PERK promotes cancer cell proliferation and tumor growth by limiting oxidative DNA damage. *Oncogene*. **29**, 3881–3895 (2010).

235. S. Yamasaki, N. Yagishita, T. Sasaki, M. Nakazawa, Y. Kato, T. Yamadera, E. Bae, S. Toriyama, R. Ikeda, L. Zhang, K. Fujitani, E. Yoo, K. Tsuchimochi, T. Ohta, N. Araya, H. Fujita, S. Aratani, K. Eguchi, S. Komiya, I. Maruyama, N. Higashi, M. Sato, H. Senoo, T. Ochi, S. Yokoyama, T. Amano, J. Kim, S. Gay, A. Fukamizu, K. Nishioka, K. Tanaka, T. Nakajima, Cytoplasmic destruction of p53 by the endoplasmic reticulum-resident ubiquitin ligase 'Synoviolin'. *Embo j*. **26**, 113–122 (2007).

236. H. J. Lee, J. M. Kim, K. H. Kim, J. I. Heo, S. J. Kwak, J. A. Han, Genotoxic stress/p53-induced DNAJB9 inhibits the pro-apoptotic function of p53. *Cell death and differentiation*. **22**, 86–95 (2015).

237. S. L. Adams, Collagen gene expression. *Am J Respir Cell Mol Biol*. **1**, 161–168 (1989).

238. D. Kennedy, K. Mnich, A. Samali, Heat shock preconditioning protects against ER stress-induced apoptosis through the regulation of the BH3-only protein BIM. *FEBS open bio*. **4**, 813–821 (2014).

239. J. G. Tate, S. Bamford, H. C. Jubb, Z. Sondka, D. M. Beare, N. Bindal, H. Boutselakis, C. G. Cole, C. Creatore, E. Dawson, P. Fish, B. Harsha, C. Hathaway, S. C. Jupe, C. Y. Kok, K. Noble, L. Ponting, C. C. Ramshaw, C. E. Rye, H. E. Speedy, R. Stefancsik, S. L. Thompson, S. Wang, S. Ward, P. J. Campbell, S. A. Forbes, COSMIC. *Nucleic Acids Res*. **47**, D941-D947 (2019).

240. C. D. L. Nguyen, S. Malchow, S. Reich, S. Steltgens, K. V. Shuvaev, S. Loroch, C. Lorenz, A. Sickmann, C. B. Knobbe-Thomsen, B. Tews, J. Medenbach, R. Ahrends, A sensitive and simple targeted proteomics approach to quantify transcription factor and membrane proteins of the unfolded protein response pathway in glioblastoma cells. *Scientific reports*. **9**, 8836 (2019).

DECLARATION OF AUTONOMOUS WORK

Hiermit erkläre ich, dass ich die heute eingereichte Doktorarbeit selbständig verfasst und keine anderen als die angegebenen Quellen und Hilfsmittel benutzt, sowie Zitate kenntlich gemacht habe. Bei der vorliegenden Doktorarbeit handelt es sich um in Wort und Bild völlig übereinstimmende Exemplare.

Weiterhin erkläre ich, dass die digitale Abbildung nur die originalen Daten enthalten und in keinem Fall inhaltsverändernde Bilderbearbeitung vorgenommen wurde.

Schwelm, den 9. Januar 2020

_____

(Sascha Steltgens, *M. Sc.*)

ACKNOWLEDGMENTS

Zu Beginn möchte ich Herrn Prof. Dr. Guido Reifenberger danken. Nicht nur dafür, dass ich die Laborarbeiten für meine Doktorarbeit am Institut für Neuropathologie durchführen und abschließen durfte möchte ich mich bedanken, sondern auch für die Geduld, die mir gegenübergebracht wurde. Des Weiteren möchte ich mich für die Korrektur dieser Arbeit bedanken.

Bedanken möchte ich mich auch bei Frau Dr. Christiane Knobbe-Thomsen. Die mir gelassene Freiheit meiner Neugierde zu folgen und dem Vertrauen meinen eigenen Weg zu finden wird mich für immer prägen. Danke für die Unterstützung und das du mich mit einem Thema bekannt gemacht hast, dass meine Faszination für die Biologie vollkommen sättigte.

Bei Marietta, Bastian, Kerstin und Jörg möchte ich mich für die ständige Unterstützung, die geduldige Beantwortung meiner nicht enden wollenden sich oftmals wiederholenden Fragen, dem aushalten meines Humors und den jetzt fehlenden Nettigkeiten bedanken.

Miriam, Miriam, Jana. Danke das ihr mich auf dem Weg begleitet habt. Danke, dass ihr mir immer geholfen habt. Danke, dass ihr mich kritisiert habt und mir immer ehrlichen Rat gabt. Danke, dass ihr an meiner Seite wart und wir diesen Abschnitt unserer Leben geteilt haben. Ich werde Zellkulturmontage und -freitage niemals vergessen.

Dankbar bin ich auch für meine Kollegen*innen aus den anderen Arbeitsgruppen am Institut, die mir Freunde wurden und mit denen ich jeden Wahnsinn händeln konnte. Die Atmosphäre war einzigartig und unterstützend ablenkend, das habe ich gebraucht.

Meinen Freunden, die mich auf meinem Weg begleiteten, unterstützten und immer ein Ohr offen hatten möchte ich danken. Ohne euch, wäre ich weder der, der ich bin, noch hätte ich meinen Weg geschafft.

Besonderes dankbar bin ich für die Unterstützung meiner Eltern. Egal wohin ich gehe, ich konnte mir immer sicher sein, dass wenn was schief geht, ihr für mich da seit. Ihr habt mir meinen Weg bereitet und nie Steine in denselben gelegt. Danke.